JASON

Technical Report
JSR-80-15

September 1980

IRREGULARITIES IN IONOSPHERIC PLASMA CLOUDS: THEIR EVOLUTION AND EFFECT ON RADIO COMMUNICATION

J. F. Vesecky
J. W. Chamberlain
J. M. Cornwall
D. A. Hammer
F. W Perkins

SRI International
1611 North Kent Street
Arlington, Virginia 22209

JASON

(9) Technical Report JSR-80-15

(11) September 1980

(14) SRI-JSR-80-15

(1) IRREGULARITIES IN IONOSPHERIC PLASMA CLOUDS: THEIR EVOLUTION AND EFFECT ON RADIO COMMUNICATION.

(12) 135

(10) J. F. Vesecky
J. W. Chamberlain
J. M. Cornwall
D. A. Hammer
F. W. Perkins

(15) DNA001-79-C-0362

JOB

SRI International

SRI International

EXECUTIVE SUMMARY

Introduction: Both satellite radio communications, which travel through the Earth's ionosphere, and high frequency (HF) sky wave radio circuits, which use the ionosphere as a refracting medium, can be strongly affected by radio wave scintillation. By strongly disturbing the ionosphere high altitude nuclear explosions (HANEs) can cause scintillation (and other effects), thus severely degrading satellite (and HF) radio communications over a large region. Therefore an accurate assessment of the severity of nuclear communications effects is necessary in order to deploy a communications system which is adequate for projected needs, but not over-designed and hence more expensive than necessary. Since experimental evidence is limited to a few high altitude nuclear tests (before the test ban treaty of 1963), such an accurate assessment must rely heavily on computer simulations and thus on a thorough understanding of the physics involved in both the disturbed ionosphere and its interaction with radio communications signals. Fortunately, the propagation of radio waves through a given disturbed ionosphere is relatively well understood. Accordingly, our 1980 JASON Summer Study focussed primarily on some aspects of the ionospheric irregularities following a high altitude nuclear explosion. More specifically we have considered the ongoing problem of predicting irregularity characteristics (namely the outer scale length L_o , spectral index α , and regions of occurrence) following a nuclear event especially at late times (~ hours after the event). Using propagation theory these irregularity characteristics can be used to forecast the degradation of a given satellite communications system.

Computer Simulations and How They are Checked: Although large amounts of data were collected during the last series of high altitude nuclear tests before the 1963 Test Ban Treaty (Fishbowl), these data are insufficient to answer many questions which have arisen subsequently. Since no further high altitude testing is permitted under the treaty, one must simulate the effects of high altitude nuclear explosions using a rather elaborate sequence of computer codes. These codes (illustrated in Fig. 2 of the main report) are based on current understanding of the physics involved in high altitude nuclear effects. However, in some areas the physics is not well understood and simulations must be checked by experiment. Such experiments have included rocket releases of barium in the ionosphere and observations of natural ionospheric irregularities. In this report (section IV) we discuss how scaled down laboratory experiments could be used. Comparison with experiment is the key way to check whether simulations have overlooked any physical processes.

Current Issues Regarding the Physics of Ionospheric Nuclear Effects: The theoretical and empirical methods for forecasting nuclear effects currently involve a number of critical issues. A key factor in these issues is the enormous range of scale sizes involved in the problem. We are concerned with size scales as small as ~ 10 to 100 m, yet the region of interest is thousands to tens of thousands of km in size--a size range of ~ 10^5 to 10^6. Computer simulations can handle size ranges of about 10 to 100! Perhaps the most important of these issues is the physics which governs the evolution of ionospheric plasma irregularities at late times (~ minutes to hours after a nuclear event).

Do the irregularities evolve for a few linear growth times of the relevant instability (~ tens of minutes for a large barium cloud) and then "freeze" or do they continue to evolve? What are the roles of currents flowing along geomagnetic field lines and connecting across the field in a remote region, of Alfvén waves, of finite Larmor radius, etc.? How can computer simulations cope with the enormous range of scale sizes involved? We suggest a "fractal" model to help in coping with some of these questions. With regard to the question of initial seed striations, we suggest that laboratory experiments using laser exploded pellets in large vacuum tanks might be helpful.

Other issues involve: (1) the possible existence of plasma which was unobserved optically during high altitude nuclear tests, but which would still disturb radio wave propagation over a volume substantially larger than that of the optically observed plasma, (2) the possibility of magnetospherically trapped ions forming an artificial ring current and the impact of such a ring current on striated plasmas.

Conclusions, Recommendations and Action Items: Our conclusions and recommendations can largely be embodied in the following list of action items through which the recommendations can be implemented.

1. Investigate the fractal model for plasma cloud evolution by (a) finding out whether or not the evolution of ionospheric barium releases (as we now understand them) can be viewed as fractalization processes, i.e., compare observations with the implications of a fractal model and

(b) investigating whether or not the equations now used to describe plasma irregularity evolution lead mathematically to a fractal model. The fractal model is important because it can extend existing computational models to cover the million-fold size range necessary to study nuclear environment scintillation at late times and because preliminary results of the fractal model indicate that late time scintillation may be more disruptive to satellite communications than currently anticipated.

2. Do short design studies to find out whether or not meaningful laboratory experiments (involving laser exploded pellets in large vacuum tanks containing magnetic fields) can be done and for what cost. Such experiments might provide information on early time ($\lesssim$ minutes) coupling of the expanding debris cloud to the atmosphere, the influence of early time structure on late time irregularity evolution and inner and outer scale sizes of late time plasma irregularities.

3. Make observations of both strong and weak fluorescence lines during the next large barium cloud release. Because of radiative transfer effects (Horak and Whittaker, 1980) observations of large barium clouds can be misleading if only the strong resonance transition at 4554 Å is observed.

4. Theoretically investigate scintillation effects along a typical HF skywave path through a late time nuclear environment. If HF systems are to provide a viable backup communications mode, it is necessary to assess the severity of scintillation effects upon them. Nuclear effects computer codes for HF propagation do not now include scintillation effects.

5. Investigate the likelihood and consequences of an artificial energetic ion (ring) current being formed as a result of a high altitude nuclear explosion. If such a magnetospheric ring current were to be present following a high altitude nuclear explosion (and there is no direct experimental evidence one way or the other), there could be substantial consequences for the evolution of ionospheric irregularities.

6. Incorporate radio and radar data into the description of nuclear event plasma following Fishbowl (and possibly other) high altitude nuclear tests, particularly regarding spatial distribution of the plasma.

This page left blank intentionally

TABLE OF CONTENTS

This page left blank intentionally

LIST OF FIGURES

LIST OF TABLES

I. INTRODUCTION, CONCLUSIONS AND RECOMMENDATIONS

Both satellite radio communications, which travel through the Earth's ionosphere, and high frequency (HF) sky wave circuits, which use the ionosphere as a refracting medium, can be strongly affected by radio wave scintillation. High altitude nuclear explosions cause scintillation (by strongly disturbing the ionosphere) and thus severely degrade satellite radio communications over a large region. Since further atmospheric nuclear tests are banned, a thorough understanding of the physics involved in both the disturbed ionosphere and its interaction with radio waves is necessary in order to design radio communications systems which will operate satisfactorily in a nuclear environment. During the 1980 JASON Summer Study we addressed some aspects of the evolution of ionospheric irregularities following a high altitude nuclear explosion--the radio wave propagation theory being apparently well understood for the satellite link case. In particular, we have worked on irregularity evolution at late times (approx. hours) after an explosion and the impact of early time irregularity structure on late time evolution. We also raise the question of scintillation effects on HF sky wave communications.

In this first section of our report we put our investigation in perspective by first discussing the physical phenomena connected with high altitude nuclear explosions and the impact of these phenomena on radio communications systems using satellites. We then discuss the methods currently used to estimate these effects in the absence of complete data

from atmospheric nuclear tests, namely computer simulations. There are a number of ways some aspects of these simulations are or can be checked both experimentally and theoretically. We review existing methods and suggest some new ones. In checking the computer simulations a number of critical issues have arisen. These are outlined. Finally we sum up our summer study conclusions and recommendations.

A. Impact of High Altitude Nuclear Explosions on Communications via the Ionosphere

1. Phenomenology of High Altitude Nuclear Explosions

As will become clear, the complicated structure of the atmosphere and the multitude of physical processes at work following a high altitude nuclear explosion make quantitative description of the nuclear environment a difficult and complex task. The brief description which follows draws on Wittwer (1980b & c), Zinn et al. (1966) and Hess (1968). As a beginning, high altitude nuclear phenomena can be divided into three time regimes according to the principal physical processes occurring, to wit

Fast Regime: $0 < t \lesssim$ few seconds;

MHD Regime: few seconds $\lesssim t \lesssim$ minutes;

Electrostatic Regime: minutes $\lesssim t \lesssim$ hours.

In the Fast Regime the nuclear device explodes with debris having an initial velocity of ~ 1500 km s^{-1}. The kinetic energy in this debris is coupled to the surrounding air by X-ray and UV radiation which ionizes ambient air at large distances ($\gtrsim$ 100's of km) and by local processes such

as collisions and charge exchange. In this regime the burst debris expands to about one cyclotron radius perpendicular to the magnetic field (~ 30 km for the Starfish event) and much larger distances along the geomagnetic field. Assymetries in the device disassembly and in the ambient atmosphere aided by various kinetic plasma instabilities tend to produce structure in the expanding debris cloud and ambient air to which it couples.

Within a few seconds a magneto-hydrodynamic (MHD) shock wave forms and begins to expand initiating the MHD Regime. As the shock 'snow plows' through the now partially ionized ambient medium it loses energy locally by collisions and charge exchange. In the downward direction this 'magnetic bubble' is stopped by local energy losses. If the burst is at a high enough altitude (such as the 400 km Starfish event), the upward motion cannot be stopped by the very diffuse upper atmosphere. The upward traveling plasma moving through the geomagnetic field generates an electric field $\vec{E} = -\vec{v} \times \vec{B}$ which polarizes the cloud. Polarization and conduction currents flow in the lower portion of the magnetic bubble. These currents result in a viscous-type drag on the upward motion, eventually halting it when the bubble is ~ 500 km in radius (for Starfish). The magnetic bubble collapses having dissipated a large fraction of the debris energy over a large region of space (~ 500 km radius perpendicular to $\vec{B}$ and from southern to northern conjugate zones along the geomagnetic field). Following the bubble collapse the heated atmosphere begins to expand, 'heaving' large amounts of plasma upwards along geomagnetic field lines into the magnetosphere (see Fig. 1). This process continues in the next regime. In addition to the irregularities existing from the fast regime,

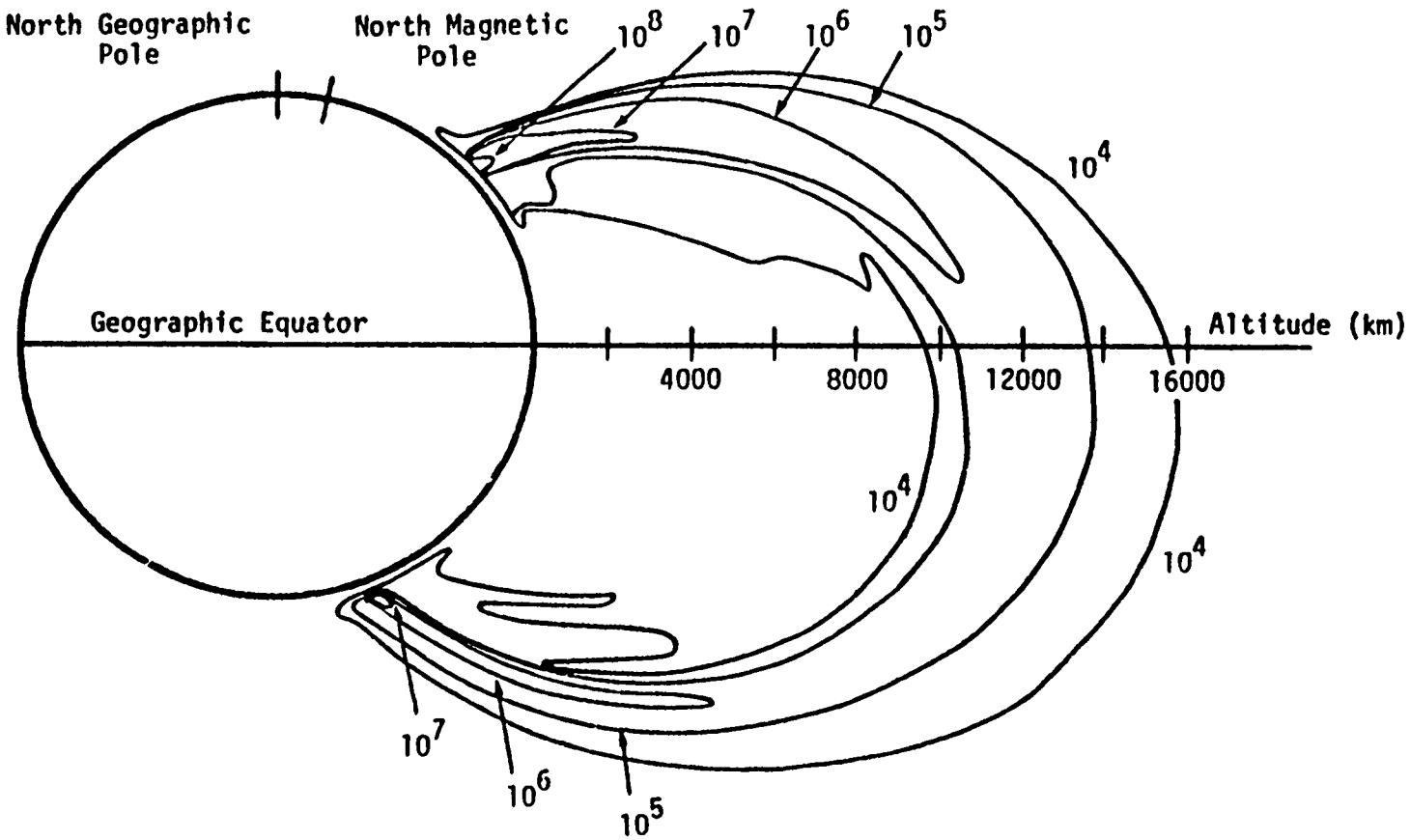

Figure 1 Electron density contours (cm^{-3}) 30 minutes after a large high altitude nuclear explosion. Note the large amounts of plasma stored in the magnetosphere. For comparison peak electron densities in the undisturbed ionosphere normally run from $\sim 10^5$ to 10^6 cm^{-3}.

Rayleigh-Taylor and $\vec{B}$ field line curvature instabilities introduce further structure.

At "late times" of from minutes to many hours large amounts of plasma continue to be stored in the magnetosphere as illustrated in Fig. 1 for t ~ 0.5 hr. This plasma subsequently descends, continually injecting plasma into the ionosphere. This curtain of plasma, only several degrees wide in the geomagnetic east-west direction, extends to larger distances north and south along the geomagnetic field. The principal plasma processes of interest at this time cause this period to be called the Electrostatic Regime. Here the geomagnetic $\vec{B}$ field is taken to be constant so that current systems and electric fields are the primary agents affecting plasma transport. As shown in Fig. 1, there are large gradients in plasma density perpendicular to the geomagnetic field. These gradients in conjunction with strong neutral winds (either induced by the explosion or at late times of natural origin) cause the plasma to be unstable to the $\vec{E} \times \vec{B}$ gradient drift instability and small scale (~ 10 m to 100's of km) plasma density irregularities develop on a time scale of $\gtrsim$ 10 minutes, lasting for hours. The fact that these irregularities exist over such an enormous range of size scales (~ 10^5 to 10^6) makes computational simulation inherently difficult. This difficulty is discussed in Section III below.

2. Propagation Effects on Radio Communications

The large extent, high density and small-scale irregularity structure of the plasma curtain shown in Fig. 1 make it a major barrier to radio communication links passing through the curtain from

ground to satellite terminals. HF sky wave communications links passing through the disturbed ionosphere are also seriously affected. For the first few minutes to tens of minutes after the nuclear explosion (depending on geometry, link frequency, and so forth) plasma densities and collision frequencies are high enough in the curtain that radio waves are highly absorbed. Thus satellite communications links passing through the plasma curtain are interrupted by excessive signal loss. This situation is often referred to as "absorption outage."

As plasma densities decrease and the absorption outage period ends, the major radio communications effects are due to small scale size irregularities in plasma density and hence in radio refractive index. As discussed briefly above and in more detail in Sections II and III below, the plasma shown in Fig. 1 is unstable and tends to form irregularities extended along the geomagnetic field and having scale lengths ~ 10's of m to 100's of km perpendicular to the geomagnetic field. Because these irregularities are intense (variance ≈ mean) along the ray paths connecting ground and satellite terminals and have scale lengths less than the appropriate Fresnel zone size ($\lesssim$ few kilometers), they can cause intense signal amplitude scintillation lasting for hours. For phase scintillation and strong scatter amplitude scintillation scale sizes larger than the Fresnel zone are also important. Signal scintillation is a general term referring to some or all of the following more specific effects:

- Deep fades in signal power (10's of dB)
- Signal phase fluctuations (10's to 100's of radians)

- Frequency selective effects
- Fluctuations in pulse propagation (group delay) time
- Fluctuations in angle of arrival at the receiving antenna
- Decorrelation of satellite signals arriving at spatially separated earth terminals

The aforementioned irregularities in plasma density also affect HF sky wave communications which propagate at dekameter wavelengths between earth-based terminals via refraction in the ionosphere. The effects on communications signals are similar to those for transionospheric links mentioned above, including both absorption outage and signal scintillations. However, HF links generally use small bandwidths (~ 20 kHz) and must deal with ionospheric variability under normal conditions. So the HF effects of high altitude nuclear explosions may in a relative sense be less severe than effects on transionospheric microwave links.

While the communications effects of high altitude nuclear explosions are indeed severe, they can be circumvented entirely or at least mitigated by appropriate system design. Some straight-forward techniques include the following:

- Increased transmitter power and/or antenna gain
- Increased operating frequency
- Receiver (MODEM) design, e.g., coding schemes, phase tracking loops, etc.
- Alternate link paths to go around the disturbed region
- Two or more antennas spatially separated
- Operational procedures, e.g., use of smaller bandwidths during disturbed periods

These techniques can certainly be effective. However, they significantly increase the cost of communications systems. Hence an accurate assessment of the severity of nuclear communications effects is necessary in order to deploy a communications system which is adequate for projected needs, but not over-designed and hence more expensive than necessary. Such an accurate assessment requires a thorough understanding of the evolution of plasma irregularities following a high altitude nuclear explosion. Much research has been done to understand this evolution, including the research reported here.

B. Simulation of High Altitude Nuclear Effects Using a Sequence of Computer Calculations

The last series of high altitude nuclear tests by the United States occurred during the Fishbowl series of 1962. Further atmospheric testing was banned by treaty in 1963. Although much data was collected during the Fishbowl series, this data set is insufficient to answer many questions which have arisen since then. Since no further testing is permitted under the treaty, one must simulate the effects of high altitude nuclear explosions using a rather elaborate sequence of computer codes. These codes are based on current understanding of the physics involved in high altitude nuclear effects.

In Figs. 2a and 2b we illustrate a possible simulation scheme. The figure takes up the calculation after device disassembly. The fast regime ($0 < t <$ few seconds) is handled by a combination of six interrelated computer codes. KLYSMA handles the coupling of device debris

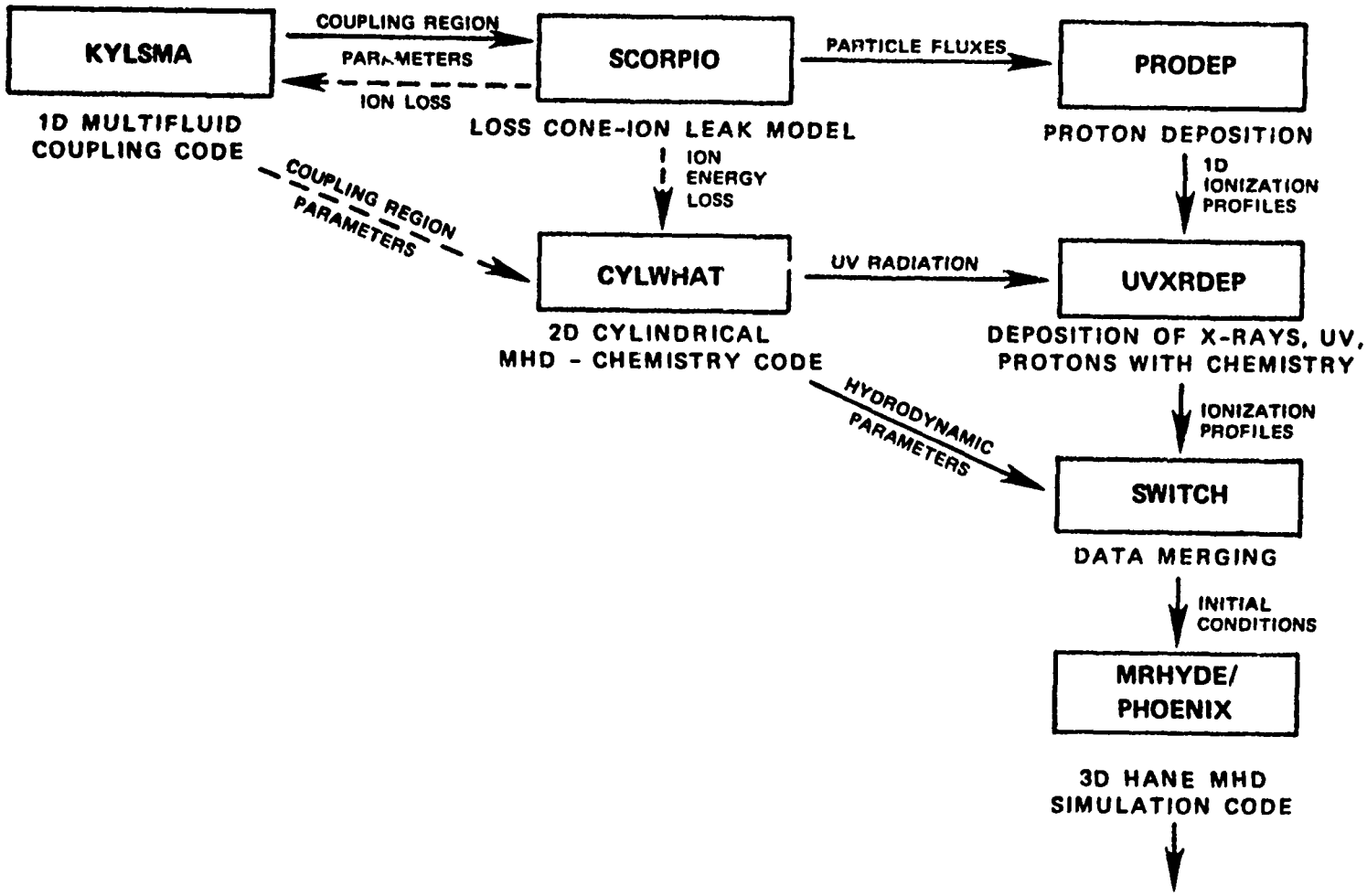

Figure 2a Flow chart for computer codes used in the simulation of high altitude nuclear explosion (HANE) events. The sequence is continued in Figure 2b. After Ossakow (1980).

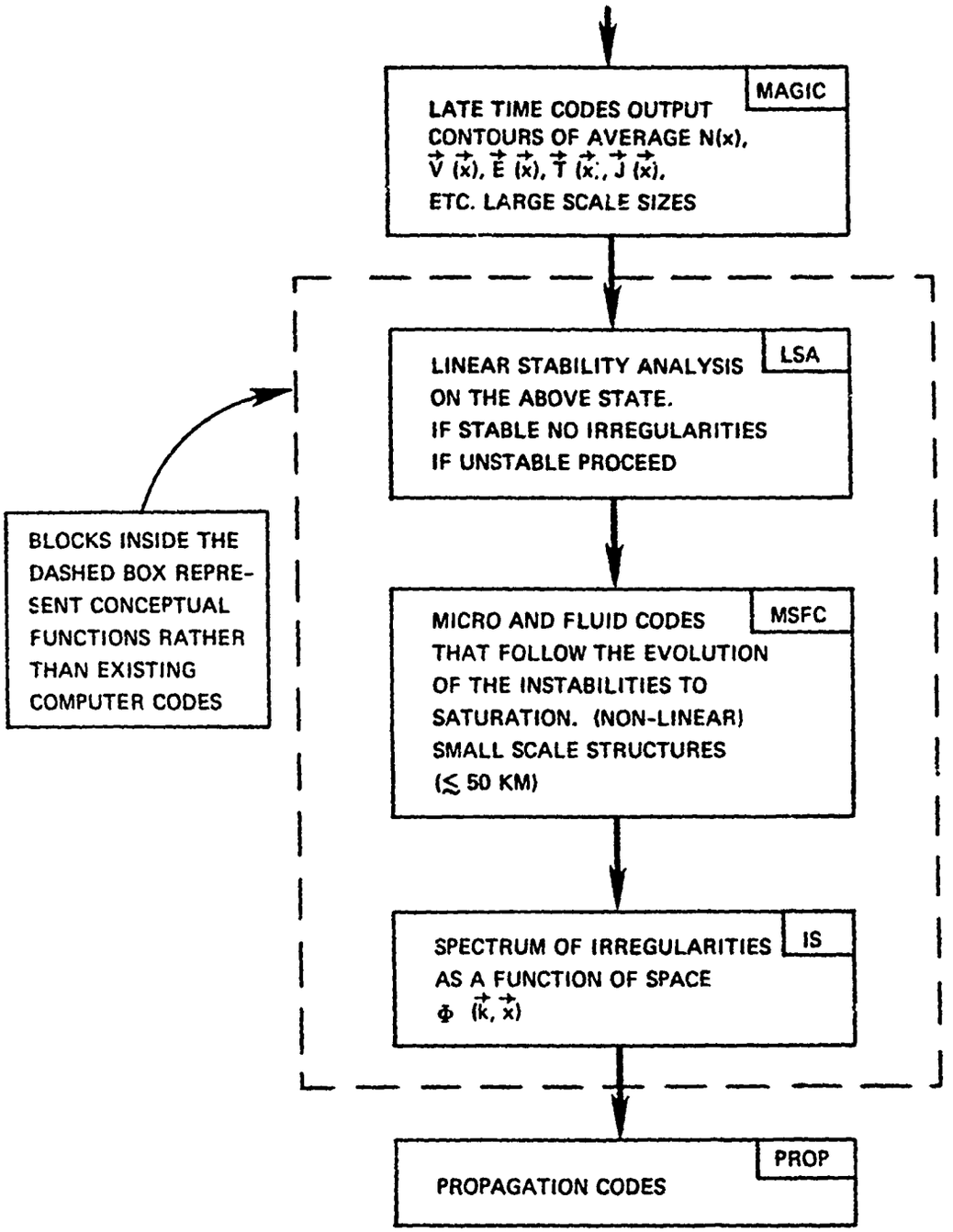

Figure 2b Continuation of flow chart for computer simulation of high altitude nuclear explosion (HANE) events. After Ossakow (1978).

energy to the ambient plasma, heating ions and electrons. The SCORPIO and CYLWHAT codes use coupling region parameters generated by KLYSMA to calculate fluxes of energetic ions and UV and X-ray photons emerging from the coupling region. The CYLWHAT code handles the blast wave and magnetic bubble expansion beginning the MHD regime (few seconds $\lesssim$ t $\lesssim$ minutes). The particle and photon fluxes are deposited over a large region by the PRODEP and UVXRDEP codes for particles and photons respectively. SWITCH merges the data from the aforementioned codes into an input to three dimensional MHD codes such as MRHYDE/PHOENIX, which calculate the atmospheric motion of coupled ion and electron fluids as large amounts of plasma are heaved upwards into the magnetosphere. At this stage (Fig. 2b) an electrostatic code MAGIC follows the subsequent motion of the plasma produced by the nuclear explosion as well as neutral atmosphere disturbances at lower altitudes. We are now in the electrostatic regime (minutes $\lesssim$ t $\lesssim$ hours) where the plasma distribution in space is evolving relatively slowly. Here the time evolution of plasma density N(x), velocity $\vec{V}(x)$, temperature T(x) current $\vec{J}(x)$ is calculated on a ~ 50 km grid. Since we are interested in irregularities on scales $\lesssim$ 50 km, further calculations must be performed as shown in Fig. 2b. At this point in the sequence we move from existing computer codes to conceptual functions which do not yet exist as running codes in the sense indicated in Fig. 2a. At each of the widely spaced (~ 50 km) grid points calculated by MAGIC a linear stability analysis (LSA) calculation would indicate whether or not the plasma is unstable to the $\vec{E} \times \vec{B}$ gradient drift instability. If so, a small-scale size, electrostatic fluid model (MSFC) of the plasma would be used to follow the non-linear evolution of the plasma irregularities. This calculation would

yield a description of the irregularity structure $\Phi(\vec{k})$ on scale sizes of ~ 50 km and less which is the input needed by the radio wave propagation codes. These propagation codes ultimately calculate the statistical characteristics of radio signals transmitted through the disturbed ionosphere resulting from the nuclear explosion. These signal statistics are in large measure the "bottom line" of the simulation so far as late time radio communications effects are concerned.

At the present time the conceptual functions described above and in Fig. 2b are implemented by an abbreviated set of calculations along the lines indicated above but using only a restricted set of parameters rather than the full output of the MAGIC code. For example, in the plane perpendicular to $\vec{B}$ the outer scale is set at 10 km, the mean square electron density fluctuation $\langle(\Delta n_e)^2\rangle$ at $\langle n_e^2\rangle/4$, the spectral index α for plasma turbulence at $\alpha = 2$ and so forth. Calculations made on this restricted set of parameters are then used as input to the radio wave propagation codes. Multiple-level-three-dimensional codes are presently under development.

There are two principle difficulties in such an involved set of computations. First, the physics on which the computing algorithms are based must be correct enough to provide useable answers. Second, the sheer size of the problem coupled with limited storage and computer time means that variables of interest, like plasma density, cannot possibly be calculated with fine resolution in time and space. Current computational

capabilities limit the range of temporal or spacial scales covered by a given computation to a factor of from about 10 to 100. Thus the MAGIC code which handles a region of space covering thousands of km must use a computational grid with a spacing of ~ 50 km. Yet we are ultimately interested in irregularities up to 5000 times smaller. Thus this "dynamic range" problem necessitates approximations in the calculational scheme. The discussion above indicates how the problem is currently being handled; namely, small scale sizes are left out of the computation until the linear stability analysis stage (LSA in Fig. 2b).

C. How Can the Computer Simulations be Checked?

The computational simulation described above covers an enormous range of scale sizes in both time and distance as well as being complex physically. Clearly such a complicated simulation requires experimental verification. Although some features of the computer simulation are verifiable using data from the Fishbowl test series, many questions remain and no more high altitude nuclear tests are planned because of the test ban treaty. Nevertheless some aspects of the computer simulation can be checked by comparison with experiments involving the same physical processes which are active in the nuclear case. Such experiments include releases of barium in the ionosphere, observations of natural ionospheric irregularities and scaled down laboratory experiments. Further the algorithms used in the simulation codes can be examined to find the impact of any physical mechanisms which are not currently included. Plasmas can be treated by both fluid and particle models. While the particle models are necessarily limited due to relatively small numbers of

particles, comparisons of results from both models are possible and could be used to check the fluid models now being used. Below we discuss each of these methods for checking the computer simulations mentioned above.

1. Barium Releases in the Ionosphere

In the electrostatic regime (minutes $\lesssim t \lesssim$ hours) probably the most pertinent experiment short of an actual test is the release of some kilograms to tens of kilograms of barium in the ionosphere such as the Secede, Stress (McDaniel, ed., 1978) and Avefria (Simons et al. 1980 and McDonald et al. 1980) experiments. The barium released is ionized either in the release process or by solar UV radiation. These Ba ions can be observed optically in resonance emission lines (e.g., 4554 Å). However, the resonance lines can be optically thick and observations in optically thin fluorescence lines (e.g., 5854, 6142 and 6497 Å) provide necessary additional information for mapping the distribution of a Ba ion cloud in some situations (Horak and Whitaker, 1980). In Fig. 3 we see the unstable plasma formed into striations oriented with the long dimension along the geomagnetic field. Such barium clouds have been observed in situ by rocket probes and remotely by optical wavelength photometry, backscatter radars and forward scatter radio transmission through the cloud. Because high altitude nuclear events and barium releases are both subject to the $\vec{E} \times \vec{B}$ gradient drift instability, these barium release experiments provide much experimental data which is relevant to the evolution of ionospheric plasmas resulting from high altitude nuclear explosions. Although the barium releases are not completely analogous to the nuclear case, they provide an excellent opportunity to exercise and check the computational algorithms

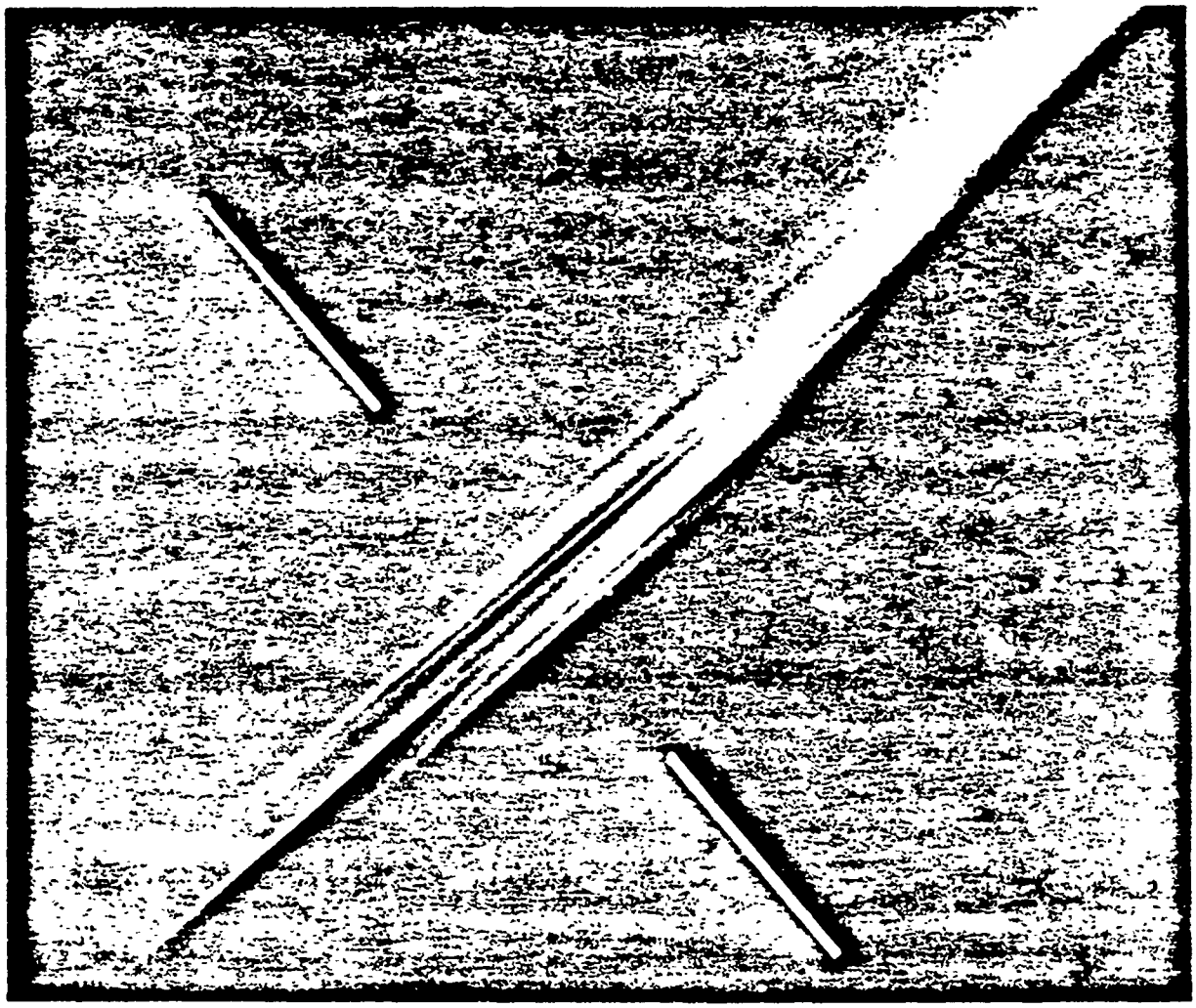

Figure 3 Striated barium plasma oriented with long dimension along the geomagnetic field. This photograph of the mature ion cloud was taken about 40 minutes after the release of 48 kg of Ba at about 180 km altitude. After Boquist (1977).

used for the electrostatic regime. So far barium plasmas have been observed for up to about three hours after release. Simulations by computer have carried out for times up to about 10 minutes after release and are in substantial argument with the observations over this time period. However, simulations have not been carried out over longer time periods and there are questions (discussed below) as to plasma behavior at these late times (~ hours).

2. Natural Ionospheric Irregularities

Natural ionospheric irregularities occur predominately at equatorial and auroral latitudes. As with the barium plasma clouds, the natural ionospheric plasma in these regions is subject to (among others) the same instability thought to cause plasma irregularities during the electrostatic regime of high altitude nuclear events. Thus a thorough understanding of these natural ionospheric irregularities provides another opportunity to check the physics used to construct nuclear event simulation algorithms. Fejer and Kelly (1980) provide an in-depth review of the current understanding of ionospheric irregularities. Perusal of this review will reveal that many of the people active in the simulation of high altitude nuclear events have also contributed to the understanding of ionospheric irregularities.

3. Laboratory Experiments

Experiments with laboratory plasmas have not so for been particularly relevant to the simulation of high altitude nuclear explosions. However, we argue in Section IV below that laboratory

experiments, specifically involving laser exploded pellets, can probably provide important information on the following:

- Coupling of the expanding debris cloud to the ambient ionosphere in the fast and MHD regimes
- Importance of "early time" phenomena, particularly spatial structure, on subsequent evolution of the plasma
- Inner and outer scale sizes of plasma irregularities in the electrostatic regime

Well conceived laboratory experiments could provide a valuable complement to the barium release and natural ionospheric irregularity experiments discussed above by their ability to explore early time phenomena and to explore late time effects in a highly controlled environment. Laboratory experiments begun at this time would benefit from the large scientific effort devoted to controlled thermonuclear fusion and space plasma related laboratory experiments.

4. Impact of Physical Mechanisms not Currently Included in Computational Simulations

Computational simulations currently used to simulate high altitude nuclear explosions must deal with an almost incredibly complex series of events involving a large number of physical processes. In order to make the problem tractable, only those effects thought to be dominant are included. In order to make the simulation valid, any effects not included in the simulation should be considered and either included or shown to be insignificant. For example, in the electrostatic regime finite

Larmor radius and some three dimensional effects are not currently included. High altitude nuclear explosions inject large numbers of high energy particles into the magnetosphere, some of which are trapped for a significant period of time. The interaction of these disturbances of the magnetosphere with the ionosphere is not now included and may be important at late times.

5. Comparison of Fluid and Particle Simulations of Plasma Dynamics

Electrostatic fluid simulations of a plasma are valid over a large range of conditions. However, fluid simulations are macroscopic and thus do not include particle effects such as the finite Larmor radii of ions and electrons in the plasma. Particle simulations such as those by Goede, Dawson and Humanic (1980) and Goede (1980) can simulate situations which are relevant to the evolution of ionospheric irregularities. While these particle simulations cannot at present attack the ionospheric irregularity problem itself (because of computer speed and memory limitations) they can help check the electrostatic codes now used by Keskinen, McDonald and Ossakow (1980), McDonald, Ossakow and Zalesak (1978), Keskinen, Ossakow and Chatervedi (1979), Ossakow, Zalesak and Zabusky (1977). This cross-checking process would involve finding a relevant domain of physical parameters which both methods could handle and comparing the results of electrostatic and particle simulations for the non-linear evolution of an unstable plasma. It should also be kept in mind that fully electromagnetic particle simulations are available.

D. Current Issues Regarding the Physics of Ionospheric Plasmas Resulting from High Altitude Nuclear Explosions

Above we have discussed theoretical and empirical methods for checking existing computer simulations of high altitude nuclear effects. This checking process currently revolves around a number of critical issues. Below we outline a number of these issues which are of importance in the research reported here. Our conclusions regarding these questions and recommendations for investigating these issues are summarized in section E below.

1. Evolution of Plasma Irregularity Structure During the Electrostatic Regime (minutes $\lesssim t \lesssim$ hours)

Both experimental studies using barium releases in the ionosphere (McDaniel, 1978) and theoretical studies using numerical simulations of non-linear plasma dynamics (Ossakow et al. 1977) indicate that ionospheric plasmas unstable to the $\vec{E} \times \vec{B}$ gradient drift instability will tend to form "fingers" along the $\vec{E} \times \vec{B}$ drift direction (see Fig. 18) and that these fingers will bifurcate forming further smaller fingers. After a few linear growth times (~ tens of minutes for a large barium release) the statistical properties of the irregularities can be characterized by a one-dimensional spectral index α of about 2 and an outer scale size (L_o) on the order of the cloud size (see Section II). The question at issue is what happens next? Does the cloud continue to bifurcate and evolve with time or does it become stable and "freeze," i.e., retain the same statistical properties (α and L_o), while moving in space, dispersing and recombining? Put another way, what physics governs the irregularity evolution at late times and what eventually limits

irregularity evolution? What are the roles of currents flowing along geomagnetic field lines and connecting across the field in a remote region, of Alfvén waves, of finite Larmor radius, etc.? As explained above and in detail in Section II α and L_o are crucial parameters in the design of satellite communications systems for use in a nuclear environment.

Experimentally and theoretically the ability to answer these questions is now limited. Barium clouds have only been observed for at most a few hours and usually less, and computer simulations are limited to a few generations of bifurcation by memory size and computation time. Further, one should continue to critically examine the extrapolation of knowledge gained from surrogate experiments with barium clouds to the nuclear case.

2. Origin, Character and Impact of Fast and MHD Region Structure on Irregularity Evolution at Later Times

Observations during high altitude nuclear tests indicate that small scale ($\lesssim$ km's) structure exists at very early times. Since the MHD regime simulations (see Fig. 2) only yield data on a ~ 50 km grid, smaller scale ($\lesssim$ 50 km) structure has not been considered prior to the linear stability analysis (LSA in Fig. 2b). The question is, then, what sort of small scale structure exists at early times, if any, and how does it affect the structure at later times? Current computations beginning at LSA in Fig. 2b assume a given structure on scales less than ~ 50 km. How close to the truth are the assumed "seed" irregularities? How would alternate choices of "seed" irregularities on important size scales

($\lesssim$ km's) affect the stability of the plasma and the non-linear growth of irregularities? As a first step, Pongratz and Simons (1979) and Simons et al. (1980) have addressed the impact of kinetic plasma instabilities on this problem both experimentally (Avefria) and theoretically. Of course, such linear analyses must be supplemented by further non-linear analysis. Ossakow (1980) plans to address the problem by inserting "seed" irregularities (on size scales $\lesssim$ 50 km) into existing simulation codes such as those reported by Ossakow et al. (1977). We argue that laboratory experiments discussed in E below and in Section IV could be helpful here.

3. Possible Magnetospheric Effects

It is well known that high altitude nuclear explosions inject enormous numbers of energetic ions into the magnetosphere (Hess, 1968). While conventional wisdom indicates that these ions are cooled by collisions and fall back down into the ionosphere, it is possible that pitch angle scattering could establish energetic (> 1 keV) ions in high altitude, virtually collisionless orbits. If this should happen, a partial ring current (analogous to the natural ring current at L ~ 4) would be established lasting from ~ hours to days.

Since ground based optical observations would not reveal such ions and no relevant satellite data from past high altitude nuclear tests exists (to the author's knowledge), we can neither confirm nor deny the existence of such an artificial ring current. Further, there is apparently no theoretical work bearing on the problem.

Here we simply raise the question of the possible impact of such magnetospheric effects on the scintillating environment following a high altitude nuclear explosion. For example, this artificial ring current would presumably have sharp gradients which would drive field-aligned currents which could, in turn, interact with conventional ionospheric striation mechanisms by, for example, driving a current convective instability. Electric fields parallel to the geomagnetic field might also be generated providing cross-field electron transport which would alter conventional striation processes by allowing ion diffusion. A modest theoretical effort seems in order to assess the likelihood of such an artificial ring current being formed and, if so, what its likely impact on striation physics would be.

4. Geophysical Distribution of Plasma Following a High Altitude Nuclear Explosion

Much effort has been expended in trying to understand the photographic data collected during the Fishbowl series of high altitude nuclear tests. Work by Kilb (1980) and others has documented the large scale distribution of plasma including the existance of jets moving across field lines and deposition of plasma in unexpected regions, e.g., far south of the Southern Conjugate Region. Most of this work has centered on photographic data from a number of sites. However, large amounts of plasma can remain undetected by optical means, especially at late times. Chesnut (1980) mentioned several ground and air based radio and radar observations during Fishbowl which apparently sensed plasma unobserved optically. Examination of these pieces of radio and radar data could substantially

change our picture of where and over what time scale enhanced ionospheric plasma densities and/or irregularities exist following a high altitude nuclear explosion.

E. Conclusions and Recommendations

Below we summarize the conclusions and recommendations arising from the 1980 JASON Summer Study on the topic of irregularities in ionospheric plasmas and their impact on radio communications. Both satellite radio communications links, which travel through the ionosphere, and HF sky wave circuits, which use the ionosphere as a refracting medium, can be strongly affected through radio wave scintillation caused by plasmas generated by high altitude nuclear explosions. Since further atmospheric tests are banned, a thorough understanding of the physics involved in both the ionospheric plasma and its interaction with radio waves is necessary in order to design radio communications systems which will operate satisfactorily in a nuclear environment. As the radio wave propagation theory is apparently well in hand for the satellite link case, we have directed our efforts toward understanding the physics of ionospheric plasma irregularities following a high altitude nuclear explosion and in particular the evolution of irregularities at late times (~ hours) after an explosion. We also raise the question of scintillation effects on HF sky wave communications.

1. Large Dynamic Range and Fractalization

The scale-free equations used (e.g., by Perkins et al. 1973 and Ossakow et al. 1977) to study the evolution of plasma

irregularities in the electrostatic (late time) regime suggest that the irregularity evolution can be described by a fractalization process (fingers have fingers have fingers, etc.) Using the fractalization model one can estimate the very important spectral index α of a fully developed irregularity cloud (see Sections II and III) using only information available from a computer simulation of the first couple of fractalizations (bifurcations). Since limitations of time and memory size virtually prohibit computer simulations for more than a few generations, the fractal model could be extremely useful in estimating the evolution of plasma irregularities at late times (~ hours) after a high altitude nuclear burst. Because fractalization leaves large scale features substantially unchanged as time progresses, it is possible that a plasma cloud is "frozen" in visual appearance as it drifts across the sky, but is nevertheless evolving according to a fractal model on such small size scales that no changes are noticed in overall appearance. Probably most important the fractal model implies that plasma irregularities could eventually evolve such that the spectral index of the irregularities α becomes substantially less than 2 ($\lesssim 1.5$). This result is unexpectedly low and, if accurate, would imply more severe communications disruptions following a high altitude nuclear explosion than are now anticipated!

Because it applies to time regimes otherwise inaccessible and has preliminary results which are surprising, we recommend that the fractal model be pursued further both in terms of the model itself and its consistency with existing knowledge, i.e., can the evolution of a barium cloud as we now understand it be viewed as a fractalization process?

2. Laboratory Experiments

We suggest that laboratory experiments, specifically laser exploded pellet experiments in large vacuum tanks containing magnetic fields, could be useful in obtaining a more complete understanding of high altitude nuclear explosions. After preliminary examination it appears that such experiments can provide information regarding the following:

a. The 'early time' (fast and MHD regimes) coupling of the expanding debris cloud to the ambient atmosphere

b. The importance of early time phenomena, e.g., spatial structure, in determining phenomena at subsequent times

c. The inner and outer scale sizes of plasma irregularities in the late time (electrostatic regime)

These experiments would impact current understanding both from the experiments themselves and the improvements in theory and computer simulations which would follow from efforts to understand the experimental data. Our discussion does not constitute an experimental design; instead it provides a strong indication that relevant experiments can be designed.

We recommend support of short term (~ 3 month) design studies by organizations having the necessary pieces of major equipment, e.g., high power lasers, large vacuum tanks, etc. If these design studies indicate that meaningful experiments can be performed, we recommend that they be undertaken with provision for participation by the appropriate research groups engaged in the simulation of high altitude nuclear effects.

3. Impact of Scattering by Small-Scale Ionospheric Irregularities on High Frequency Sky Wave Communication

Although satellite, cable and microwave relay links carry the bulk of U.S. military and civil communications, point to point communications by HF(3-30 MHz) sky wave (ionospheric refraction) propagation are frequently the best (and often the only) backup systems available for long distances. If HF sky wave systems are to provide viable backup communications when satellite links are unavailable, they must function when the ionosphere is disturbed by high altitude nuclear explosions. While large scale nuclear effects on sky wave propagation have been investigated extensively, the effects of signal scintillation by small-scale irregularities have, to the author's knowledge, been ignored. Since small-scale irregularities will presumably exist for hours after a high altitude nuclear explosion and since natural irregularities of similar characteristics, though probably less intense, severely disrupt sky wave communication in the equatorial and auroral regions, we recommend that the impact of small-scale irregularities on HF skywave propagation should be assessed. If this impact is significant, which we anticipate it will be, we recommend it be included in the computer simulations of HF propagation in a nuclear environment. This would enable communication system designers to mitigate these scintillation effects by appropriate design modifications.

While small-scale ionospheric irregularities are a nuisance so far as HF communications are concerned, they make possible VHF (~ 30 to 50 MHz) ionospheric scatter propagation over 1500 km distances. Ionospheric

scatter communications utilizing natural irregularities were, in fact, used to affect communications between the U.S. and Europe (via Canada, Greenland, Iceland, and Britain) prior to satellite systems.

4. Radiative Transfer Effects in Optical Observations of Barium Ion Clouds

The barium ion has two resonance transitions at 4934 and 4554 Å with three fluorescent transitions at slightly longer wavelengths 5854, 6142 and 6497 Å. In the past the common procedure has been to observe only the strong resonance line emissions at 4554 Å (and occasionally the other member of the pair at 4934 Å). We have studied work still in preparation by Horak and Whitaker (1980) and agree with their conclusion that observations in the resonance lines alone can yield erroneous values of the column density of barium ions and that observations can be unambiguously interpreted if supplemented by simultaneous photometry of the fluorescence lines. We also note that strontium is an almost unavoidable contaminant of barium and therefore neutral Sr is likely to be present in ionospheric barium clouds. The neutral Sr has a resonance line at 4607 Å which could contaminate the 4554 Å barium ion line measurements. This again argues for redundant spectral observations (both resonance and fluorescence lines) in cases where large optical depths are anticipated--the forthcoming PLACES experiment should produce optical depths of ~ 50 and saturation effects in the resonance line at 4554 are certainly likely. We therefore recommend that both resonance and fluorescent line observations be made during PLACES and other future barium releases where large optical depths at 4554 Å are anticipated.

5. Possible Magnetospheric Effects

High altitude nuclear explosions inject large numbers of energetic ions into the magnetosphere. Some of these ions may become trapped for considerable periods (~ hours to days) in collisionless orbits. If such an artificial ring current were to be present following a high altitude nuclear explosion, there could be substantial consequences for the evolution of ionospheric irregularities. A modest theoretical effort seems in order to assess the likelihood of such a partial ring current being formed and, if so, what its likely impact on striation physics would be.

II. IMPACT OF PLASMA IRREGULARITIES ON COMMUNICATIONS VIA THE IONOSPHERE

Since the refractive index for electromagnetic waves varies from unity in even a weakly ionized plasma, the large amounts of ionospheric and magnetospheric plasma generated by high altitude nuclear explosions (Figure 1) are likely to have a significant influence on radio communication signals propagating through these ionized regions. For radio signals of interest here the refractive index of a simple ionized medium is given by $n^2 \approx 1 - (f_{pe}^2/f^2)$ where f is the wave frequency and the electron plasma frequency is $f_{pe} \approx 10^4\sqrt{N}$ where N is the number density of electrons in cm^{-3}. Thus one finds that (other factors being equal) communication effects are more pronounced at lower radio wave frequencies and at higher plasma densities. These effects apply both to signals propagating completely through the nuclear disturbed ionosphere and magnetosphere, e.g., to communications satellites, and to signals propagating via ionospheric refraction between two surface locations, e.g., sky wave HF communications. At times not long after a high altitude nuclear explosion, i.e., $\lesssim$ tens of minutes, the nuclear generated plasma is so dense and so strongly coupled to the ambient neutral atmosphere that absorption effects dominate and received radio signals are simply too weak, too greatly attenuated, to be useful. As time passes, absorption effects decay and scattering effects dominate, lasting hours. In assessing scattering effects the spatial size distribution of the plasma irregularities is of great importance. The evolution in time of the spatial distribution of

nuclear produced plasma is the primary subject of this report. Hence we will deal with propagation and communications effects only long enough to indicate the motivation for studying the plasma spatial structure.

A. Summary of Communications Effects Caused by Plasma Irregularities

The propagation of UHF and microwave communications signals ($\gtrsim$ 300 MHz) through the plasma generated by a high altitude nuclear explosion has been studied in great detail by Rino, Vondrak, and Hatfield (1975), Johnson, Chesnut, and Rino (1976), Wittwer (1976), Wittwer et al. (1977), Hendrick (1977), Knepp (1977), Wittwer (1978), McDaniel (1978) and Wittwer (1980a) among others. Although refractive index irregularities introduce a variety of signal effects including multipath and group delay jitter, angle of arrival jitter and spatial decorrelation, we will focus on what are probably the most important effects, namely signal amplitude and phase fluctuations.

In Fig. 4 we illustrate the propagation of a radio signal through an irregular medium consisting of multiple layers, each containing irregularities in the plasma electron number density $N(\vec{r})$ and hence in the radio refractive index $n(\vec{r})$. As the radio ray path moves relative to the irregularities the received radio signal scintillates, i.e., undergoes variations in amplitude and phase with time. The twinkling of stars is another example of scintillation caused by propagation through an irregular medium.

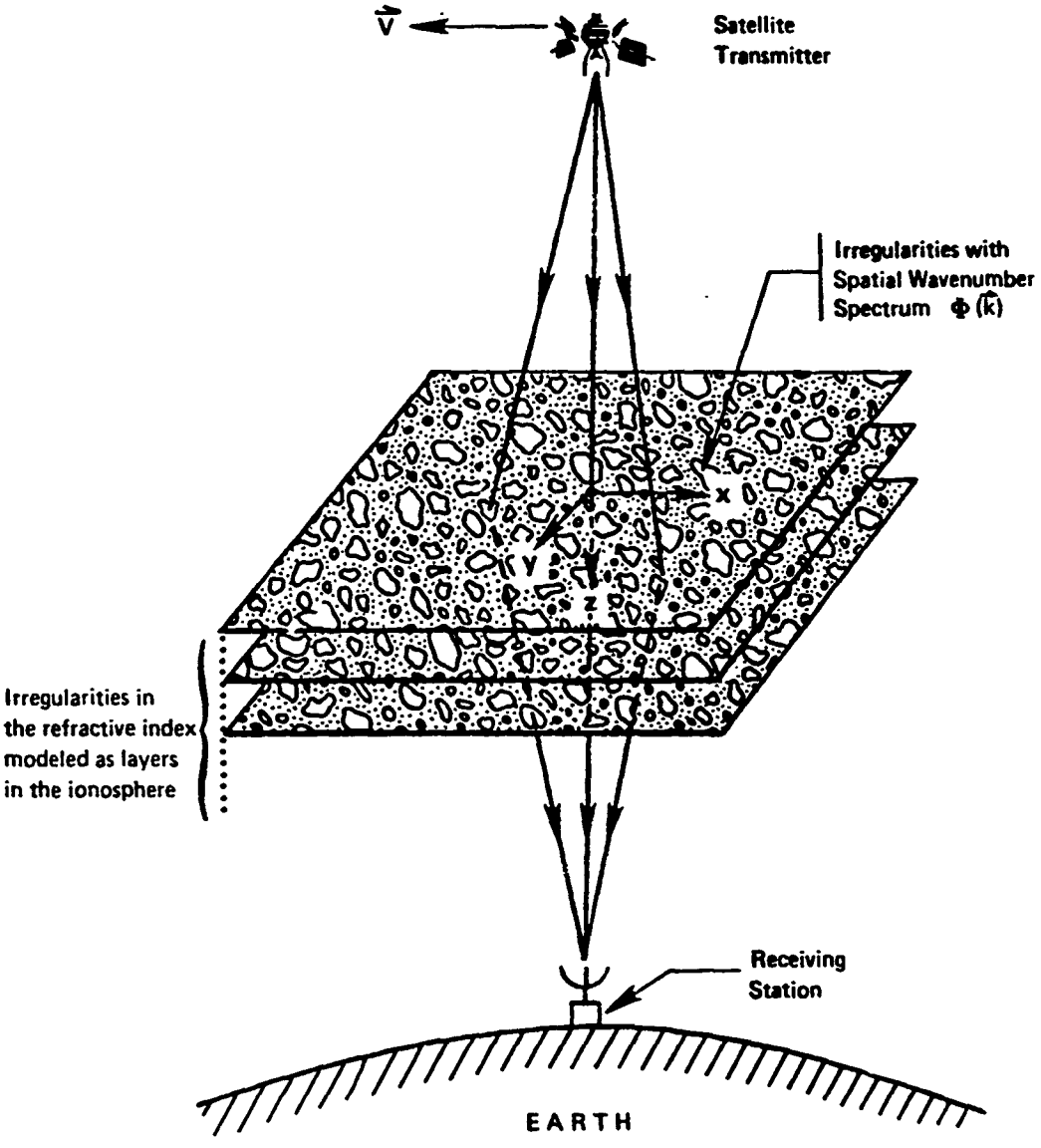

Figure 4 Geometry for a simplified propagation model. As the radio ray path from satellite to Earth moves relative to the refractive index irregularities (modelled as layers in the ionosphere), these irregularities introduce random fluctuations in the received signal's amplitude and phase (see Figure 5) known as signal scintillation.

A useful way to think of the scintillation process, described by Uscinski (1977, Ch. 4), is shown in Fig. 5. Here we visualize the complex electric field $\vec{E}(z)$ observed at some point z along the straight line ray path from transmitter to receiver (see Fig. 4) as being composed of a non-scintillating component $\langle\vec{E}\rangle$ and a scintillating, i.e., randomly fluctuating, component $\vec{E}'$ such that

$$\vec{E}(z) = \langle\vec{E}(z)\rangle + \vec{E}'(z) \quad . \tag{II-1}$$

The average power in the wave field is therefore

$$\langle\vec{E}\vec{E}^*\rangle = \langle\vec{E}\rangle^2 + \langle\vec{E}'\vec{E}'^*\rangle \quad . \tag{II-2}$$

At the top of the scintillating medium, but still in free space, we take z to be zero increasing downward through the medium. At $z = 0$ the power in the wave field in all in the coherent component $\langle\vec{E}\rangle^2$, i.e., $\langle\vec{E}\vec{E}^*\rangle = \langle\vec{E}\rangle^2 = E_o^2$. As z increases $\langle\vec{E}(z)\rangle^2$ decays exponentially:

$$\langle\vec{E}\rangle^2 = E_o^2 \exp(-\beta z) \tag{II-3}$$

where β^{-1} can be thought of as the mean free path for radio photons propagating through a layer of the scintillating (irregular) medium (Uscinski, 1977, ch. 4). After propagating some distance $\lesssim \beta^{-1}$ through the medium $\langle\vec{E}\rangle^2$ has decreased by e^{-1} and some power is now resident in the fluctuating component $\langle\vec{E}'\vec{E}'^*\rangle$ as shown in Fig. 5a. Since the variance σ_ϕ^2 of the phase of $\vec{E}$ is still small ($\sigma_\phi^2 < 1$ radian), the

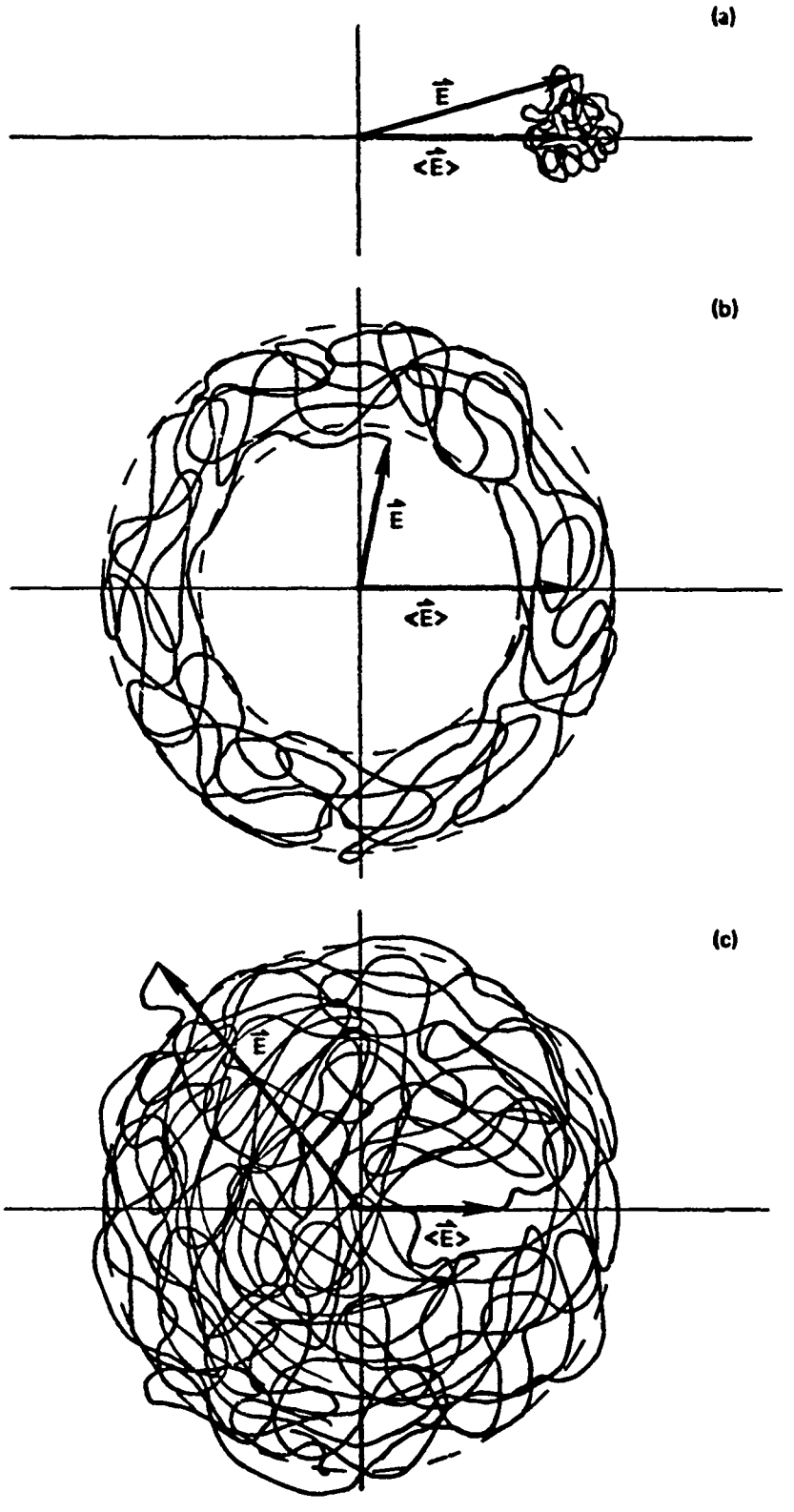

Figure 5 Argand (phasor or complex plane) diagram showing the total electric field $\vec{E}$ being composed of a mean field $\langle\vec{E}\rangle$ along the abscissa (real axis) and a fluctuating component $\vec{E}'$ such that $\vec{E} = \langle\vec{E}\rangle + \vec{E}'$. For weak scatter (a) amplitude fluctuations are small ($|\vec{E}'| << |\langle\vec{E}\rangle|$) and phase fluctuation much less than a radian. In the case of intermediate scatter (b) amplitude fluctuations are still small, but phase fluctuations have become large. For strong scatter (c) both amplitude and phase fluctuations are large ($|\vec{E}'| \sim |\langle\vec{E}\rangle|$); signal statistics approach a Rayleigh distribution for amplitude and uniform for phase.

signal is said to be only weakly scattered. Although we take β to be constant here for simplicity, it could of course be a function of z.

If the thickness of the scintillating medium is $\Delta z \lesssim \beta^{-1}$, then the received signal is weakly scattered as in Fig. 5(a). On the other hand, if propagation continues through the medium for $z > \beta^{-1}$, the phase fluctuations become more severe (eventually approaching a uniform distribution over 2π radians); but with only small amplitude fluctuations, i.e., a stage (b) is reached between (a) and (c) in Fig. 5. Finally for $z >> \beta^{-1}$ [Fig. 5(c)] the $\langle \vec{E} \rangle^2$ component becomes much smaller than the fluctuating component $\langle \vec{E}' \vec{E}'^* \rangle$ and the signal statistics approach a Rayleigh distribution, i.e., the signal amplitude is Rayleigh distributed and the phase is uniformly distributed over 2π (see Papoulis, 1965, for reference). This case is often referred to as saturated scattering or the Rayleigh limit. Since it is a worst case, it can be used as a bound on scintillation effects.

A parameter commonly used to measure the degree of the scattering is the scintillation index S_4^2 where

$$S_4^2 = \frac{\langle I^2 \rangle - \langle I \rangle^2}{\langle I \rangle^2} \qquad \text{(II-4)}$$

and the intensity, $I = \vec{E}\vec{E}^*$. For weak scatter $S_4^2 << 1$, and for strong scatter $S_4^2 \gtrsim 1$.

A variety of methods exists for dealing with wave propagation through a random medium, e.g., some recent work on phase screens by Rino, Vondrak and Hatfield (1975), Rino (1979a & b) and Wittwer (1980a) and on Feynman path integrals by Flatté et al. (1979). Of primary importance in all these methods is the spatial size distribution of the irregularities in refractive index, i.e., the blobs shown in Fig. 4. For weak scatter fluctuations in amplitude $|\vec{E}'|$ and hence in power $\langle \vec{E}' \vec{E}'^{*} \rangle$, only refractive index fluctuations on spatial scales (ℓ) of the order of the Fresnel zone size (in the scintillating medium) and smaller are important. In the case of ionospheric amplitude scintillation for UHF signals ($\lambda \sim 0.5$ m) only size scales of $\ell \lesssim \sqrt{\lambda R} = \sqrt{0.5 \times 3 \times 10^5} \approx 400$ m are important. R is the distance from the receiver to the scattering medium. As scattering becomes strong, larger size scales become significant for amplitude scintillation. In the case of phase scintillation, refractive index fluctuations on size scales larger as well as smaller than the Fresnel zone size are important for both strong and weak scattering. The upper limit on important size scales for phase scintillation is set by the length of time during which phase is observed, relative velocity of the ray path through the scintillating medium and the propagation geometry (Rino, 1979a). Since fluctuations of significant strength exist down to size scales of $\lesssim 10$ m, a range of size scales well over an order of magnitude can be important in determining the scintillation of radio signals propagating through a disturbed ionosphere.

As discussed above, a signal with Rayleigh distributed amplitude and uniformly distributed phase (i.e., saturated scintillation) can be used

as a bounding approximation for signals which are strongly scattered upon passage through a disturbed ionosphere (see Figs. 4 and 5). Fig. 6 shows an example of saturated phase and amplitude scintillation on a UHF signal propagating through a disturbed ionosphere. Communication using such a Rayleigh fading channel is not unique to transionospheric satellite links, but is encountered in communications via HF skywave as well as VHF ionospheric and tropospheric scatter circuits. Because of these many practical applications, Rayleigh-fading channels have been studied extensively (Schwartz, Bennet and Stein, 1966). Such a Rayleigh-fading channel can be described to first order by two parameters τ_o and f_o. The signal decorrelation time τ_o measures the autocorrelation property of the complex electric field signal at the receiving antenna, i.e., τ_o corresponds to the time lag required for this autocorrelation function to drop by a factor e from its value at zero time lag. Thus τ_o gives the time scale over which the $\vec{E}$ vector in Fig. 5 moves along its "ball of string" paths in the Argand diagrams. In Fig. 6 τ_o corresponds to the mean duration of fades at the -3 dB level. The other parameter f_o, called the frequency selective bandwidth, measures the correlation of fading characteristics at two separated frequencies. DNA defines f_o as $1/2\pi\sigma_\tau$ where σ_τ^2 is the variance of the random, time-delay-jitter (excluding jitter associated with the total electron content along the ray path). By this definition f_o is the frequency separation required to reduce the complex signal correlation by a factor 0.697 below its value at zero frequency separation. These parameters are the primary output of computational simulations of radio signal propagation through a nuclear disturbed ionosphere. The spatial distribution and strength of plasma

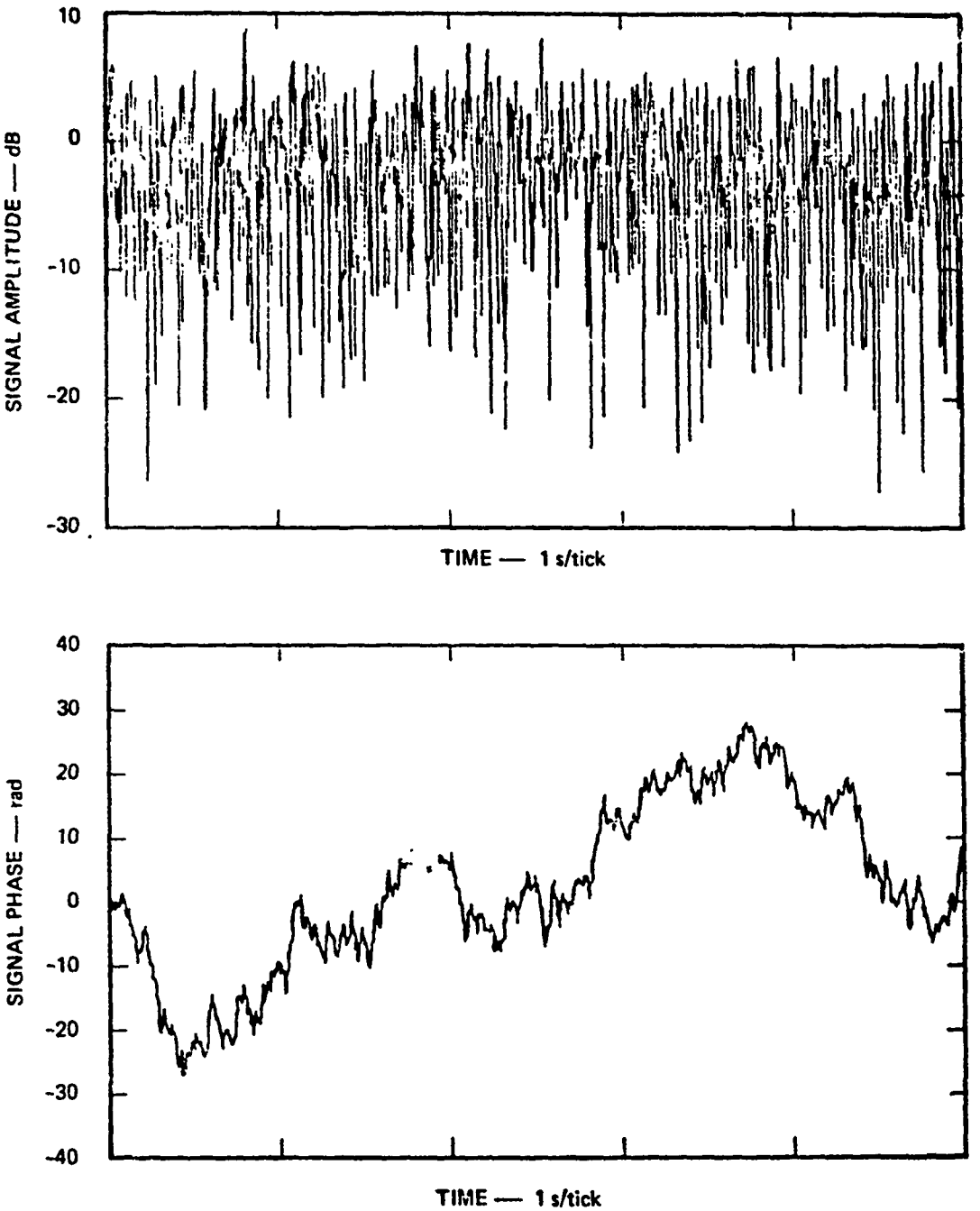

Figure 6 Example of UHF signal amplitude and phase scintillation for strong scatter conditions in a disturbed ionosphere with signal decorrelation time $\tau_0 = 8$ ms. Signal statistics approach the saturated regime in which amplitude is Rayleigh distributed and phase is uniformly distributed. Scintillations can be faster or much slower, depending on link geometry and ray path velocity with respect to the plasma irregularities. After McDaniel (1978).

irregularities, ray path speed with respect to the irregularities, propagation path geometry and operating frequency all influence τ_o and f_o .

A communications channel can be described by

$$R(t) = \int_0^\infty h(t,\tau)\ S\ (t - \tau)\ d\tau \qquad \text{(II-5)}$$

where R is the received signal, S the transmitted signal and h the impulse response of the channel. Aside from signal effects associated with propagation geometry, absorption, integrated electron content along the ray path and angle of arrival variations, $h(t,\tau)$ for the Rayleigh-fading case can be characterized by the two parameters τ_o and f_o . Since for most communications systems scintillation effects parametrized by τ_o and f_o are most important and since knowledge of h enables one to calculate error rates for various communication systems, operating frequencies, modulation schemes, etc., scintillation effects on communications systems can be at least bounded by knowing τ_o and f_o . Further discussion is given by Wittwer (1980a & b).

In Figs. 7 and 8 we show as a function of operating frequency the ranges of τ_o and f_o expected for communications through a nuclear disturbed ionosphere. For reference, FLTSATCOM operates at UHF; Global Positioning System (GPS) at L band; Defense Support Program (DSP) at S band; WESTAR, RADUGA and INTELSAT IV (and V) at C band (4-8 GHz); Defense Satellite Communication System, (DSCS) and INTELSAT V at X band

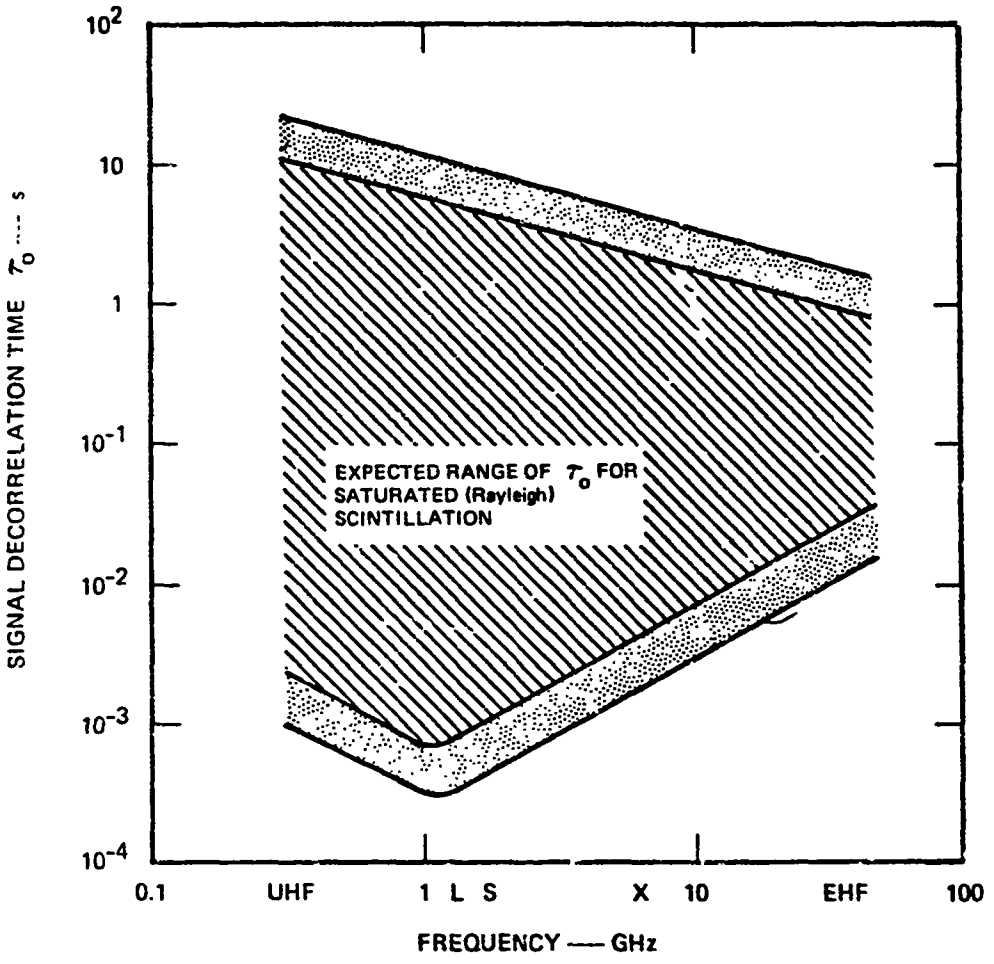

Figure 7 Expected range of signal decorrelation times or fading rates (τ_0) for strong scintillation conditions encountered in a nuclear environment. After McDaniel (1978).

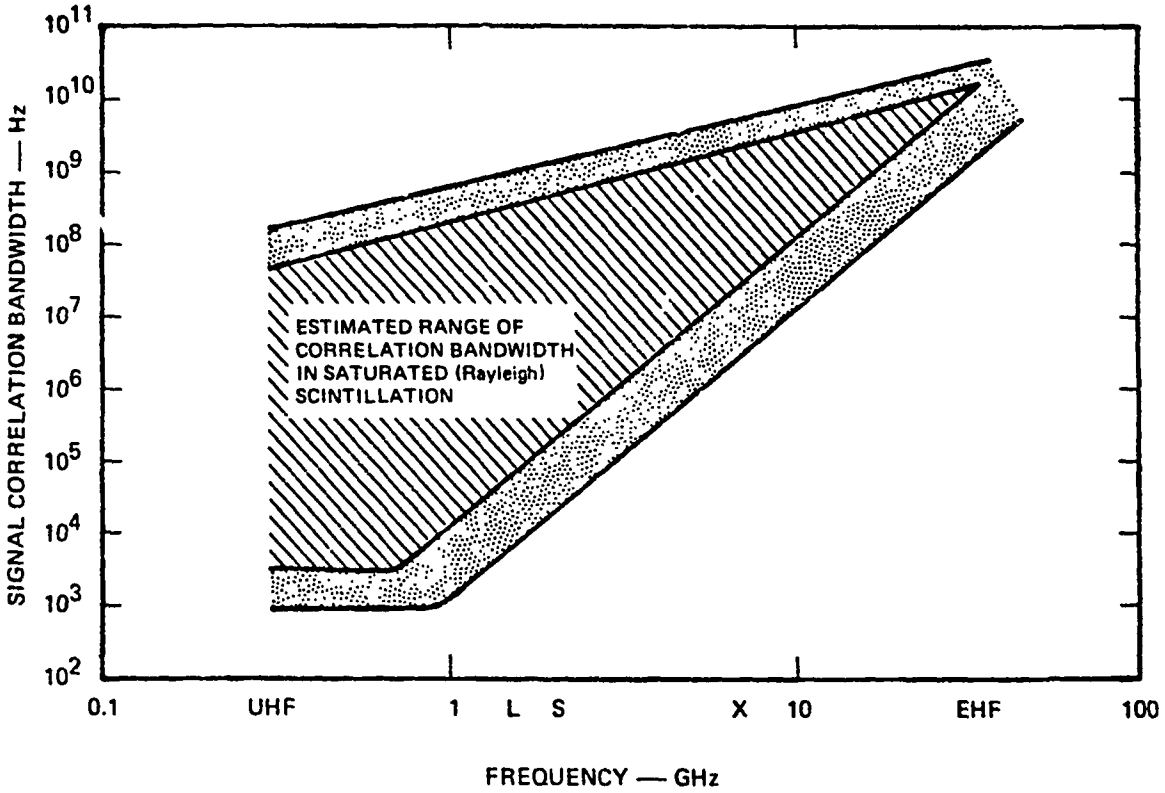

Figure 8 Estimated range of signal correlation (or frequency selective) bandwidths (f_0) for strong scintillation conditions encountered in a nuclear environment. The minimum values represent very severe environments and are less likely to be encountered on a given link. After McDaniel (1978).

(8-12.5 GHz) and the planned Strategic Satellite System (S^3) at EHF. The frequencies corresponding to these various bands are shown in Figs. 7 and 8.

Although various system parameters and modulation schemes determine the detailed structure of error rates in terms of τ_o and f_o, some qualitative feeling for the severity of scintillation effects can be obtained by comparing τ_o and f_o with the time scale T for significant signal variation. T would usually be equivalent to the time required to transmit one bit of information with $(1/T)$ being the information transmission rate or one half the required system bandwidth (except for spread spectrum systems.) Thus for all systems one would expect catastrophic disruption for $\tau_o \lesssim T$ and/or $f_o \lesssim (2/T)$, i.e., for fades lasting on the order of the symbol period or less and for frequency selective bandwidths less than the required system bandwidth. For coherent systems catastrophic degradation occurs for $\tau_o \lesssim 1/B_L$, where B_L is the phase-tracking loop bandwidth, because the system cannot handle the rapid phase changes. For $\tau_o > T$ (or $\tau_o > 1/B_L$ for coherent systems) amplitude scintillation will still cause some degradation. For example, a communication system operating at one megabit data rate at S band could certainly anticipate problems in view of Figs. 7 and 8 if remedial action were not taken. By remedial action we refer to various mitigation techniques discussed, for example, by McDaniel (1978) and Wittwer (1980a). These include frequency shift or differential phase shift keying in place of absolute phase shift keying, high transmitter power (gain margin), large loop bandwidth phase trackers, higher operating frequencies, etc.

To emphasize the importance of scintillation effects we illustrate in Fig. 9 the large area of the United States which would be affected by a high-altitude nuclear explosion similar to that shown in Fig. 1.

To summarize briefly, the parameters τ_o and f_o determine or at least bound error rates for a given communication system, geometry, etc. To find τ_o and f_o we need to know the time history of how the strength of the refractive index irregularities is distributed with respect to their size, call it Φ, for locations $(\vec{r})$ along the ray path between transmitter and receiver. If $\Phi(\vec{r})$ is known with confidence, scintillation effects and techniques to reduce them can be investigated with confidence.

B. Parametrization of Spatial Structure of Plasma Irregularities

Since the wave propagation theory is in reasonably good order, the question of calculating scintillation effects on communications systems hinges on the specification of the scintillating environment, namely $\Phi(\vec{r},t)$. Our particular emphasis lies in the evolution of Φ at "late times" (electrostatic regime), i.e., tens of minutes to hours. Some aspects of the physics of this evolution are considered in Section III below.

Although one could probably construct a deterministic model for the refractive index irregularities shown in Fig. 2, a statistical model makes better sense for two reasons. First, for propagation through a nuclear disturbed ionosphere, waves would have to propagate through a

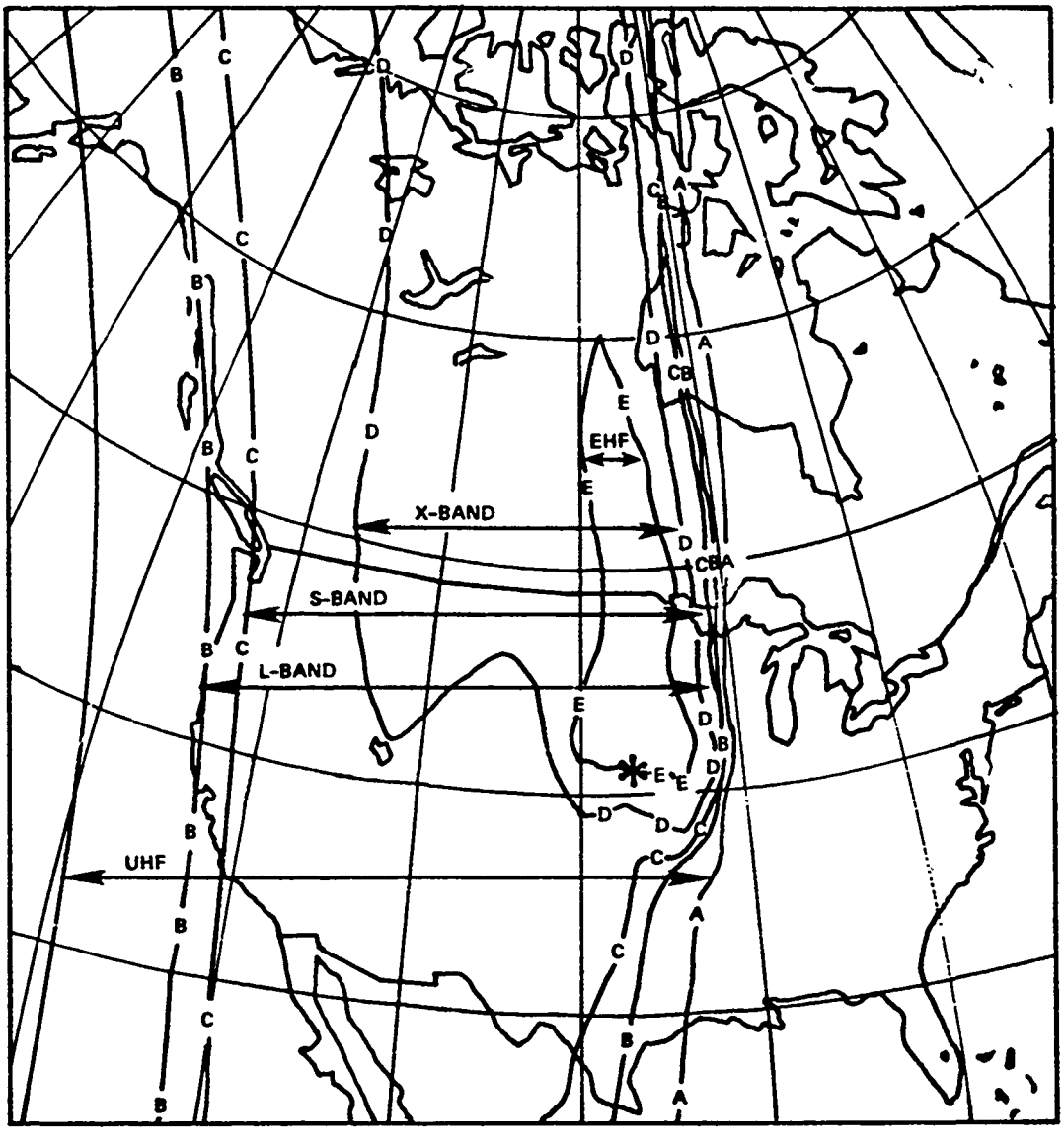

Figure 9 Geographical extent of strong scintillation along links between ground and synchronous satellite terminals one half hour after a high altitude nuclear burst. Note the wide geographic area affected by a single burst and the strong frequency dependence. The extent of EHF strong scintillation is particularly sensitive to uncertainties and may be smaller than shown. After McDaniel (1978).

number of structures such as shown in Fig. 2 and after scattering from about six such structures the resultant wave is indistinguishable from a wave propagating through an analagous environment described statistically. Second, because one would not know just exactly what sort of deterministic structures would exist in a nuclear disturbed ionosphere except in a statistical sense, a statistical model represents "average" conditions.

A convenient way to describe the distribution of the strength of refractive index irregularities with respect to size is to use a spectral density function Φ where the size (δx) of an irregularity is given in terms of a spatial wavenumber $k = 2\pi/\delta x$. As discussed above, refractive index fluctuations δn in the ionosphere arise because of electron density fluctuations δN where for small values of (f_{pe}/f), $\delta n \approx \frac{-80.6\ \delta N}{2f^2}$. From this we see that the Φ for refractive index fluctuations (δn) is simply related to the Φ for electron density (or plasma density in the ionosphere) fluctuations δN. Further, this relation is scaled by the inverse fourth power of the operating frequency f, i.e., $\Phi_n \approx (40.3)^2\ f^{-4}\ \Phi^n$ (mks). Ionospheric plasma irregularities arising from both natural causes and high altitude nuclear explosions are reasonably well fitted by power law $k^{-\alpha}$ curves when described in one-dimensional spatial wavenumber space, i.e., by measurements along some straight line in space. Thus the irregularities can be described by $\Phi(\vec{k};t,\vec{r})$ where Φ is the spectral density function for refractive index fluctuations, $\vec{k}$ is the three dimensional wave number vector, t is time, $\vec{r}$ gives location along the ray path and the three-dimensional spectral index (p) is

related to the one-dimensional spectral index (α) by $p = \alpha + 2$ for isotropic fluctuations (Fejer and Kelley, 1980; Rino, 1978). Since the power law region is usually bounded by a lower limit $\vec{k}_o$ below which the wavenumber spectrum is relatively constant with respect to $\vec{k}$ and an upper limit $\vec{k}_i$ above which the spectrum decreases rapidly with increasing $\vec{k}$, it is reasonable to describe such plasma irregularities by analogy with fluid turbulence although the physical processes involved are different.

For three-dimensional, isotropic turbulence we can generalize the von Karman spectrum (Ishimaru, 1978, ch. 16) to arbitrary spectral index and write

$$\Phi(k;t,\vec{r}) = C^2(k^2 + k_o^2)^{-[(\alpha + 2)/2]}\exp(-k^2/k_i^2) \qquad \text{(II-6)}$$

where C is a "structure constant" describing the strength of the turbulence; $k_o = 1/L_o$ and L_o is the outer scale size; $k_i = 1/L_i$ and L_i is the inner scale size; and α is the one-dimensional spectral index. In terms of turbulent eddies L_o is the size of the largest eddy and L_i the size of the smallest. In Kolomogorov fluid turbulence $\alpha = 5/3$. For plasma striations such as those of Fig. 2 which are dominated by sharp gradients, $\alpha \sim 2$. A sketch of (II-6) is given in Fig. 10.

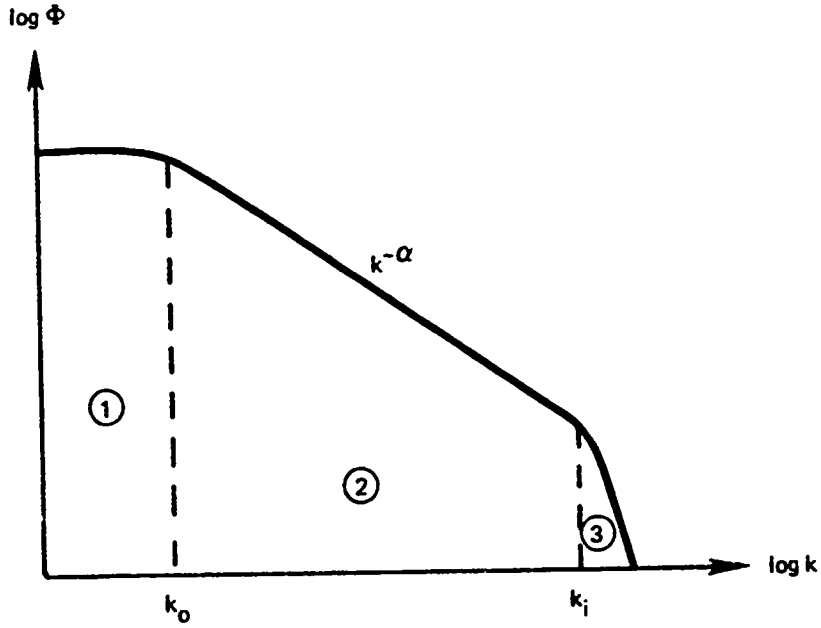

Figure 10 Sketch of the turbulence model given by eg. (II-6). The outer scale L_o corresponds to $k_o = 1/L_o$ while the inner scale L_i corresponds to $k_i = 1/L_i$. For Kolmogorov fluid turbulence the regions labeled 1, 2 and 3 are referred to as the input range, the inertial subrange and the dissipation range respectively and $\alpha = 5/3$. For the plasma irregularities considered here different physical processes are at work and $\alpha \sim 2$.

Due to the geomagnetic field in the ionosphere, irregularities are not isotropic as one can easily see in Fig. 2. Hence one must generalize Eq. (II-6) to include scale lengths along three directions as done by Wittwer (1980a):

$$\Phi(\vec{k}) = \frac{8\pi^{3/2}\langle\Delta n^2\rangle L_x L_y L_z [\Gamma(0.5\alpha + 1)\Gamma(0.5\alpha - 0.5)]}{\left(1 + L_x^2 k_x^2 + L_y^2 k_y^2 + L_z^2 k_z^2\right)^{(\alpha + 2)/2}} \qquad \text{(II-7)}$$

where $\langle\Delta n^2\rangle$ is the total variance of the refractive index fluctuations; L_x, L_y, and L_z are the outer scales sizes in the x, y, and z directions, Γ denotes the Gamma function and α the one-dimensional spectral index. Although no inner scale is included in Eq. (II-7) one could be included as in Eq. II-6 by using a multiplicative exponential term.

Once the spatial wavenumber spectrum of refractive index irregularities is specified as in equations II-6 and II-7, the spatial and temporal characteristics of signal amplitude (or intensity) and phase fluctuations can be calculated. That is, one can calculate the signal decorrelation time τ_o and frequency selective bandwidth f_o as well as many other signal statistics, for example, the temporal frequency spectra of signal amplitude and phase fluctuations. For phase fluctuation statistics the detrend time or length of observations in time, whichever is shorter, is also important (Rino, 1979a).

It is instructive to consider the simple case of Fig. 11 where a plane wave propagates through a statistically homogeneous and isotropic medium. The irregular medium and ray path are moving relative to each other with a velocity V_t which is transverse to the ray path. In this simple case of weak scattering the temporal frequency spectra of amplitude $P_A(\omega)$ or phase $P_\phi(\omega)$ fluctuations can be written as integrals of the wavenumber spectrum of refractive index fluctuations $\Phi(k)$ weighted by the appropriate filter function. From Ishimaru (1977, ch. 19)

$$P_{A,\phi}(\omega) = \frac{8\pi^2 \langle n \rangle^2 \omega^2 L}{c^2 V_t} \int_0^\infty f_{A,\phi}(k) \Phi(k) dk' \qquad \text{(II-8)}$$

where $\langle n \rangle$ is the average refractive index, ω the wave frequency, L the length of the ray path (the scintillating medium covers the length L of the ray path), c the velocity of light, V_t the velocity of the ray path with respect to the medium and $k = \left[k'^2 + \left(\omega^2/V_t^2\right)\right]^{1/2}$. The filter functions f_A and f_ϕ for amplitude and phase are illustrated in Fig. 12.

The important feature of the filter functions is that for weak amplitude scintillation the wavenumber spectrum of irregularities is effectively high-pass filtered, i.e., the influence of Φ at $k < \left(\sqrt{2}\pi/\sqrt{\lambda L}\right)$ is restricted. Put another way, only refractive index fluctuations at scale sizes less than the Fresnel zone size $\left(\sim \sqrt{\lambda L}\right)$ are effective in producing signal amplitude fluctuations for the weak

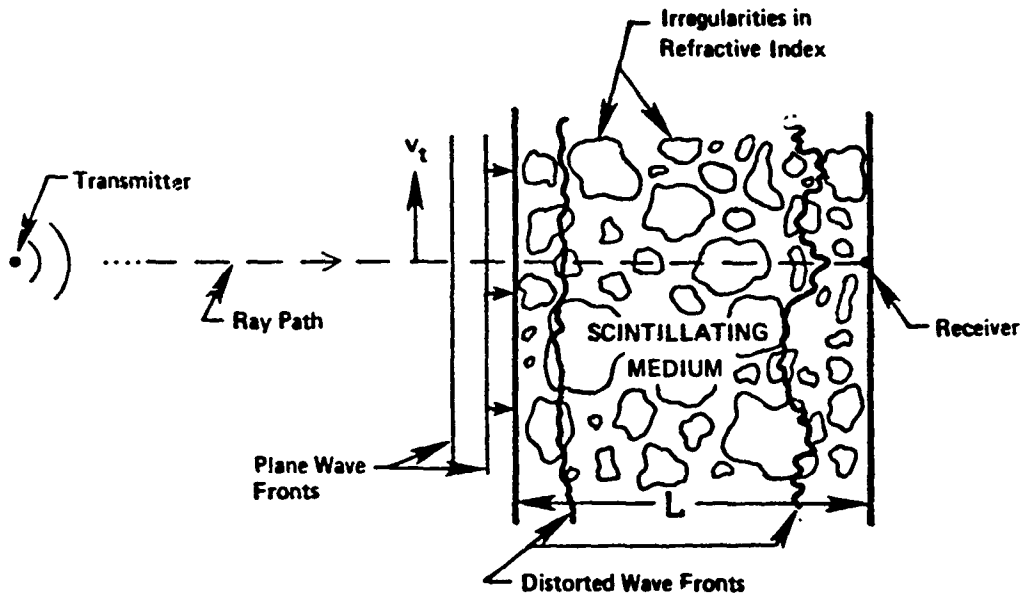

Figure 11 Simple example of plane wave propagating through a statistically homogeneous and isotropic scintillating medium. The ray path (and hence transmitter and receiver) move with a transverse velocity v_t relative to the medium.

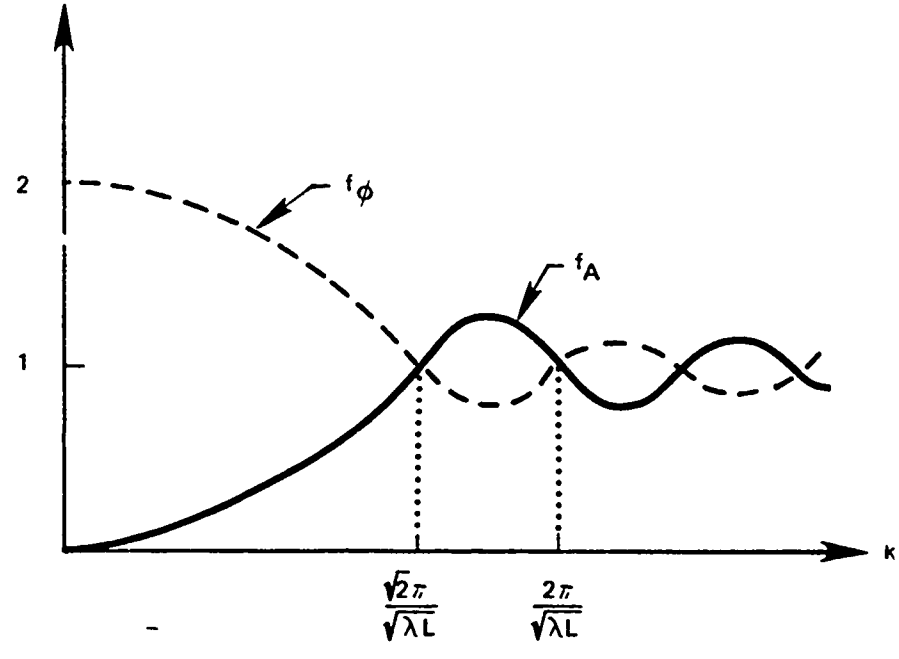

Figure 12 General shapes of weak scatter weighting or filter functions f_A and f_ϕ for signal amplitude and phase respectively. Note that in performing the integral of eq. II-8 the functions f and Φ are evaluated at k such that $k^2 = k'^2 + (\omega^2/V_t^2)$ where k' is the variable of integration. Figure taken from Ishimaru (1977, ch. 17).

scattering case. For strong scatter, size scales larger than Fresnel zone size become involved in amplitude scintillation. On the other hand all scale sizes potentially influence signal phase fluctuations in either weak or strong scatter. However, Rino (1979a) has pointed out that the largest scale sizes which can influence phase fluctuations are limited by the detrend time or total observation time, whichever is shorter. The point we make here is that the wave-number spectrum of refractive index fluctuations $\Phi(k)$ along with various known geometrical and radio system parameters are the essential ingredients used in calculating the signal statistics one would expect upon propagation through an ionosphere disturbed by a high altitude nuclear explosion (or by natural ionospheric disturbances, for that matter). Although we have illustrated this point by discussing $P_{A,\phi}(\omega)$, it applies equally well to other signal statistics such as τ_o and f_o, the signal decorrelation time and frequency selective bandwidth. Since the propagation geometry and radio system factors are known and since the radio propagation theory is relatively well understood, the weak link in the calculation turns out to be $\Phi(k)$, the spatial distribution of refractive index irregularities. Hence the bulk of this report focusses on the determination of $\Phi(k)$, the ultimate objective being to accurately model $\Phi(k)$ as a function of time, spatial location and scenario.

C. Sensitivity of Signal Statistics to Plasma Irregularity Structure

Now that we have identified the spatial wavenumber spectrum of refractive index irregularities $\Phi(k)$ as a weak link in our ability to

calculate radio signal propagation through a disturbed ionosphere, it is appropriate to ask how sensitive signal statistics are to errors in our knowledge of $\Phi(k)$, i.e., to errors in the turbulence strength, outer scale L_o and spectral index α. Wittwer (1980c) has calculated signal decorrelation time (τ_o) and frequency selective (i.e., available) bandwidth (f_o) as functions of the spectral index α and outer scale size L_o. These calculations are for a nominal Rayleigh fading case. When L_o is the independent variable, α is held at 2. Both τ_o and f_o can be closely approximated by power law functions of L_o over the range of L_o encountered in the ionosphere, namely $\tau_o \propto [L_o/\ell n(L_o/L_i)]^{0.5}$ or $\tau_o \approx 1.7\ L_o^{+0.42}$ and $f_o \propto L_o/\ell n(L_o/L_i)$ or $f_o \approx 1.3\ L_o^{+0.84}$ for $L_i = 10$ m and $1\ \text{km} \lesssim L_o \lesssim 30$ km where τ_o is in msec, f_o in MHz and L_o in km. Both τ_o and f_o turn out to be strong functions of the spectral index α as illustrated in Fig. 13!

It is clear from these nominal case calculations that signal statistics are indeed sensitive to errors in the parameters characterizing the spatial distribution of refractive index irregularities in the disturbed ionosphere $\Phi(\vec{k})$. The spectral index α has a particularly strong influence for $\alpha \lesssim 2$. The current canonical value for α is 2 for late times. If plasma irregularities were to evolve at late times such that α is substantially below 2, then current projections which take $\alpha = 2$ would be seriously underestimating the signal distortion produced by propagation through a disturbed ionosphere. The evolution of L_o and α with time are discussed in Section III below.

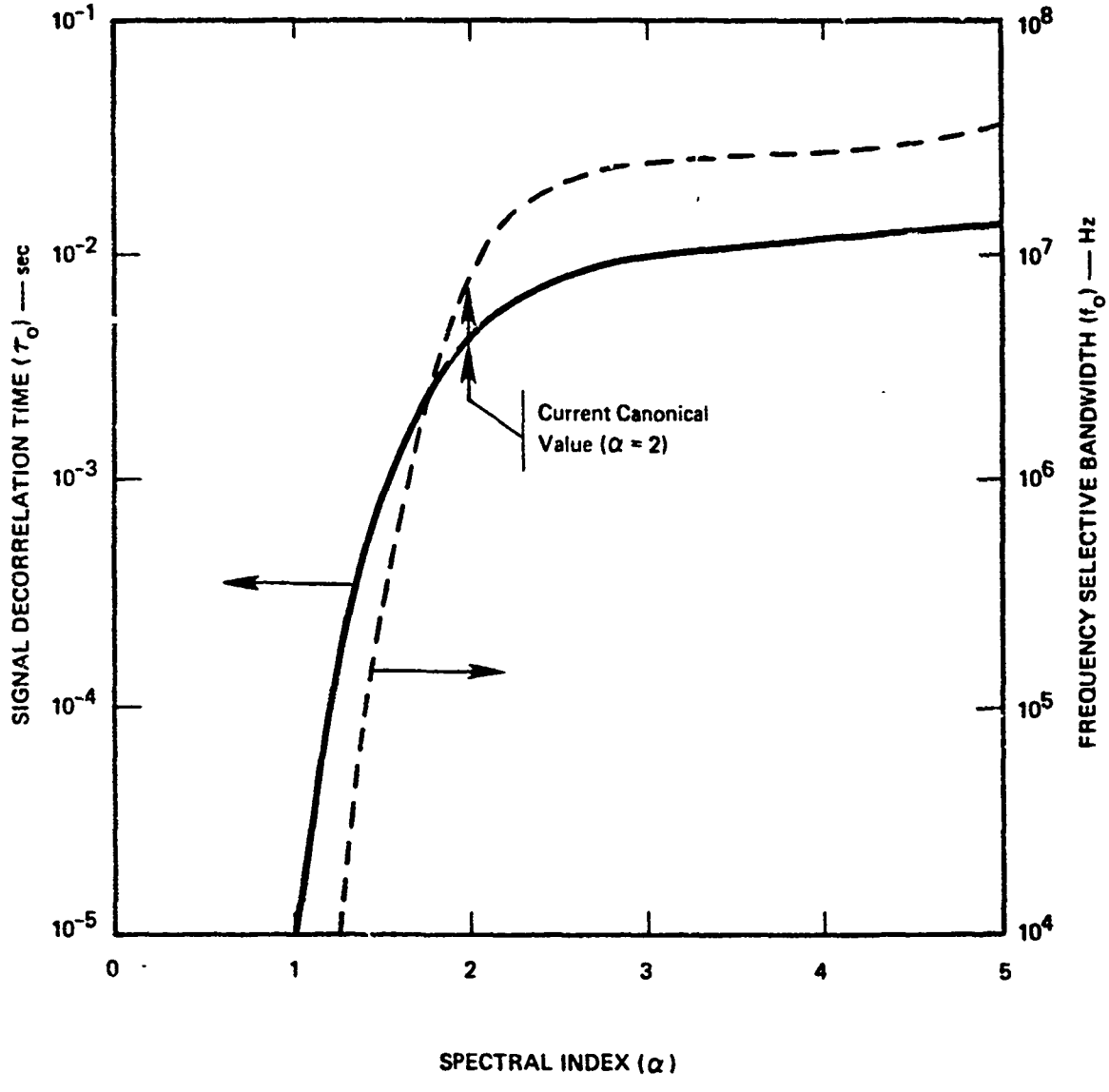

Figure 13 Signal decorrelation time (τ_o, solid curve) and frequency selective bandwidth (f_o, dashed curve) as functions of the spectral index α of a power law model for the wavenumber spectrum $\Phi(k)$ of refractive index fluctuations. After Wittwer (1980c).

D. Effects of Plasma Irregularities on HF Communications via Ionospheric Refraction and Scattering

1. Importance of HF Communications Effects

Although satellite, cable and microwave relay links carry the bulk of military and civil communications, point to point communications by HF (~ 3 to 30 MHz) sky wave (ionospheric refraction) propagation are frequently the best (and often the only) back-up system available for long distances. Soviet forces apparently rely on HF systems for much of their primary, as well as secondary, communications needs. If HF sky wave systems are to provide viable back-up communications for use when satellite links are unavailable, they must naturally function as well as possible when the ionosphere is disturbed by high altitude nuclear explosions. Many nuclear effects on HF communications have been extensively studied, e.g., increased absorption due to increased ionization at relatively low altitudes. Propagation codes which model such large scale effects have existed for over a decade, e.g., NUCOM (Owen and Bailey, 1978; Baumann, Hatfield and Owen, 1973; and Neilson, Lomax and Turner, 1967). However, to the author's knowledge such codes do not include the effects of scattering from small scale ($\lesssim$ 50 km) irregularities. Since such small scale ionospheric irregularities will presumably exist for hours after a high altitude nuclear explosion, it is necessary to assess their impact on existing and planned HF sky wave communications systems which must operate in a nuclear environment. Below we discuss the probable nature of these scattering effects, an approach to dealing with them theoretically and how they might be used in a VHF (35-50 MHz) ionospheric-scatter communications system.

2. The Impact of Scattering by Small-scale Ionospheric Irregularities on HF Sky-Wave Communications

Since ionospheric irregularities caused by high altitude nuclear explosions are in many ways analagous to ionospheric irregularities occurring naturally in equatorial and auroral regions, one can argue by analogy that study of sky wave communications circuits propagating through these natural irregularities should provide information relevant to the nuclear case. The ionospheric irregularities are identified by a condition known as "spread F." Spread F refers to ionospheric conditions in which vertically transmitted HF waves are reflected not by a single well defined ionospheric layer, but by irregularities spread over a range in altitude. Further information on spread F and ionospheric irregularities is given by Davies (1965) and Fejer and Kelley (1980).

HF sky wave propagation paths passing through spread F regions, i.e., regions containing ionospheric irregularities, are not refracted by the ionosphere in a smooth fashion, but rather a number of wavelets originating in various regions arrive at the receiving antenna where their vector sum is sensed by the receiving system. Interference between the arriving wavelets causes signal amplitude and phase to fluctuate in a random manner as with the satellite signals discussed above. In the sky wave case the propagation ray path is relatively stationary and relative movement between ray path and ionospheric irregularities is caused primarily by irregularity movement.

Experience with sky wave communications along paths where spread F is common, i.e., through the auroral zone or through equatorial regions

(particularly transequatorial paths), shows that flutter fading is common with fading rates from a few to perhaps 100 Hz (Davies, 1965, Ch. 5). These fading rates correspond to irregularity motion of ~ 100 ms^{-1}. The frequency selective bandwidth typically ranges from ~ 3 kHz for CW signals to ~ 40 kHz for short pulses (op. cit.). Such flutter fading is disastrous to conventional voice communication.

A potential source of further experimental information would be HF sky wave transmission experiments carried out during the 1962 Fishbowl series of high altitude nuclear tests. Oblique ionospheric sounders between various points in the Pacific were run for periods (~ hours) after high altitude explosions and spread F type conditions were observed, e.g., along the 2500 km path between Canton Is. (2° S, 172° W) and Raratonga Is. (21° S, 159° W) from about 50 minutes after the Kingfish test to 130 minutes and presumably longer (Nielson, 1972).

One should bear in mind here that fading is a relatively common phenomenon on HF sky wave paths and arises from a number of mechanisms in addition to the small-scale irregularities at issue here. Hence the users of HF sky wave communications circuits have always had to cope with signal fading and have adjusted system designs accordingly. On the other hand the flutter fading on auroral and transequatorial paths is very severe relative to that typically experienced at mid-latitudes. In addition fading effects associated with a nuclear disturbed ionosphere are likely to be worse still. In sum it would be prudent to investigate the impact of small-scale ionospheric irregularities on HF sky wave circuits which are to operate in a nuclear environment.

3. A Theoretical Approach to Scattering of HF Signals by Small-Scale Ionospheric Irregularities

The effects of small-scale irregularities on HF wave propagation in the ionosphere were studied by Pitteway (1960a & b) and the results applied to measurements of the movements of ionospheric irregularities, Wright (1968 and following papers) and Pitteway (1971). While extension and application of Pitteway's work could be fruitful, it is probably better to pursue a different course, taking advantage of more recent work by Flatté et al. (1979) and Haugstad (1978). The problem of HF sky wave propagation through an irregular medium has much in common with the transionospheric propagation problem discussed above. The principal difference is that in the HF case the background medium (in which the irregularities exist) is important--it refracts the HF wave back to Earth. In the transionospheric (satellite) case the background medium is not important in this sense since little large-scale refraction occurs. The importance of the background medium is clear in the case of sound transmission in the ocean (SOFAR) channel and hence is included in the work of Flatté et al. (1979). Similarly Haugstad also included background effects in his study of EM wave propagation through planetary atmospheres. It would appear that HF sky wave propagation through a disturbed ionosphere could in some cases be treated by applying the work of Flatté et al. and/or Haugstad to a model of the ionosphere disturbed by a nuclear explosion as discussed briefly in Section I above. The cases where this method would likely fail would be those where the irregularities were very strong, causing large angle scattering. At late times when small angle scattering would presumably dominate, these methods should work.

4. Ionospheric Scatter Communication Using Irregularities Produced by High Altitude Nuclear Explosions

Irregularities in the ionosphere can be used to communicate at 30-50 MHz over ~ 1500 km paths in a manner similar to tropospheric scatter systems at UHF frequencies. In fact an ionospheric scatter communications system was constructed by the Air Force stretching from Massachusetts via Canada, Greenland, Iceland and Britain to Europe (JTAC, 1960). This system depended on relatively large antennas (~ 20 dB gain), high powers (~ tens of kW) and allowed communications bandwidths relatively small (~ 10 kHz) compared to tropospheric scatter systems. Irregularities at D-region altitudes provided the scattering medium. The principal advantages over troposcatter lay in the longer path lengths possible and more simple apparatus required.

The ionospheric irregularities caused by high altitude nuclear explosions would provide an abundance of scatterers which could be used for communications. The point here is that ionospheric scatter communications systems are practical and might provide a viable back-up (with respect to satellites and landline) mode for long distance (~ 1500 km) point to point communications in a nuclear environment. While the data rate of ionospheric scatter channels is only comparable to HF sky wave channels, the higher operating frequencies would reduce absorption along the path due either to natural phenomena or to the nuclear environment. In addition the nuclear explosion related irregularities at F-region altitudes would presumably provide lower loss and longer distance paths than the E-region irregularities used in the natural environment.

In a nuclear disturbed ionosphere adaptive HF-VHF systems might be able to use refractive (as opposed to scatter) paths. This could be a better option than the scatter system suggested above. However, neither option has been explored quantitatively to the author's knowledge.

III. PHYSICS OF PLASMA IRREGULARITY EVOLUTION AT LATE TIMES

A. Important Physical Mechanisms for Late Time Evolution of Striated Plasmas

We are concerned here with plasmas (whether from a high-altitude nuclear explosion, a barium release, or a laboratory simulation) whose size and shape scale lengths are very much larger than a set of scale lengths identified below. Under these circumstances, the plasma clouds evolve, under the influence of a differential electron-ion drift, by spontaneously generating smaller scale lengths. This process--usually idealized as the $\vec{E} \times \vec{B}$ gradient-drift instability (Linson and Workman, 1970; Perkins et al. 1973, and Völk and Haerendel, 1971)--has one important feature in common with inertial-range turbulence: the evolution equations make no reference to any of the small length scales of the problem. We sketch a plausible outcome of the long-term behavior of scale-free evolution in Sec. III B; here we are concerned with the questions of what are the small scale lengths, and how do they affect the evolution from large to small length scales.

In general, scale-free evolution yields a power-law spectrum for plasma irregularities [Eqs. (II-6 & 7) and Sec. III B], and at k-values comparable to the inverse of the smallest scale length the spectrum is cut off (see Fig. 10). It is not known whether the cutoff is exponential, as in Eq. (II-6), but it hardly matters, as long as the cutoff is sharp enough. One does not know a priori exactly how the cutoff in k-space

depends on the inverse scale length, and large ratios can occur (like turbulent Reynolds numbers), so that one must be prepared to study the dynamics associated with a given physical scale length.

In Table I, we list candidate scale lengths for the three types of plasma clouds of interest to us at times well after cloud formation. These length scales are found by simple dynamical arguments, e.g., finding a damping term which just balances the linear $\hat{E} \times \hat{B}$ gradient-drift growth rate. We comment briefly on the effects listed in the Table.

Electron Diffusion. To our knowledge, this is the only physical scale length whose effects are claimed to be observed in large-scale simulations (McDonald et al. 1978). Roughly speaking, the electron diffusion coefficient D_e is given by

$$D_e = \frac{\nu_e}{\Omega_e^2} \frac{(T_e+T_i)}{m_e} \qquad \text{(III-1)}$$

where ν is a collision frequency, Ω a gyrofrequency, T a temperature (in energy units), and e, i refer to electrons and ions. To find the scale length equate $k_\perp^2 D_e$ to the linear growth rate $\gamma = k_\perp U$ ($U = cE_o/B$, the convective drift velocity). It is easy to superimpose diffusion dynamics on the scale-free equations, because neither kinetic effects nor three-dimensional geometries need be considered, and presumably this is the reason why electron diffusion is the only process included in the large computer simulations. This is an unfortunate state of affairs, because electron diffusion is the smallest scale length listed in the Table and one

TABLE I

Physical Scale Lengths for Striating Plasma Clouds:
High-Altitude Nuclear, Ionospheric Barium Release, and Laboratory Simulation

Physical Process	High-Altitude Nuclear	Ionospheric Barium Release	Laboratory Simulation
Typical Cloud Size L	100-1000 km	1-10 km	1 m
Electron Diffusion	1-10 cm	1-10 cm	<< 1 mm
Ion Diffusion - Parallel Resistivity: Multi-level Clouds	?	~ 100 m	<< 1 mm
Ion Inertia: Vortices, Convective Cells, Low-Frequency Drift Modes	Ion Larmor Radius $R_{Li} = \bar{v}_i \Omega_i^{-1}$ ~ 1-10 m	~ 10 m	~ 1 mm
Higher-Frequency Modes	Variable - Ranging from R_{Li} to R_{Le}	same	same

expects important phenomena at the larger scale sizes listed there. [Inner scale lengths, which are substantially smaller than the Fresnel zone size of ~ 400 m are not likely to be important so far as radio communication systems are concerned.]

Ion Diffusion. The analog of (III-1) for ions yields a diffusion coefficient (and scale length) about ten times as large, but it is inappropriate to invoke this length scale for a two-dimensional problem. The well-known reason is that ions cannot diffuse any faster than the electrons can move across field lines; that is, normally ion diffusion is exactly cancelled by the effect of the polarization potential in the cloud. However, if the plasma cloud is immersed in a background (e.g., ionospheric) plasma of sufficiently high conductivity, electrons can in effect move across field lines by short-circuiting through the background plasma (Volk and Haerendel, 1971, and Francis and Perkins, 1975). This has been described in detail by Francis and Perkins who show that if the height-integrated background Pedersen conductivity Σ_b is large enough, ion diffusion is allowed but at a rate reduced by the factor $\Sigma_b(\Sigma_b + \Sigma_c)^{-1}$ (Σ_c is the plasma cloud integrated conductivity). On the other hand, these authors show that a relatively compressible (collisional) background may actually enhance striation growth, rather than lead to diffusive damping. For nuclear disturbances of the ionosphere Σ_c is usually much larger than Σ_b with Σ_c becoming relatively smaller at late times.

Perkins, Zabusky, and Doles (1973) have described another somewhat similar mechanism involving parallel resistivity: the electrostatic potential is not constant along a magnetic field line. In this case, one loses the constraint that all electrons on a given field line have the same $\vec{E} \times \vec{B}$ drift, and limited transverse ion diffusion can occur. The ion diffusion scale length for barium clouds given in Table I is based on the discussion in Perkins et al. (1973). We do not give an ion-diffusion length for the nuclear or laboratory cloud in the Table, because of many uncertainties in the properties of the background plasmas which determine whether ion diffusion is important or not.

The important fact about ion diffusion is that it is governed by three-dimensional effects, which clearly complicate large-scale computer simulations. There have been some attempts to mimic three-dimensional effects by doing two-level simulations [a uniform background cloud below a uniform plasma cloud, (Scannapieco et al. 1976)], but we are not aware of any in which ion diffusive damping could have been seen.

Ion Inertia Effects. Often one is concerned only with cases where Ω_i is the largest frequency in the problem; in particular, $\Omega_i \gg k_\perp \bar{v}_i$, where $\bar{v}_i$ is a typical ion velocity. Linear ion-inertia effects are easily accounted for (Linson and Workman, 1970, and Ossakow et al. 1978), but non-linear effects which might affect the evolution of situations whose size is comparable to the Larmor radius $R_L = \bar{v}_i \Omega_i^{-1}$ have not been considered (as far as we know) for the striation problem, although the general physical picture has been appreciated for very similar spread-F

phenomena (see the review of Fejer and Kelley, 1980; also Costa and Kelley, 1978a & b).

A particularly important effect is the coupling of the gradient $\vec{E} \times \vec{B}$ drift instability to drift waves. The scale frequency for drift waves is ω^* :

$$\omega^* = \frac{2k_\perp T_i}{m_i \Omega_i d} \qquad \text{(III-2)}$$

where d is a typical cloud gradient scale length, and $k_\perp R_L \simeq 1$ for the fastest growing modes (if the drift wave is unstable). The drift-wave frequency is comparable to the gradient-$\vec{E} \times \vec{B}$ growth rate $\gamma \simeq Ud^{-1}$ $(U = cE_o B^{-1})$ when the average ion velocity is comparable to U, a not untypical condition for the plasma clouds of interest. In order that the usual linear electrostatic drift-wave theory apply, for which $\omega^* < \Omega_i$, one should have $R_L < d$, but it will be necessary to consider the evolution of gradient scales all the way down to the Larmor radius in a complete theory.

In the absence of exotic ion distributions in velocity space, drift-wave instability is controlled through a <u>three-dimensional</u> effect: a finite $k_{||}$ such that $k_{||} \bar{v}_i \ll \omega^* < k_{||} \bar{v}_e$. This means that the cloud must be no longer (along the field) than about $d \bar{v}_e \bar{v}_i^{-1} \gg d$, a condition which may or may not be satisfied.

It is not particularly important whether these modes are stable or unstable. Unstable modes will eventually be damped, by a variety of mechanisms: ion diffusion (remember, $k_{||} \neq 0$) , or interesting non-linear interactions like coupling to convective cells (Okuda and Dawson, 1973) which is a kind of enhanced diffusion, or coupling to what Dupree (1978) calls clumps (of particles in a BGK-like mode). All of these effects can only be treated adequately by taking into account some features of kinetic theory, which raises new problems for computer simulations. (These problems are sufficiently important and specialized that we have devoted another subsection to them.) But it may very well be possible to model most of the interesting drift-wave effects in a way which is amenable to computer codes now in use (2-d electrostatic). We have in mind a development analogous to the quasi-three-dimensional treatment of Hasegawa and Mima (1978), who take into account the parallel motion of electrons along the magnetic field, yet derive completely two-dimensional non-linear electrostatic equations which describe important features of drift-wave and convective-cell turbulence.

We believe that the phenomena described here under the heading of ion inertia may well be dominant in setting the inner scale length where the gradient-associated free energy of the $\underset{\sim}{E} \times \underset{\sim}{B}$ gradient drift instability is dissipated.

Higher-Frequency Unstable Modes. There is a very considerable literature on such modes as applied to F-region irregularities and barium clouds (Fejer and Kelley, 1980; Huba et al. 1978; Huba and Ossakow, 1979,

and Simons et al. 1980). We will not go into details; the modes invoked are (besides the drift waves discussed above) the electron or ion-cyclotron-drift, lower-hybrid drift, and drift-loss-cone. Frequencies are comparable to Ω_i, and wave lengths run from the ion Larmor radius to the electron Larmor radius. The theory is fully kinetic, thus not amenable (without drastic simplification) to the usual electrostatic fluid simulation codes. (It should be noted that some of these modes are fully two-dimensional, and unstable when $k_{||} \equiv 0$.) Whatever effects these modes have can be accounted for in particle-kinetic simulations, although even these simulations will be difficult for electron-driven modes.

The Los Alamos group (Simonds et al. 1980) has interpreted the prompt striations observed in the barium shaped-charge cloud Buaro as due to a drift-loss-cone instability. These authors have suggested to us in briefings that very early-time spatial structures of size $\lesssim R_{Li}$, spread through the initial cloud, are important in determining the way the late-time gradient-$\vec{E} \times \vec{B}$ drift instability evolves. However, kinetic instabilities such as considered by the Los Alamos group saturate at a modest level ($\delta n/n$ a few percent), and it is hard to see how these are involved in the 100% spatial modulations actually observed in barium clouds.

B. The Problem of Large Dynamic Range and Fractalization

We have already said in Sec. I that the plasma physics of a high-altitude nuclear cloud (or, to a lesser extent, that of a barium cloud) covers an enormous range of spatial scales at late times (~ hours

after cloud formation). This range is so large (perhaps up to 10^6) that conventional approaches to computer simulation, or even the largest laboratory plasma devices (see Sec. IV), cannot begin to cover it. Just how large the dynamical range is depends on what one believes governs the physics at short distances (at the inner scale); Fig. 14 shows schematically the late-time divergence of the outer and inner scales of a nuclear plasma cloud for two candidate inner scales: the ion Larmon radius R_L and the electron diffusion length (gotten by equating $k^2 \left(\frac{T}{m_e}\right)\left(\frac{\nu_e}{\Omega_e}\right)^2$ to the gradient-drift growth rate $k_\perp U$). Also shown is an estimate of a computer's dynamical range, based on a 100 x 100 spatial mesh and assuming that 3 mesh points are needed to model the smallest spatial features.

There are other, larger candidates for an inner scale (discussed above), and a barium cloud might only reach an outer scale of 10 km, instead of 1000 km for a nuclear cloud, so there are circumstances when the dynamical range of spatial scales for an ionospheric barium cloud may be accessible to straightforward computer simulation or even laboratory analog experiments. But it is clearly of interest to study, in a semi-analytical way, the problems raised by a virtually infinite dynamic range. In fact, it is common in the computer simulations to make the range actually infinite by throwing out of the equations of motion all terms which refer to a fundamental length scale. Since the resulting scale-free equations--termed by us the canonical equations--have only a few specialized analytic solutions, there has been little progress in analysis of the full non-linear problem.

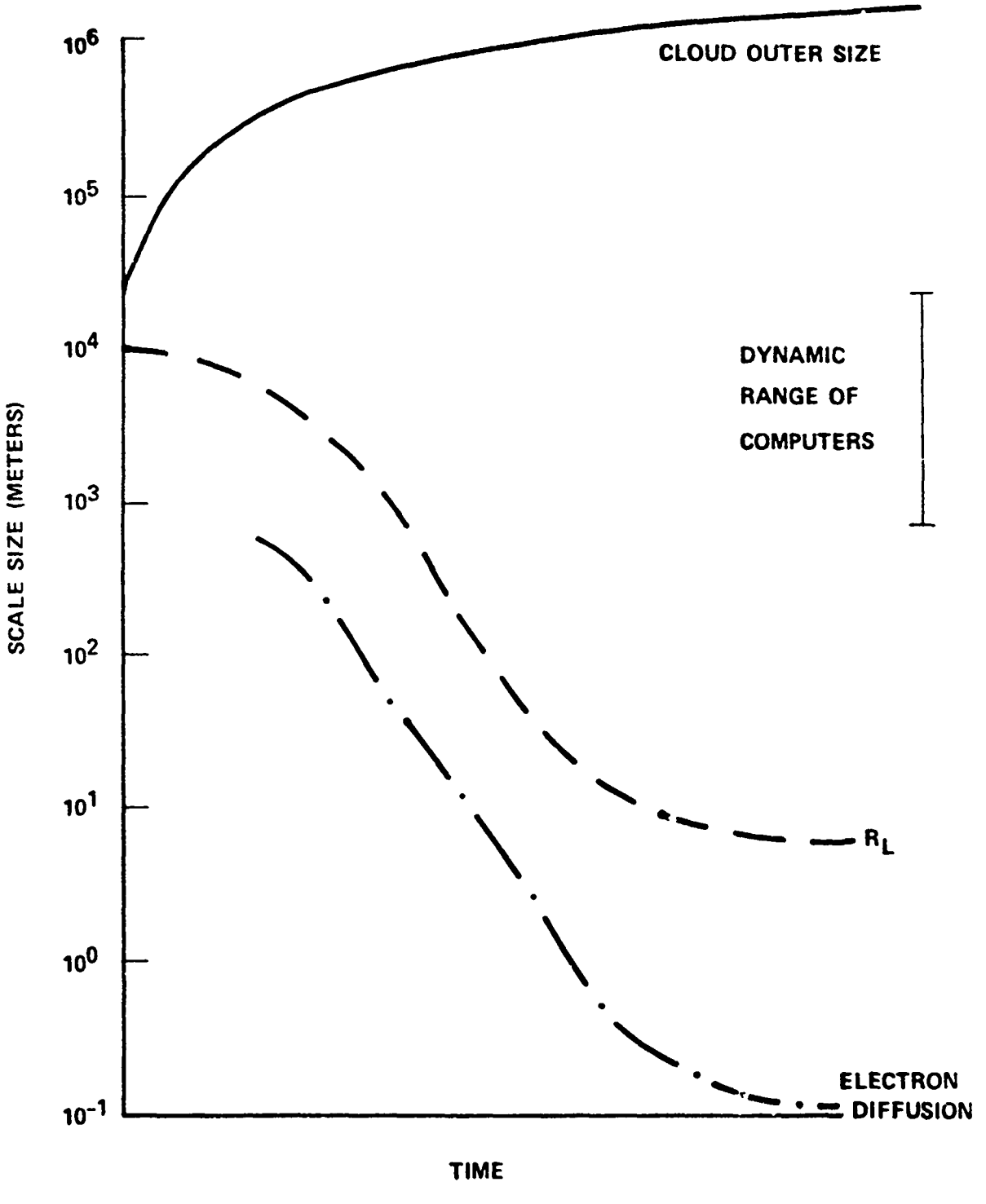

FIGURE 14 Schematized range of scale sizes for striating plasma clouds.

The last sentence is (or was, until recently) true of many physical problems in quantum field theory, hydrodynamical turbulence, second-order phase transitions, etc. The common feature is an enormous dynamical range; the common method of attack is to exploit the self-similarity of the scale-free equations. (That is, the contours in Figs. 15 and 16 are all made of figures of the same shape, but sizes which get smaller as the fractal evolves. A fractal, discussed more fully below, is a continuous but non-differentiable curve of infinite length.)

We have carried out a preliminary investigation of the self-similarity properties of the canonical equations, with the result that a plasma cloud subject to these equations fractalizes, that is, isodensity contours (always enclosing the same area) bifurcate to infinitely small spatial scales and become of infinite length in a finite time. The term fractal was invented by B. Mandelbrot (1977) to describe a class of continuous plane contours which have infinite length and no derivatives; examples of (almost) fractals are shown in Figs. 15 and 16 (taken from Mandelbrot, 1977). Given some plausible assumptions listed below, it turns out that the power spectrum of a plasma cloud whose outer contour is a fractal is reasonably well described by the Rufenach power spectrum (see equation (II-7)

$$P(k) = \frac{\text{Const.}}{\left(1 + k^2 L^2\right)^{\alpha/2}} \qquad \text{(III-3)}$$

with L (the outer scale) of the order of the overall cloud size and with α significantly less than 2. The consequences of $\alpha < 2$ have already been pointed out (see Section II. C).

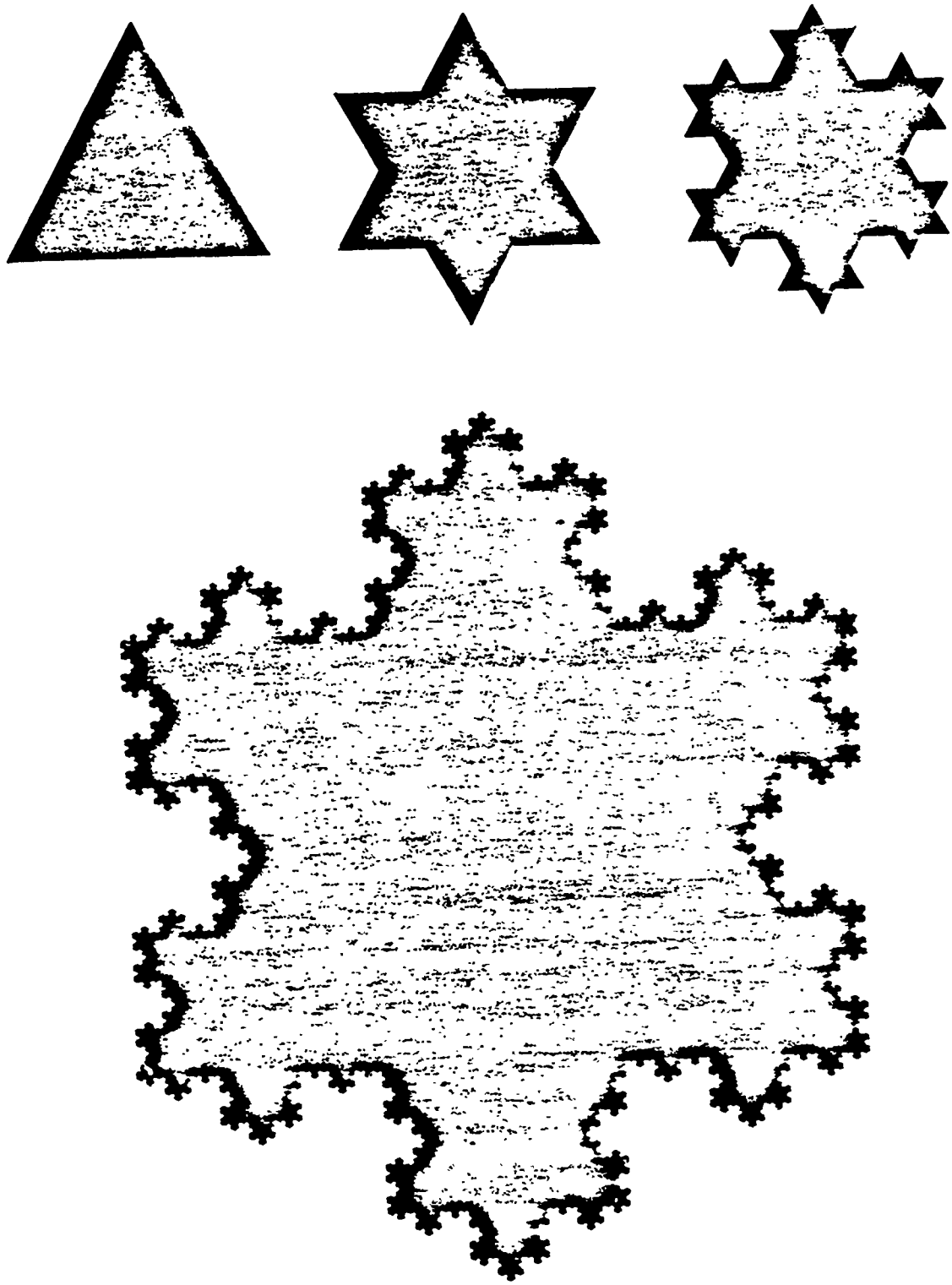

Figure 15 Evolution of a fractal (in this case, the Koch triadic).
Taken from Mandelbrot (1977).

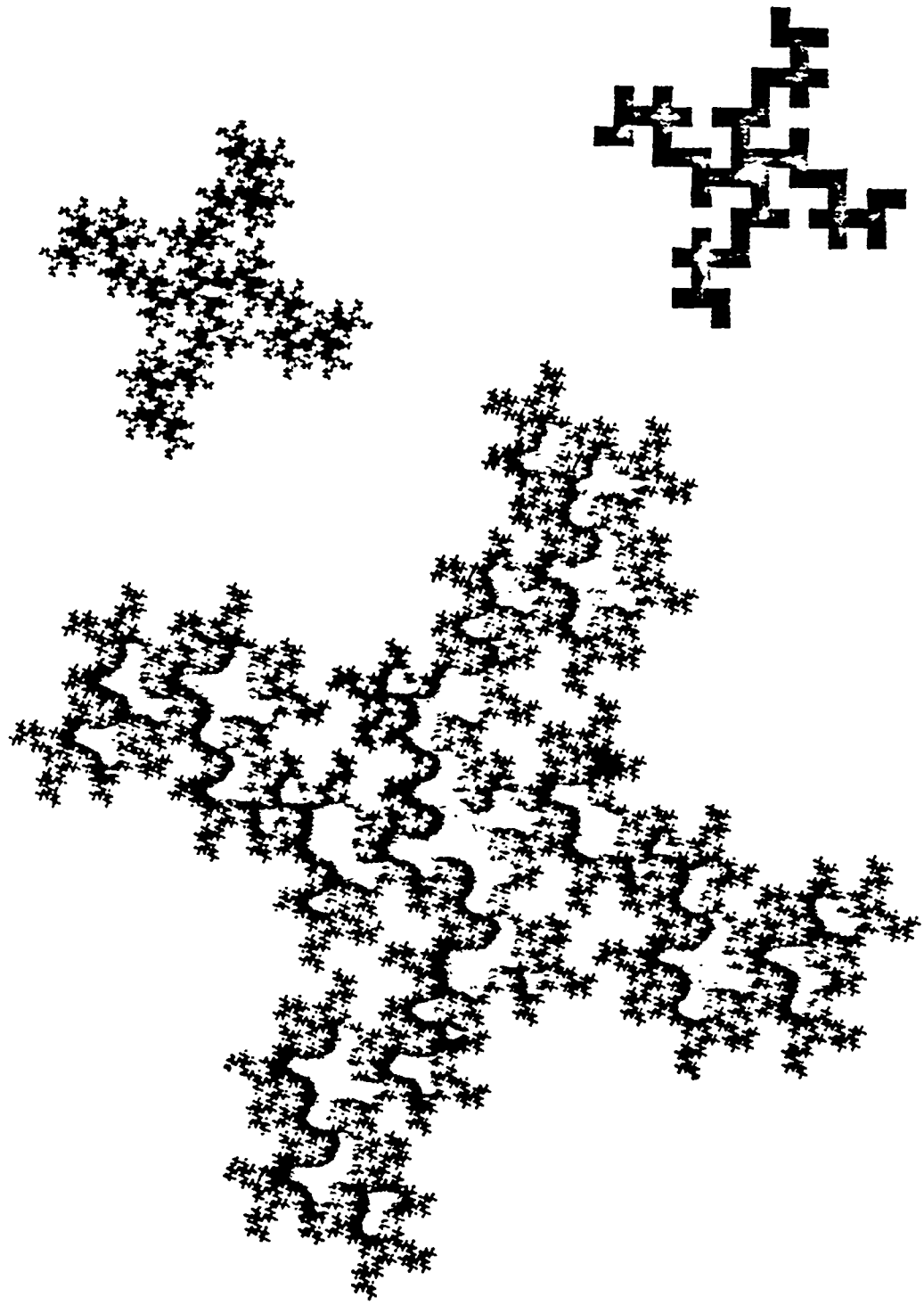

Figure 16 Evolution of another fractal (taken from Mandelbrot).

For a geometric fractal like those in Figs. 15 and 16, α is a unique number, but for actual plasma clouds there will be an ensemble of α's clustered around a mean value. It is an important conclusion of our investigation that these α's --which refer to a fully-fractalized cloud-- can be determined from computer simulations that have a dynamic range no greater than now available (≈ 30) .

No physical cloud can ever fully fractalize, because at a sufficiently small spatial scale there is physics not included in the canonical equations (e.g., electron diffusion), which destroys the self-similar evolution of the cloud, as we have discussed in Sec. III A. But it is worth knowing that an idealized scale-free cloud can fractalize in a finite time, of the order of twice the time it takes for the first generation of striations to appear. This is because each new striation generation evolves on a time scale faster than that of the previous generation, in proportion to the size ratio between the old and the new generation.

1. The Canonical Equations and Fractalization

These are (e.g., Perkins et al. 1973; McDonald et al. 1978).

$$\frac{\partial n}{\partial t} + \frac{c}{B}(\hat{z}\times\vec{\nabla}\phi)\cdot\vec{\nabla}n = 0 \qquad \text{(III-4)}$$

$$\vec{\nabla}\cdot(n\vec{\nabla}\phi) = \vec{E}_0\cdot\vec{\nabla}n \qquad \text{(III-5)}$$

Here the magnetic field B points in the z direction, ϕ is an effective electrostatic potential induced by the plasma cloud of (ion or electron) density n, and $\vec{E}_0$ is an externally-imposed electric field in the xy plane. The cloud potential ϕ vanishes at spatial infinity; $\vec{E}_0$ summarizes the effects of ion-neutral drag and of gravity. The fields n, ϕ are independent of z.

Long ago Dungey (1958) proved that these equations have no equilibrium solutions (aside from some special cases which will not concern us here). Again, aside from some special cases, there are no known analytic time-dependent solutions, but it is well-understood that dense parts of the cloud tend to short out the background electric field $\vec{E}_0$ and thus move more slowly than the background drift velocity $U_0 = cE_0B^{-1}$. As a result, the back side of the cloud tends to steepen, then to split into fingers. The NRL simulations show that when the first few backside fingers have formed, the edges of the fingers have density gradients perhaps an order of magnitude steeper than the interior of the fingers and of the rest of the cloud; these gradients become larger as time goes on. In view of this, it has been suggested that the power spectrum is dominated by the steep edges (Zabusky and Block, 1978, and Costa and Kelley, 1978).

For a steep-edged plasma cloud of well-behaved shape in the xy planes and typical dimension L, this means $P(k^2) \sim k^{-2}$ when $kL >> 1$ (but k^{-1} is greater than the edge thickness). But there is no reason to suppose that the cloud does have a well-behaved figure, simply because

there is no intrinsic scale length. A roughly circular cloud of dimension L will develop fingers of dimension (1/2-1/3) L (say) in a time scaled by $T = LU_0^{-1}$ (however, the time scale may be a fraction of the actual time). If there are no collective mechanisms by which one finger interacts with remote parts of the cloud (and none has been demonstrated), each finger will develop fingers just as the original cloud did; but now with a time scaled by $(1/2\text{-}1/3)\ LU_0^{-1}$. It is easy to see that the cloud develops a spectrum of finger sizes reaching all the way down to zero length, and it does this in a finite time, measured on a scale $(1.5 - 2)LU_0^{-1}$. Furthermore, it is likely that in this idealized cloud the cloud length (measured along a specific isodensity contour at the edge) is infinite (of course, its area is unchanged since the velocity field is incompressible).

Mandelbrot has termed such geometric oddities fractals. They do not have the same dimension as ordinary curves. Here the dimension is defined, not in the usual topological sense, but as the Hausdorff-Besicovitch dimension (which is 1 for ordinary curves). Nor is the power spectrum of a steep-edged cloud whose cross-section is a fractal $\approx k^{-2}$ for $kL \gg 1$; instead, it is roughly of the form (III-3) with $\alpha < 2$. (α is not, unfortunately, the same as the Hausdorff-Besicovitch dimension.)

In the rest of this Section we 1) discuss a special geometry for equations (III-4) and (III-5) which hints at fractalization; 2) compute the power spectrum of some fractals, and 3) deduce from 2) the physical

ingredients necessary to calculate α in the general case. These ingredients can be read off a computer simulation with limited dynamical range.

The physics is cartooned in Fig. 17, showing how a plasma cloud which has already developed steep (backside) edges and fingers begins to evolve smaller fingers in a self-similar way. We have idealized the cloud to have a uniform density except for an infinitely steep edge where the density drops to ambient; this is a popular and well-justified idealization, judging from the simulation results. Equation (III-5) shows that polarization charges develop on the sides, but not the backs, of the striations, in the approximation $\vec{E} \approx \vec{E}_0$. These polarization changes distort $\vec{E}_0$ by an amount $\delta\vec{E}$, producing wiggly field lines (two of which are shown as dotted lines in Fig. 17). The velocity flow field $\vec{U} = cB^{-1}\hat{Z} \times (\vec{\nabla}\phi - \vec{E}_0)$ carries plasma out of the center of the striation, and toward the edges. As a result, the density-depleted center cannot short out the electric field as well as the edges can, and the center moves more rapidly (to the right, in Fig. 17) than the edges do. So each finger develops an indentation, ultimately resulting in two new fingers of about 1/3 the size of the original ones.

The idealized outcome of several such generations of finger creation is shown in Fig. 18, which illustrates an evolving fractal. This many generations would be calculable in standard simulations as far as spatial dynamic range goes, but ordinarily time constraints allow at most

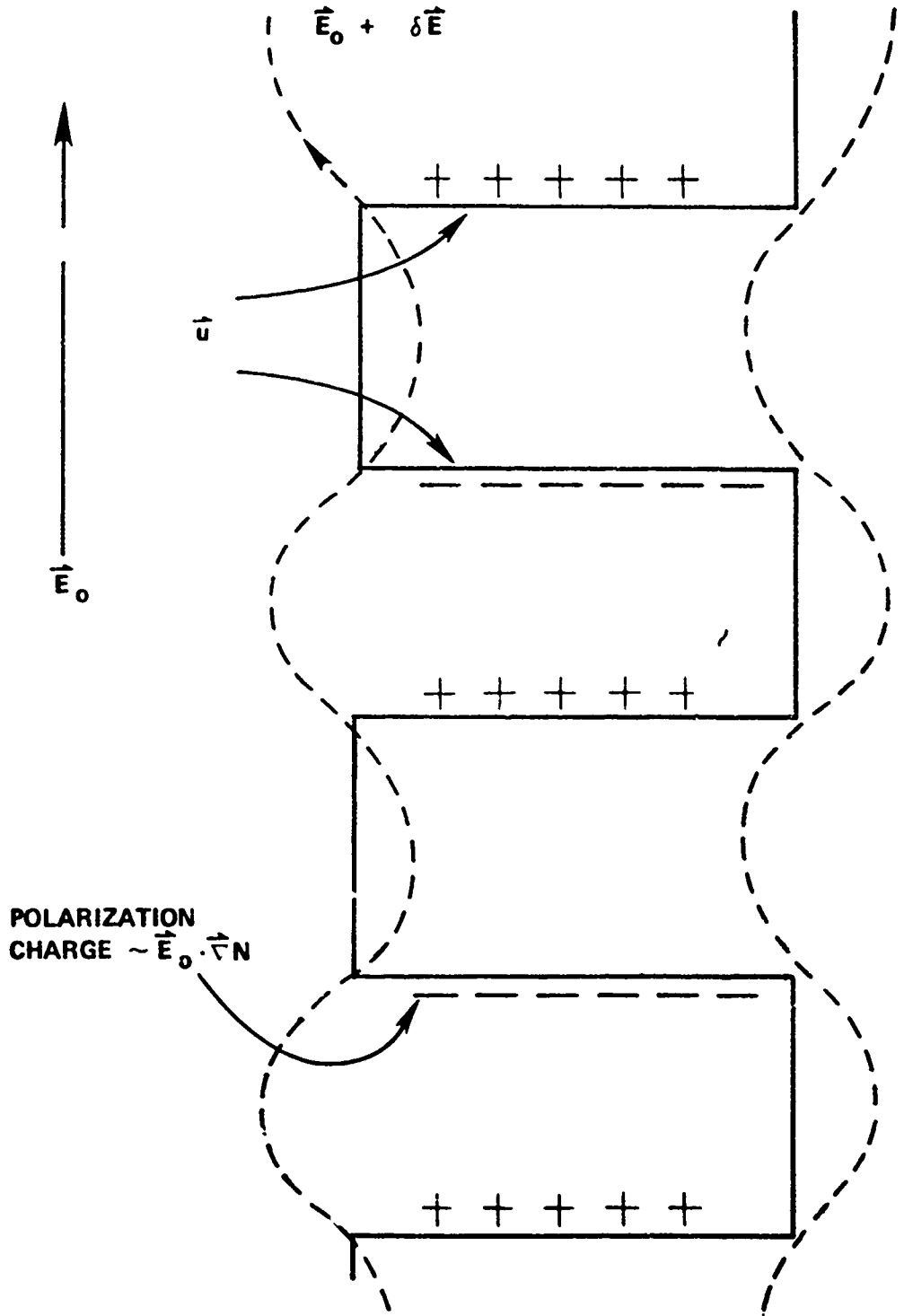

Figure 17 Perturbed electric field caused by, and causing, striations. The background plasma is to the left and cloud to the right.

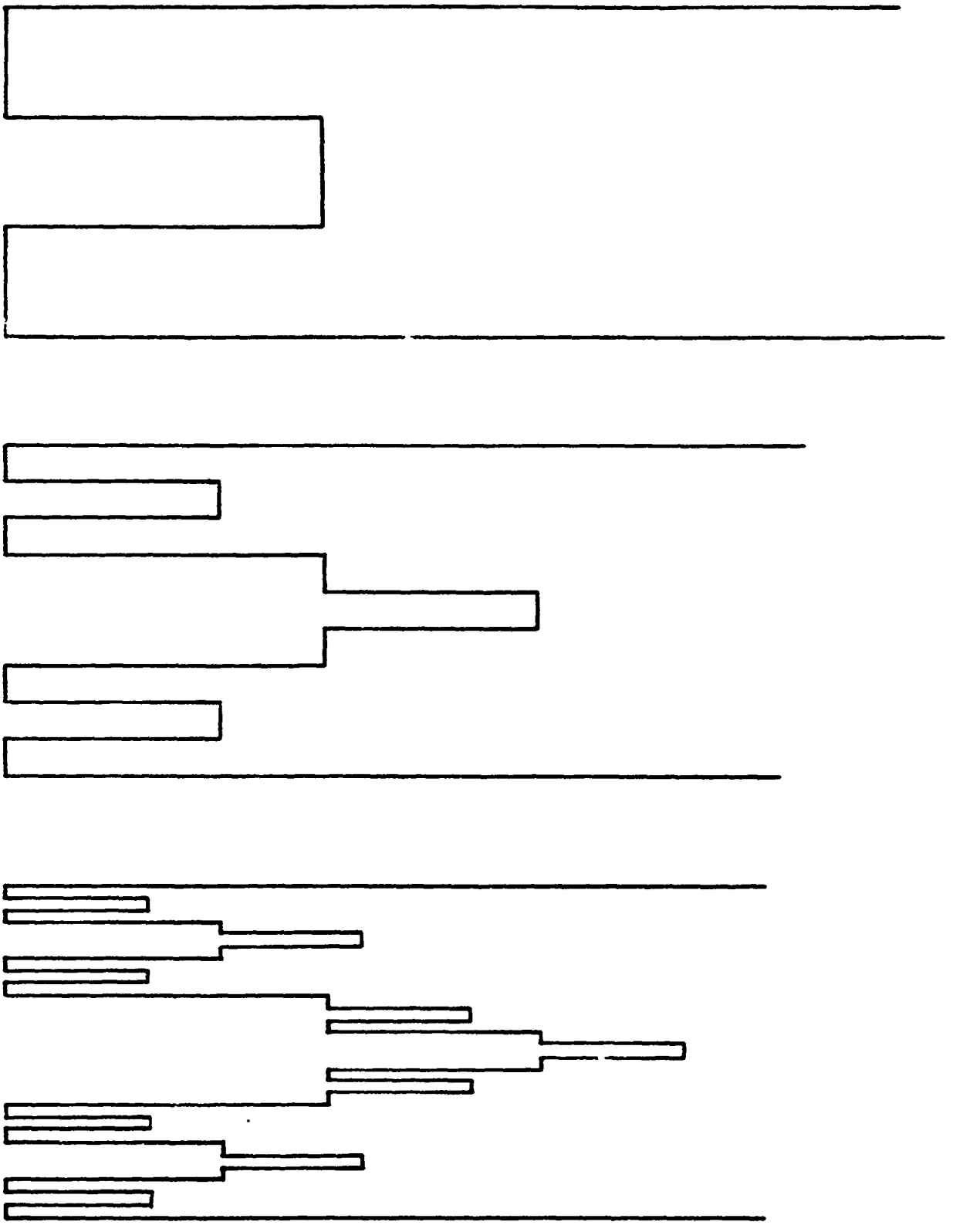

Figure 18 Idealized fractalization of an ionospheric plasma cloud.

two generations to be followed [see, for example, Figs. 2, 3, 4 of Ossakow et al. (1977)].

By now it is evident that the peculiar structure of a fractal looks the same no matter what power magnifier is used to study it. Everything that can be said about a fractal follows from knowledge of how one generation evolves into the next, which requires study of a rather limited dynamical range. We show how this works in determining the power spectrum of a fractal.

The power spectrum of equation (III-3) is defined as

$$P(k) = |\tilde{n}(k)|^2 \qquad \text{(III-6)}$$

where

$$\tilde{n}(k) = \int dx\, dy\, e^{i\vec{k}\cdot\vec{x}}\, n(\vec{x}) \qquad \text{(III-7)}$$

is the Fourier transform of the density n. We assume n is constant inside a certain isodensity contour, dropping to (nearly) zero outside, and take $\vec{k} = (k,0,,0)$ (thus $\vec{k} \cdot \vec{B} = 0$). Consider first $\tilde{n}(k)$ for a non-fractal shape, such as the topmost triangle in Fig. 15. Let the length of a side be L. For $kL \ll 1$, $\tilde{n}(k) \approx \tilde{n}(0) = A$, where $A \sim L^2$ is the area of the figure, and for $kL \gg 1$ $\tilde{n}(k) \sim k^{-1}$ times an oscillating function like $\sin kL$. Then $P(k) \sim k^{-2}$, after averaging out rapid oscillations $(\sin^2 kL \to 1/2)$. Then for a non-fractal shape $\alpha = 2$, which we call the

canonical value of α ; it is often invoked as a rough approximation for actual plasma clouds (Zabusky and Block, 1978, and Costa and Kelley, 1978).

Now consider the power spectrum of a fractal, for a given kL . In Fig. 15 the fractal is formed by adding triangles of 1/3 size to the existing triangle of any generation; similarly, $\tilde{n}(k)$ is formed additively from triangles of size $L \times 3^{-M}$, where M is the generation number ($M = 0$ for the original triangle, or "unperturbed cloud"). Let us choose k so that

$$kL = 3^{\overline{M}} \qquad \text{(III-8)}$$

for some integer $\overline{M}$ rather larger than 1, so $kL \gg 1$. Then in computing the contribution to $\tilde{n}(k)$ from triangles of the Mth generation, if $M \gg \overline{M}$ the exponent ikx in (III-7) hardly varies across such a triangle, and the contribution to $\tilde{n}(h)$ is just A_M , the <u>area</u> of the Mth generation triangles. Similarly, if $M \ll \overline{M}$, ikx varies rapidly and these triangles yield a term in $\tilde{n}(k)$ which is k^{-1} times an oscillating function. We drop such terms, because the terms we save do not decrease as rapidly.

It is a reasonably good approximation to replace the inequality $M \gg \overline{M}$ by $M > \overline{M}$ in the above discussion, which leads us to the approximation for $kL \gg 1$:

$$\tilde{n}(k) \approx \sum_{M=\underline{M}}^{\infty} A_M \qquad \text{(III-9)}$$

For the fractal of Fig. 15, it is an easy calculation to find

$$A_M = \frac{3}{4} A_0 \left(\frac{4}{9}\right)^M \qquad (M > 1) \qquad \text{(III-10)}$$

where $A_0 = 1/4\ 3L^2$. (Incidentally, this means that Fig. 15 does not quite evolve incompressibly, since the full fractal area is (8/5) A_0, but this is <u>not important</u>; it is quite easy to change Fig. 15 into an incompressible fractal by rescaling the whole figure a slight amount at each generation.) Then from (III-9), for $kL \gg 1$

$$\tilde{n}(k) \approx \frac{27}{20} A_0 e^{-\underline{M} \ln(9/4)} \qquad \text{(III-11)}$$

and using (III-8),

$$\tilde{n}(k) \approx \left(\frac{27}{20}\right) A_0 (kL)^{-\ln(9/4)/\ln 3} \qquad \text{(III-12)}$$

So by reference to the Rufenach spectrum (III-3)

$$\alpha = \frac{2\ln(9/4)}{\ln 3} \approx 1.48\ ! \qquad \text{(III-13)}$$

We can fit the power spectrum to the Rufenach spectrum at another point, say $k = 0$, where $\tilde{n}(k) = A = 8/5\ A_0$. This shows that the outer scale is

$(32/27)^{(1/\alpha)} L \approx L$, which is intuitively obvious: the sub-fractal generations of Fig. 15 do not change their overall shape very much, only their edge structure. (This last point is related to the phenomenon of freezing; it shows that there is a kind of shape freezing even in the presence of infinitely detailed bifurcation.)

It should now be clear how to calculate α for any fractal. The formula is

$$\alpha = 2 \ln\left(\frac{A_{M-1}}{A_M}\right)(\ln\lambda)^{-1} \qquad \text{(III-14)}$$

where A_M is the area of the Mth generation part of the fractal, and λ is the generation ratio (ratio of length scales of the Mth to the (M + 1) generation. Applying this to the fractal of Fig. 18 (with the x axis running <u>vertically</u>) gives a disturbingly small value of α , about 0.75! This is because the generating elements in Fig. 18 are much longer than they are wide, so λ is not quite well-defined. Special techniques involving coupling of more than two generations are needed, but we will not describe them here. Nevertheless, it is a case that is of practical importance judging from the long thin fingers of the computer simulations.

Since no physical cloud can ever fully fractalize, the next question is, how accurate are these considerations? One can redo the problem, replacing the upper limit $M = \infty$ in (III-9) by a finite upper limit M_u , determined by

$$L/\ell \approx \lambda^{M_u} \qquad \text{(III-15)}$$

where ℓ is the inner scale, or scale of physical effects left out of the canonical equations (e.g., $\ell \approx R_L$) . If $L/\ell = 10^6$, $\lambda = 3$, then $M_u \approx 13$, and the error committed by using an upper limit of ∞ is (for the Fig. 15 fractal) of order $(4/9)^{M_u} \sim 3 \times 10^{-5}$ as long as $kL \gg 1$, $k\ell \ll 1$. For $k\ell > 1$, there is a peak in the power spectrum which now begins to fall at least as k^{-2} and possibly faster, depending on the details of how steep the density gradient is on the scale length ℓ . These questions are taken up in Sec. III A.

C. Comparison of Instability Evolution in Fluid and Particle Computer Simulations of a Plasma

Until recently there have been, in effect, two different kinds of computer simulations: fluid codes (like that used by NRL) which handle complicated spatial structure, but not particle-kinetic effects; and particle codes, used primarily for infinite homogeneous plasmas. Now, however, it is possible to follow, to some extent, the evolution of gradients in particle-kinetic codes, as John Dawson and his colleagues at UCLA have shown.

A group at UCLA under the direction of John Dawson has done simulations in the following geometry (see Fig. 19, taken from Goede's thesis, Goede, 1980): a line current I in the y direction creates a magnetic field B_z decreasing as x increases. A plasma cloud (of

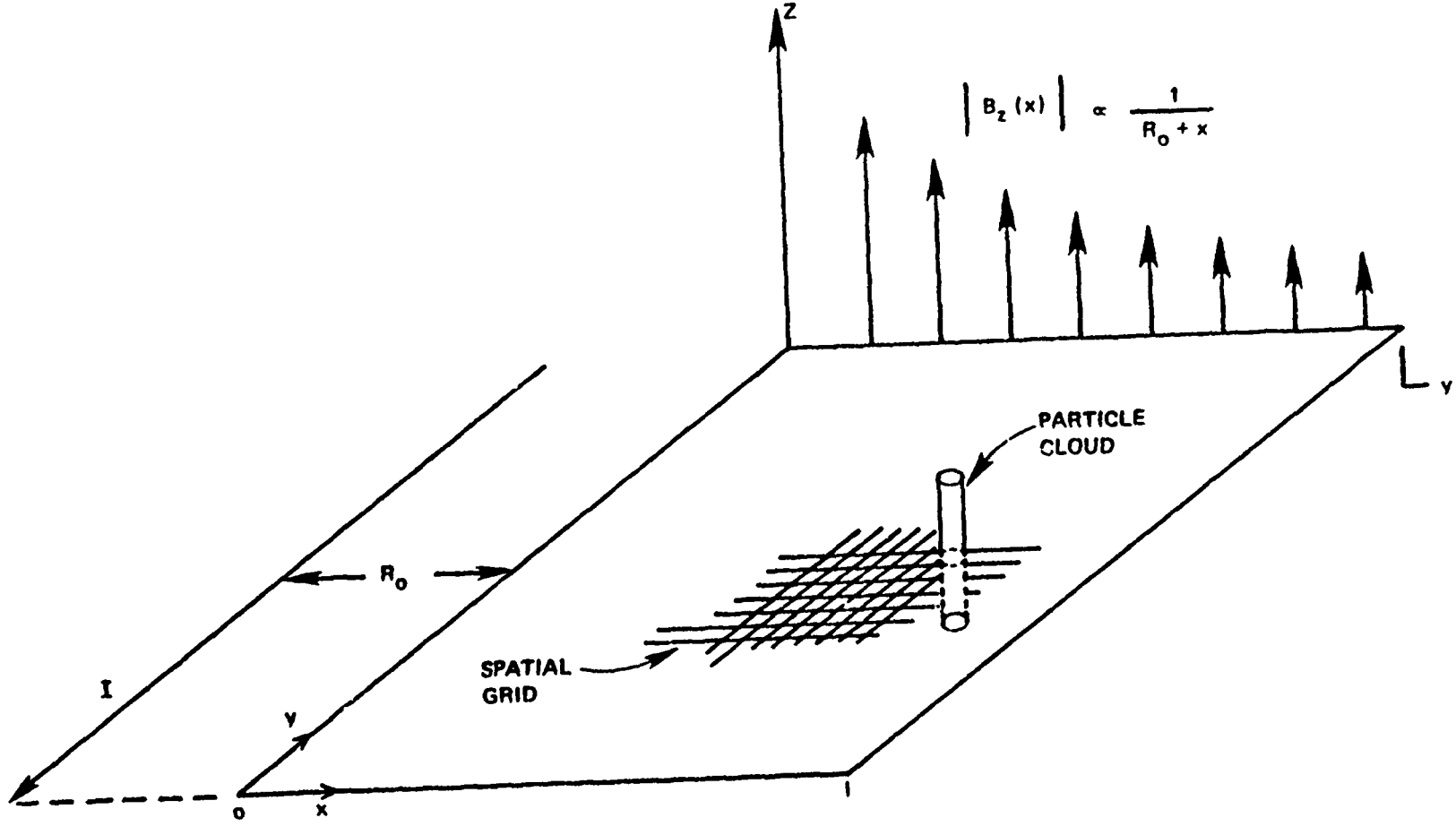

Figure 19 Geometry of spatially inhomogeneous particle simulations, taken from Goede(1980).

particle "rods" extending along $\vec{B}$) is supplied, also with a gradient in the negative x direction; of course, this is Rayleigh-Taylor unstable. The plasma is collisionless; the ion/electron mass ratio $M_i/M_e = 4$, and $T_e/T_i = 2$. The evolution of the particle cloud is shown at four successive times, in Fig. 20a,b,c,d. The cloud moves in the positive x direction, as would be expected from the linear Rayleigh-Taylor instability (with "gravity" g given by $-\mu BM^{-1}$, where μ is the magnetic moment), and reaches a terminal velocity $\sim g\nu_{eff}^{-1}$. The effective collision frequency is not yet completely understood, but it may arise from the generation of convective cells (Okuda and Dawson, 1973). Computer printouts of the electrostatic potential associated with Fig. 20 are not yet available, but printouts for similar runs in Goede's thesis show the formation of convective cells which appear to be responsible for the induced drag on the moving blob of plasma.

The simulations show unstable electrostatic modes, but the growth rates of these modes is not at all well-fit by simple collisionless theory. We have pointed out to Goede and Dawson that the growth rates may possibly be fit by a collisional Rayleigh-Taylor form, using ν_{eff} as given from the terminal blob velocity.

For those interested in striations, the most interesting aspect of the simulations is the formation of fingers on the blob (Fig. 20d). These fingers are precisely of the type expected to form as a result of the $\vec{E} \times \vec{B}$-gradient drift instability, which is mathematically the same as the

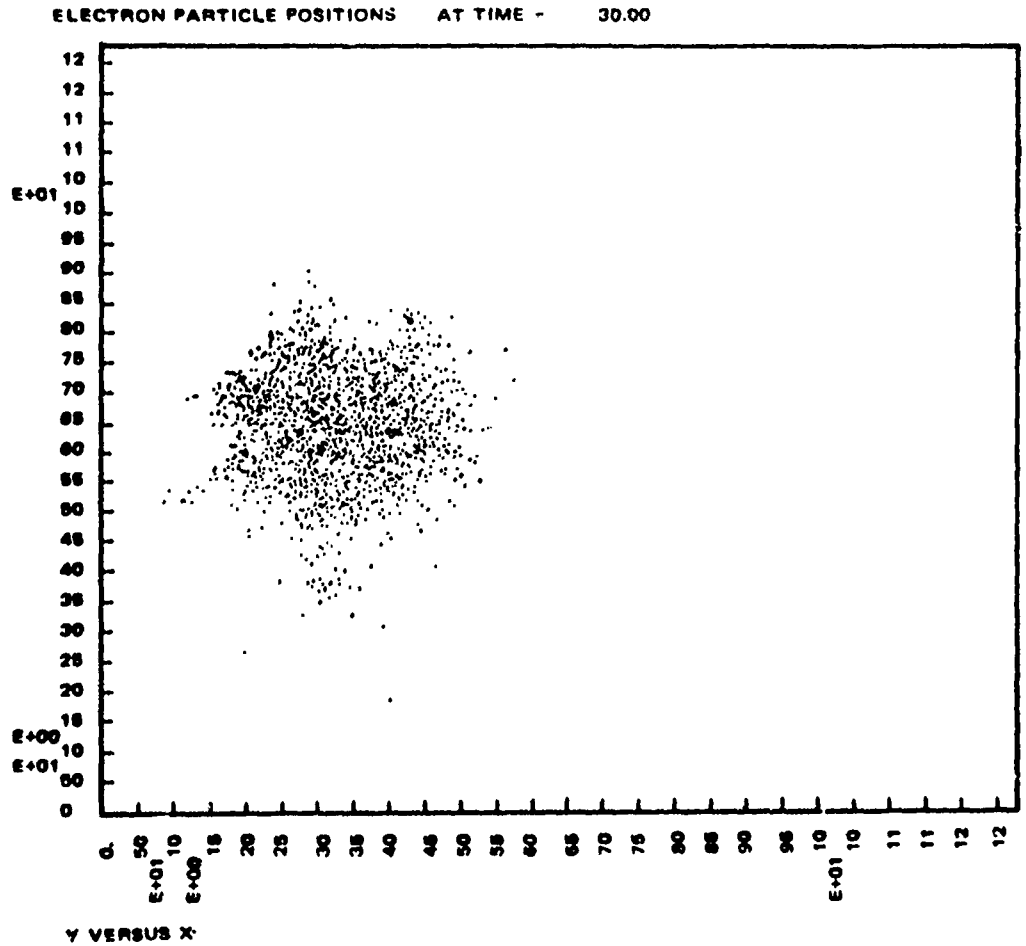

Figure 20a One of four snapshots of a plasma cloud evolving in the geometry of Fig. 19. Time is in units of the electron plasma frequency, and $M_i/M_e = 4$. (Furnished by John Dawson.)

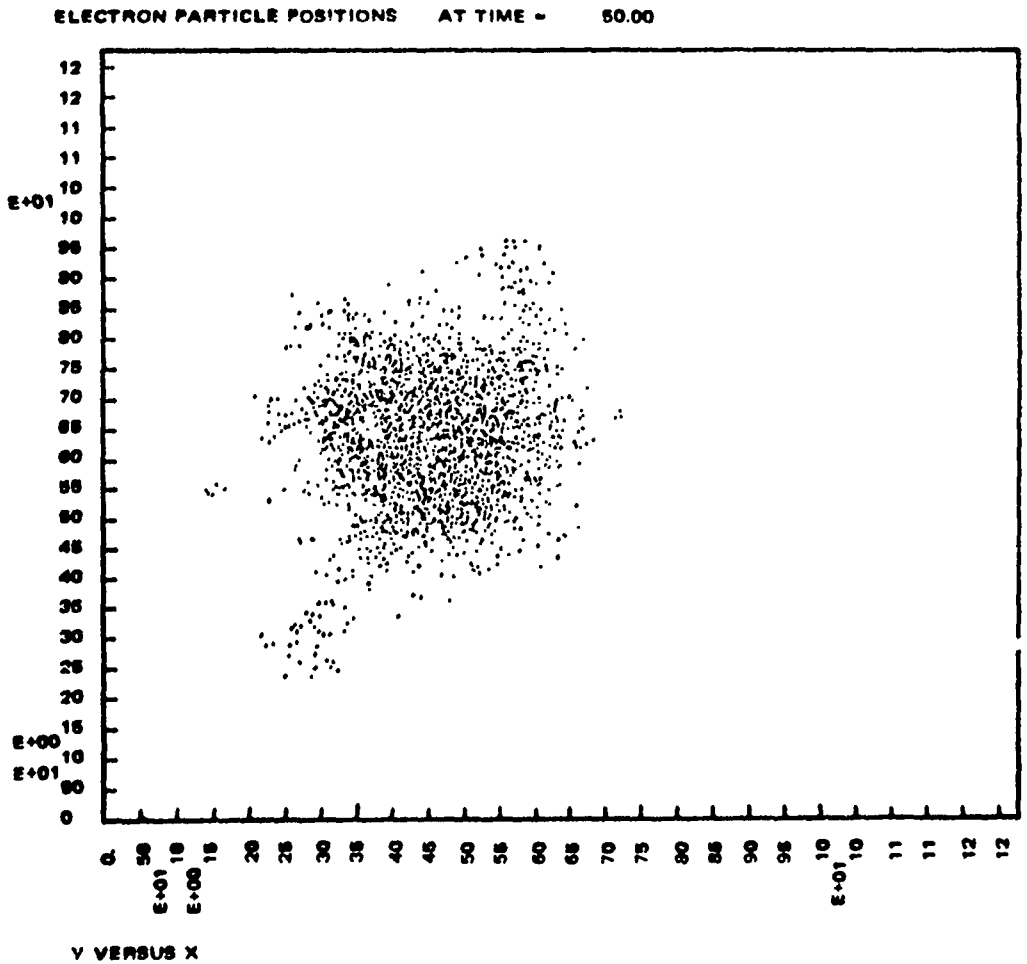

Figure 20b One of four snapshots of a plasma cloud evolving in the geometry of Fig. 19. Time is in units of the electron plasma frequency, and $M_i/M_e = 4$. (Furnished by John Dawson.)

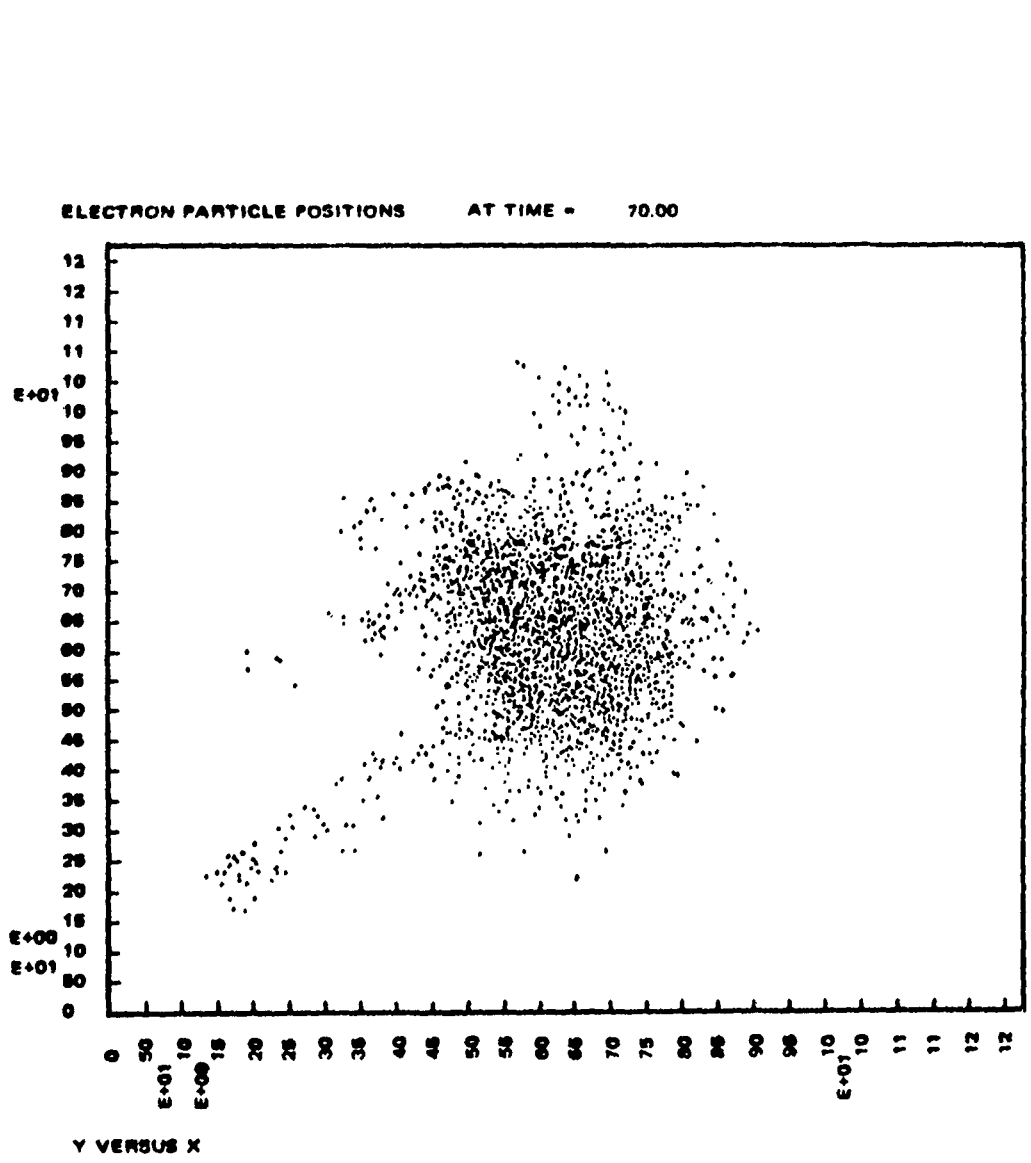

Figure 20c One of four snapshots of a plasma cloud evolving in the geometry of Fig. 19. Time is in units of the electron plasma frequency, and $M_i/M_e = 4$. (Furnished by John Dawson.)

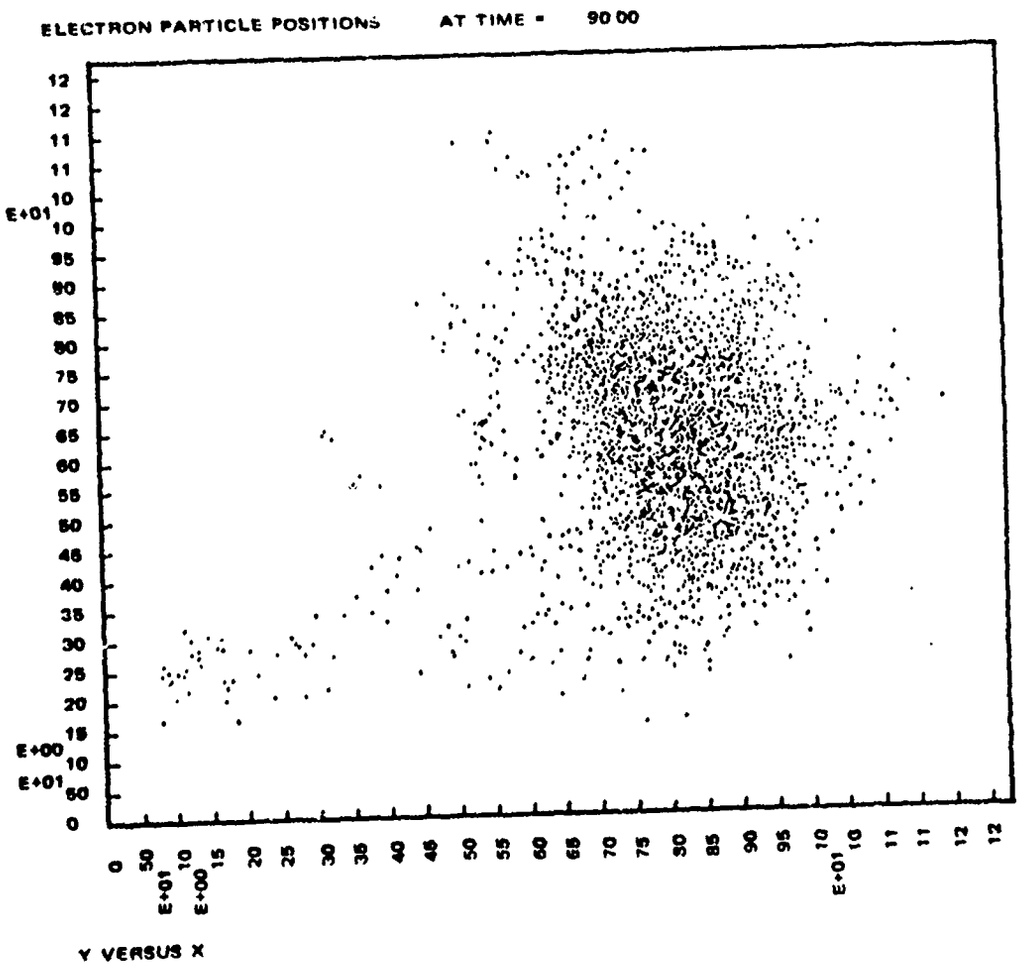

Figure 20d One of four snapshots of a plasma cloud evolving in the geometry of Fig. 19. Time is in units of the electron plasma frequency, and $M_i/M_e = 4$. (Furnished by John Dawson.)

collisional Rayleigh-Taylor instability (with effective electric field $E = (M/e)g(\Omega/\nu_{eff})$) .

The way now lies open to combine large-scale fluid codes and smaller-scale particle codes, since there is a real overlap in their domains of applicability. Dawson and colleagues' results indicate that convective cells are formed; in the presently available simulations, cell formation is enhanced by having a strong magnetic field ($\Omega_i > \omega_{pi}$) . It will be most interesting to study weak-field simulations, looking for convective cell generation caused by the spontaneous formation of fingers (i.e., relatively sharp gradients). We have already indicated in Sec. III A how this might work, through the mechanism of drift-wave generation and decay into convective cells. The proposed analytical research of such a mechanism must be accompanied by simulations capable simultaneously of dealing with particle-kinetic effects and with spontaneous striation formation by the standard electrostatic-fluid instabilities; these simulations now appear to be possible.

D. Possible Magnetospheric Effects

A high-altitude nuclear explosion generates an enormous number of energetic ions. It is conventional wisdom that these are eventually cooled by collisions, and fall back into the ionosphere. However, the possibility exists that substantial numbers of energetic (> 1 kev) ions undergo pitch-angle scattering at very high altitudes which puts them into orbits whose mirror points are so high that they are virtually collisionless. (The pitch-angle scattering may be caused by, e.g.,

electromagnetic ion-cyclotron waves generated by the energetic ions themselves.) These ions may live for tens of hours or days, their lifetimes being governed by charge exchange, pitch-angle scattering into the loss cone, and very slow energy degradation by Coulomb collisions.

Such energetic ions are impossible to detect directly from the ground (by, e.g., optical observation). As far as we know, there are no satellite data which bear one way or the other on trapped ions from a high-altitude nuclear explosion, because of lack of adequate instrumentation in the years 1963 and before; nor is there any theoretical work (including simulations) on the problem. The direct scintillation effects of the ion density are clearly negligible because the densities are so small. Here we are looking for effects in the more dense, lower ionosphere which are caused by the interaction of these ion currents with the ionospheric plasma.

If such a partial ring current of energetic ions is found, it is worth looking at its effect on the striation scene. This ring current will itself have sharp gradients which could influence propagation from satellites. Moreover, these sharp gradients will drive field-aligned currents which can interact with conventional ionospheric striation mechanisms (e.g., by driving a current-convective instability, or by generating high-altitude electrostatic turbulence which is mapped down field lines into the ionosphere). These currents come from gradient and curvature drift velocities of some hundreds of meters to a few km/second. One might speculate that the artificial ring current will generate a kind

of auroral environment, associated with (small) electric fields parallel to the magnetic field. (This speculation rests on recent auroral models which drive parallel electric fields by energetic ion injection.) The resulting currents and energetic electrons may influence striation phenomena by providing rapid cross-field electron transport, thus allowing ions to diffuse (see Sec. III A). It is worth a modest theoretical effort to see if any such ion ring current is actually formed, and if so, what its effects on striations are.

It has recently been established in an experiment called Trigger that auroral phenomena, including rapid acceleration of particles to energies of as much as 300 keV, can be stimulated by the sudden release of large amounts of plasma in the F region ionosphere (≈ 160 km). The Trigger experiment (Holmgren et al., 1980) consisted of an explosive release of Cs^+ ions and electrons (via an explosion of 12 kg of a TNT-Al-$CsNO_3$ mixture) which increased the conductivity by more than 2 orders of magnitude over ambient. During the few seconds to few tens of seconds of observation, the cloud expanded to a scale size of a few km. There were no energetic particles to begin with in the plasma; apparently they were created by a large transient electric pulse with a substantial component along the magnetic field line. Obviously such an electric field will accelerate ambient ions (a process which is not necessarily modeled correctly in MHD codes, since kinetic effects may dominate the parallel electric fields), so that it may well be that energetic ions in the magnetosphere are not simply bomb debris, but strongly-energized ionospheric ions.

One may well ask: Should not such phenomena have been seen in Ba^+ releases? In fact, it would not be surprising to see them, and there is some evidence that they were (see Baker et al., 1978, for an overview), but until Trigger little attention was paid to proper instrumentation and especially to insuring that instruments were on the same field line as the released plasma.

It would be very much worthwhile to conduct Trigger-like experiments in future Ba^+ releases, not only for what is learned about early-time processes, but for what might be learned about the storage and subsequent release at late times of energetic magnetospherically-trapped particles.

IV. LABORATORY EXPERIMENTS AS MODELS OF HIGH ALTITUDE NUCLEAR EXPLOSION PHYSICS

In this section, the value of laboratory experiments, specifically laser exploded pellet experiments, to obtaining a more complete understanding of the phenomenology of a high altitude nuclear explosion (HANE) is discussed. For the reasons discussed below, it appears that such experiments can provide information regarding (1) the "early time" coupling of the expanding debris cloud to the ambient ionosphere; (2) the importance of "early time" effects in determining the later time phenomena; and (3) the late time inner and outer scale sizes. This information, and the understanding of HANE phenomenology to which it would contribute, would come both from the results of the experiments themselves and from the improvement that would undoubtedly follow in the computer codes used to simulate HANE physics. The benefits of improved ability to predict the long term behavior of the ionosphere after a HANE could have a substantial impact on the effectiveness of our satellite communication system, as discussed in detail in Section II.

In the subsections which follow, we further motivate HANE simulation with laser pellet explosions, briefly describe experiments which have been performed or are in progress, and then discuss in some detail the possibility that relevant experiments can be performed using existing facilities with relatively modest additional capital cost. We shall see that two independent experiments are probably necessary to simulate early

and late time phenomenology. It is important to note that we are not providing an experimental design, but merely a strong indication that relevant experiments can be designed. In order to be sure that proper consideration of all necessary scaling laws is given, it is recommended that DNA support two to three month design studies by interested organizations who have the necessary major pieces of equipment (powerful lasers, sophisticated diagnostic capability, and/or large vacuum chambers). This would enable DNA to evaluate whether truly relevant experiments can be performed, after which an RFP for such experiments can be issued.

A. Objectives of the Suggested Experiments

The modeling of HANE phenomena with barium releases in the ionosphere, together with analytic theory and computer simulation, has led to considerable understanding of the fundamental physics underlying the behavior of artificial plasma clouds in the ionosphere during the electrostatic regime (see Section I). (Evolution at very late times is still not understood either empirically or theoretically; see Sections I and III.) Nevertheless, our inability to make continuous detailed measurements on barium clouds, and the fact that barium clouds can simulate only electrostatic regime effects, leave us uncertain as to (1) the evolution of a plasma cloud in the ionosphere, specifically its inner and outer scale lengths, and the spatial power spectrum of irregularities, and (2) the degree to which the details of early time phenomenology affect the late time behavior of HANE plasma clouds. Furthermore, we are unable to confidently infer all of the necessary details from computer simulation

coupled with theory. This is true even in time regimes where we have codes which are "validated" against barium cloud experiments. This is because limitations on the number of spatial grid points that can be used in a simulation of adequate time duration limit the range of spatial scales that can be covered to a factor of about 100, e.g., 0.8-80 km (see, for example, Keskinen, 1980). By contrast, in an actual barium release, wavelengths ranging from $\lesssim$ 10 m to about 50 km appear to be important (Baker et al. 1978). As for early times, there is still controversy over the actual debris-air coupling mechanism(s) (Clark, 1980), and these may provide initial conditions for subsequent late time plasma cloud expansion which substantially influence the important scale sizes and the power spectrum of the late time cloud structure.

Given the above background it is clear that appropriate experiments would be quite valuable. The goals would be the following: (1) an experiment which investigates the early time debris-air coupling and would thus provide information that can be otherwise provided only by a HANE; this experiment would also serve to provide information on the initial conditions which should be used in late time computer simulations; (2) an experiment which investigates the late time plasma cloud behavior, and which can be used to determine relevant length scales and to "validate" late time codes if it is well diagnosed. As we will see, it would be wasteful to tie up a laser capable of doing the first experiment to also do the second one. Therefore, two independent experiments are suggested below, one using a very high power laser and the other using a lower power laser, but a very large vacuum chamber.

B. Closely Related Laboratory Experiments

About ten years ago a laser-pellet experiment for HANE simulation was initiated at the Naval Research Laboratory (NRL) by John Stamper and Steve Dean. A 10-60J, 30 nsec pulse duration Nd:glass laser was focussed on the tip of a 250 μm diameter lucite fibre. A 1 kG magnetic field was to be used, as was a 10^{15} cm^{-3} "ambient" plasma (Stamper, 1980). However, the background plasma was found to be unnecessary because the laser-produced plasma at the target was able to substantially photo-ionize 10-200 mtorr of nitrogen or helium in the vicinity of the target. The intent was to look at the early time "collisionless" portion of the interaction. The experiment was sidetracked by the discovery and study of large spontaneous magnetic fields near the pellet (Stamper et al. 1971). These fields, which were due to the single-sided pellet irradiation at high power density (~ 10^{12} W/cm^2), dominated the early time plasma expansion. At the radius at which the spontaneous fields were no longer dominant, the electrons were no longer collisionless, although the ions were (Dean et al. 1971). No follow-on experiment with symmetric irradiation of the pellet was performed at NRL.

At the University of Maryland, an experiment to follow up the work of Stamper and Dean on HANE simulation was started in 1971. The problem of the megagauss fields was avoided by lowering the laser power density, looking at least 1 cm away from the target, and using a lower ambient plasma density. Early experiments found a collisional interaction (Koopman and Goforth, 1974), but in more recent experiments, the interaction is believed to be collisionless (Parsons, 1980). In these recent experiments

a slab target of Ba or iron is used, and it is being irradiated by a 6J CO_2 laser in ~ 100 ns. This means that the initial expansion velocity is much lower than in a HANE, namely an observed value of (1-3) x 10^6 cm/sec. Observations are made where the expanding plasma density is from 10^{15} to 10^{13} cm^{-3}. The ambient plasma of 10^{13} cm^{-3} is produced from the ~ 10^{-3} Torr (6 x 10^{13} cm^{-3}) background gas by the U.V. flash of the target. The magnetic field is variable from 0-2 kG. This experiment has observed collisionless coupling with 1 cm shock thickness using Ba, with a 1 kG magnetic field. The specific instabilities involved in the collisionless interaction have not yet been identified, but this is precisely what this experiment is now capable of doing. Apparently the experiment has been funded at a level of ~ $80k/year by the Air Force, during which its diagnostic capability was built up to a very formidable level. It is now a beautiful physics experiment capable of determining which of the standard collection of instabilities are present when one plasma expands into another. However, the experiment has been terminated due to the recent death of the principal investigator, David Koopman. An SAI group has proposed to AFOSR that the experiment be continued under their auspices.

The results of this experiment are significant to the physics of the HANE problem. The findings regarding collisionless coupling in the most recent experiments should be examined closely for potential applicability and importance to a HANE. However, the specific energy deposition (J/gm) is much lower than in a HANE [Zinn et al. (1965) give the kinetic energy yield for Starfish of about 10^9J/gm], and a slab target was used rather than a pellet. Since specific energy deposition is said to be

one of the most important scaling parameters (Clark, 1980), this may make any conclusions from the University of Maryland experiment difficult to extrapolate with confidence to the early and intermediate time regimes of the high altitude case. The recent work on this experiment was apparently under the direction of Dr. Charles Parsons, and the experiment was being carried out by G. P. Jellison, a graduate student.

A variety of other slightly related experiments have been performed which we mention only briefly: two experiments to fill mirror machines with laser-produced plasma have been performed, one by Alan Haught at United Aircraft and one by John Osher at LLL ("Baseball" experiment). An experiment by Pechacek and Greig at NRL produces a plasma in a cusp magnetic field using a laser-exploded pellet. None of these experiments involved an ambient plasma, so there was no coupling to be observed. However, data on plasma production and expansion is presumably available. An experiment at AVCO to investigate the coupling of a gun plasma to an ambient plasma was performed about ten years ago by Friedman and Patrick (1971). This experiment demonstrated collisionless coupling of a streaming plasma to a magnetized background plasma. The streaming direction, however, was strictly parallel to an applied magnetic field, so the relevance to a HANE is marginal. Nevertheless, it is worth noting that momentum transfer lengths from streaming to background plasma a factor of 100 less than the ion Larmor radius were observed.

C. Present Status of Pulsed Laser Systems

Multikilojoule laser sytems exist in several laboratories in the U.S. now, with the largest development programs being those at LASL

(CO_2 laser system) and LLL (Nd:Glass laser system). We shall use the SHIVA laser system at LLL as the basis for discussion because it delivers the most energy to a target, namely 10 kJ to a $\lesssim$ 200 μm diameter pellet. In a short pulse ($\lesssim$ 100 ps), about 25% of the energy is absorbed, and virtually 100% can be absorbed in longer (> 200 ps) pulses (Manes et al. 1980; Lawrence Livermore Laboratories, 1979). Furthermore, a pellet can be irradiated with nearly arbitrary symmetry. A typical exploding pusher target is a glass shell 150 μm in diameter, 1 μm wall thickness, filled with 10 atmospheres of D-T gas. It weighs 100 ngm, and it is irradiated in the short pulse mode with close to spherical symmetry. A specific energy deposition of over 10^9 J/gm is implied, and 6×10^9 J/gm is documented. We specifically mention exploding pusher targets because they are rather well characterized by now. For example (Manes et al. 1980), the expansion starts at $(1\text{-}10) \times 10^7$ cm/sec, depending upon the power on the silicon microballoon target. Furthermore, "other observables", e.g., shell temperature and core information, are well predicted by code calculations at the early times which interest the LLL group.

In addition to the laser itself the SHIVA system includes a multiport, 80 cm radius experiment chamber and a very sophisticated collection of diagnostics. The latter is particularly suited for very high density and temperature observations, but some of it could be useful to investigate coupling phenomena at lower density if an ambient plasma were present in the chamber. Target fabrication has also become rather sophisticated in recent years: thin shell, multishell and multilayered targets have all been made in many different materials. Therefore, it is

likely that appropriate adjustment of laser power and pellet surface material would allow the pellet to produce the ambient plasma around it by photoionization as a HANE does, while still varying other observables, such as the initial expansion velocity.

The great advantage of a laboratory experiment is evident when one realizes that the SHIVA system, for all its complication, is capable of two laser-pellet experiments at full power and with full diagnostic complement per day (Manes et al. 1980). Thus, once appropriate parameters have been determined and set up experimentally, and the diagnostics are set up, information can be collected (and analyzed) very rapidly. This information can be obtained using a variety of different pellets and laser powers, depending upon the effect under investigation. A variety of different symmetries can also be investigated.

D. Scaling from HANEs to Laser Pellets

The scaling laws to be used to guide the design of experiments to simulate a HANE are relatively straight-forward for a late time experiment, but not nearly so obvious for the early time. There are two dominant problems in the early time case: (1) it is not possible to obtain consistent scaling of all parameters, and so it is necessary to choose a set which makes the experiment "as relevant as possible"; and (2) there is no agreement as to what coupling mechanisms are the most important under given conditions (e.g., altitude and yield), and different scaling may be required depending upon the mechanisms expected. (Here is where the results of a physics experiment, such as the University of Maryland one

described in the previous subsection, would be very helpful.) Since the least information is available for the early time, it is probably the most important case to consider here, and so we shall look at it first. This case will also be able to provide information on the transition to late time, the importance of which has already been discussed.

1. Early Time Scaling

Table II presents the parameters of the Starfish Device exploded at 400 km altitude, as presented by Zinn et al. (1965), in the column marked HANE. Although we consider Starfish here, we recognize that other event parameters are probably of as much or more interest and that these would be considered in further work. Note that near the explosion the ambient air is likely to be fully ionized by the flash, but further away the plasma density will be close to ambient. Thus, two different sets of plasma frequencies are given. Because the atmospheric density scale length at 400 km is ~ 60 km, the debris expansion and shock wave are not symmetric about the burst point in the vertical direction even before the magnetic field has much of an effect. Furthermore, the symmetry is even worse when the debris energy has been degraded sufficiently that the magnetic field begins to become relevant.

With these considerations and others implied by the parameters in Table II in mind, we specify that the experiment should have the capability of depositing at least 100J in a 100 ngm target with some appropriate level of symmetry. Provisions to puff in gas to produce a neutral particle density gradient, and to produce a magnetic field oriented appropriately to

TABLE II

EARLY TIME PARAMETERS

	HANE	Experiment
Kinetic Energy Yield	10^{15} J	100 J
Mass	10^{6} gm	100 ngm
Bubble Radius	~ 200 km	5 cm
"Mass Radius"*	100 km (~ 10^{8} cm^{-3})	2 cm (~ 10^{14} cm^{-3})
Magnetic Field	$\frac{1}{3}$ G	300 G
Initial ion Larmor radius		
(10keV/Nucleon)	29/Z Km(Fe)	30 $\frac{A}{Z}$ cm
Background	Air (10^{8} cm^{-3})	Air ($\gtrsim 10^{14}$ cm^{-3})
ω_{ce}	10^{7} sec^{-1}	2 x 10^{10} sec^{-1}
ω_{ci}	10(Fe) sec^{-1}	10^{7} $\frac{Z}{A}$
ν_{e} (1eV)	3 x 10^{3} sec^{-1}	3 x 10^{9} sec^{-1}
ν_{in}	~ 1 sec^{-1}	10^{4} sec^{-1}
ω_{pe} (Fully Ionized 10^{8} cm^{3} Ambient**)	5 x 10^{8} sec^{-1}	5 x 10^{11} sec^{-1}
ω_{pi} (Fully Ionized Ambient)	6 x 10^{4} sec^{-1}	6 x 10^{8} sec^{-1}
ω_{pe} (Undisturbed Ambient 2 x 10^{5} cm^{-3})	2 x 10^{7} sec^{-1}	2 x 10^{10} sec^{-1}
ω_{pi} (Undisturbed Ambient)	2 x 10^{3} sec^{-1}	2 x 10^{7} sec^{-1}
V_{A} (Undisturbed Ambient)	~ 400 km/sec	~ 400 km/sec
V_{A} (Fully Ionized Ambient)	~ 20 km/sec	~ 20 km/sec

* The radius within which there is an ambient mass equal to the weapon mass.

** Assuming the background gas is fully ionized by the radiation in the region of interest.

that density gradient, should be made, although the first experiments could be performed without these. A magnetic field of up to ~ 1 kG is necessary to reduce length scales to laboratory size. This is seen by assuming B^2 x Volume is proportional to the kinetic energy yield (i.e., the bubble size is determined by field energy displacement by the expanding debris). Thus, if we take the desired laboratory length to be 5 cm and the remaining quantities from Table II, we obtain 300 G as our field. In order to set the density, we have two possible scaling choices: B^2/n or B/n the same. In addition we wish to have the "mass radius" approximately equal to 1/2 the bubble radius. The first density scaling retains the value of ω_c^2/ω_{pe}^2, the Alfvin speed V_A (assuming the same ion species) and transverse pressure balance (at the same temperature); it requires a plasma density of 10^{15} cm^{-3}. The B/n scaling maintains ω_{ce}/ν_e (at the same temperature) as well as the ratio of the ion Larmor radius to the ion range; the density would be only 3×10^{11} cm^{-3} here. The mass radius would be 2 cm for 10^{14} cm^{-3} air, requiring a fill pressure of 1.5 mtorr of air if the U.V. flash fully (singly) ionizes it. We choose 10^{14} cm^{-3}, although it may be necessary to drop it by an order of magnitude to avoid collisionality problems-- ν_e/ω_{ce} using table values may be too large. The other parameter poorly scaled in the experiment is the ion Larmor radius, which may cause a problem in trying to use the results of this experiment to provide initial conditions for a late time code calculation. This presumably depends upon the coupling mechanism and requires further study. A small amount of preionization can be used to make an undisturbed ambient density of 2×10^{11} cm^{-3} in order to have undisturbed ambient V_A, and ω_{pe} scale correctly. The interesting duration of this experiment

would be ~ 10 μsec at most. Extensive optical diagnostics will probably be needed, such as holographic interferometry for density and spectroscopy for temperature. Submillimeter scale measurements can be made.

2. Late Time Scaling

Here we would like the following set of relationships between various parameters:

(a) τ = experiment duration $\gtrsim 2 \times 10^4 \, \omega_{ci}^{-1}$ in order to simulate ~ 1000 sec (ω_{ci} is the ion cyclotron frequency);

(b) $\tau \gtrsim 100 \, \gamma^{-1}$ where γ = growth rate of the gradient drift instability (cE/BL, where L = density scale length, E and B are the electric and magnetic fields, respectively, and c is the speed of light);

(c) $\frac{\nu_e}{\omega_{ce}} < \frac{\nu_i}{\omega_{ci}} \ll 1$;

(d) $\frac{\omega_{pi}}{\omega_{ci}} \gtrsim 10$ in the plasma cloud;

(e) Length scale range of 1000, in order to substantially exceed that of computer simulations.

We assume we have a > 5 m diameter by many meter long tank available in which to do the experiment. Then the following set of experimental conditions will suffice:

Li^{+1} ions in the cloud; hydrogen background

B = 1 kG

T_i = 1000° K

E = 50 V/m across the 5 m tank

These give $\omega_{ci} = 1.6 \times 10^6$ sec^{-1}, ion Larmor radius ~ 1 mm, and a time of drift across the 5m tank of 10 msec. In order to have $\gamma = cE/BL \gtrsim 10^4$ sec^{-1} requires $L \lesssim 5$ cm. The densities must be determined by the requirements on the collision and plasma frequencies. In addition, we must be sure that the Li^{+1} plasma is cooled by collisions with a cold neutral background in $\lesssim$ 100 μsec ($\lesssim \gamma^{-1}$) . The following set of parameters seems reasonable based upon what the University of Maryland experiment is doing with laser produced barium plasmas from a slab target:

$$n_n \gtrsim 6 \times 10^{13} \text{ cm}^{-3} (\gtrsim 1 \text{ mTorr})$$

$$n_{Li} \approx 10^{12} \text{ cm}^{-3}$$

$$n_{amb} \approx 10^{10} \text{ cm}^{-3} \text{ or } 10^{11} \text{ cm}^{-3}$$

The two choices in the ambient density are to simulate HANE and barium cloud situations, respectively. Assuming the ambient plasma has cold ions ($\lesssim$ 0.1 eV) and electrons ($\lesssim$ 1 eV), all of the necessary frequency criteria are satisfied.

Such a situation may be produced by a modest power laser. The necessary 10^5cm^3 of 10^{12} cm^{-3} Li^{+1} is 10^{17}e-i pairs. At 10 eV to produce

each one, this requires 160 mJ. A slab target ~ 1 cm in radius would be used. The plasma would expand into the weakly ionized ambient plasma with an initial ion Larmor radius of ~ 1 cm (10 eV) and a collision frequency of $\gtrsim 10^5$(10 eV). Therefore, in 100 μsec it will have collided many times and diffused across B a few ion Larmor radii. It is now low β and "ready" to respond to a 250 V electric field across the tank perpendicular to B. The tank must be much more than 5 m long so that plasma does not reach the ends during the 10 msec experiment. Such a tank exists at the Manned Spacecraft Center near Houston (it was used for Space Shuttle system tests) and others may exist elsewhere (e.g., one of the "space chambers" that exist around the country). (A great deal of capital expense can be saved if a tank and a field coil power supply are available at the same site. The coils themselves and the laser would be relatively inexpensive.) Note that it may be possible to introduce perturbations into the initial cloud by the use of periodic barriers in the way of the plasma as it moves away from the slab, or perhaps by using several separated focal spots for the laser. Since assembling the necessary diagnostic capability is probably the most time-consuming aspect of building up this experiment, a reasonable approach is to transport the University of Maryland experiment to wherever an adequately large tank is available. (Even if this is not done, this experiment should be kept going in order to complete its collisionless coupling physics experiments.)

E. Conclusion Regarding Laboratory Experiments

The discussion of the previous section by no means constitutes an experimental design. However, it does indicate that a

complete design study is warranted if DNA is interested in using controlled and flexible laboratory experiments to simulate high altitude nuclear explosions. Recommendations are made in Section I above.

V. RADIATIVE TRANSFER EFFECTS IN Ba+ LINES IN STRIATED BARIUM CLOUDS

Ba II has two resonance transitions, $6\ ^2S_{1/2}$-$6\ ^2P_{1/2}$ (4934A) and $6\ ^2S_{1/2}$-$6\ ^2P_{3/2}$ (4554A). At slightly longer wavelengths lie three fluorescent transitions, $5\ ^2P_{3/2}$-$6\ ^2S_{1/2}$ (6497A), $5\ ^2P_{3/2}$-$6\ ^2P_{3/2}$ (5854A), and $5\ ^2D_{5/2}$-$6\ ^2P_{3/2}$ (6142A). These transitions are illustrated in Fig. 21. In the past the common procedure has been to observe only the strong resonance line, 4554A, and occasionally the other member of the pair, 4934A, to obtain column densities of Ba^+. A radiative-transfer analysis still in preparation at Los Alamos Scientific Laboratory by Horak and Whitaker (1980) shows that observations in the resonance lines alone can give erroneous values of the integrated density, but that the observations can be interpreted unambiguously if supplemented by simultaneous photometry of the fluorescent lines.

The effect is one commonly known as the curve of growth and is illustrated in Fig. 22. At column densities of Ba+ of $N = 10^{11}$ cm^{-2}, the 4554A line begins to become saturated. A correction is not simply made for the loss of radiation through attenuation, since some of the loss is restored through secondary scattering back into the line of sight. The only practical means of ascertaining the column density is through simultaneous observations of the lines 6497, 5854, and/or 6142A, which have diminished populations in their lower levels and consequently are slower to

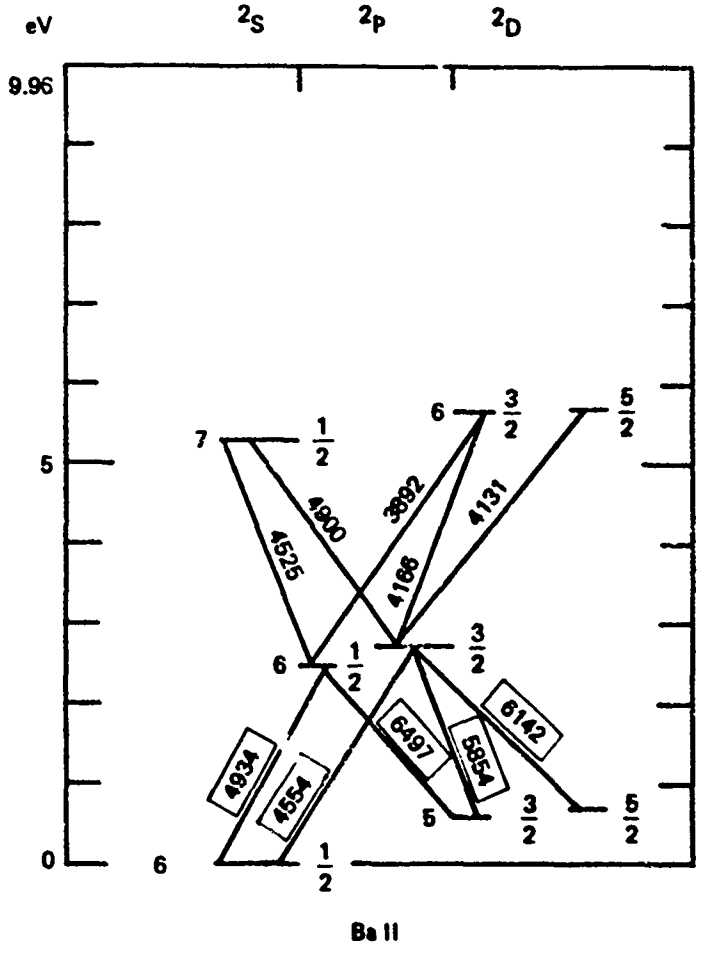

Figure 21 Energy-level diagram of Ba II, showing the low lying resonance and fluorescent transitions. After Horak and Whitaker (1980).

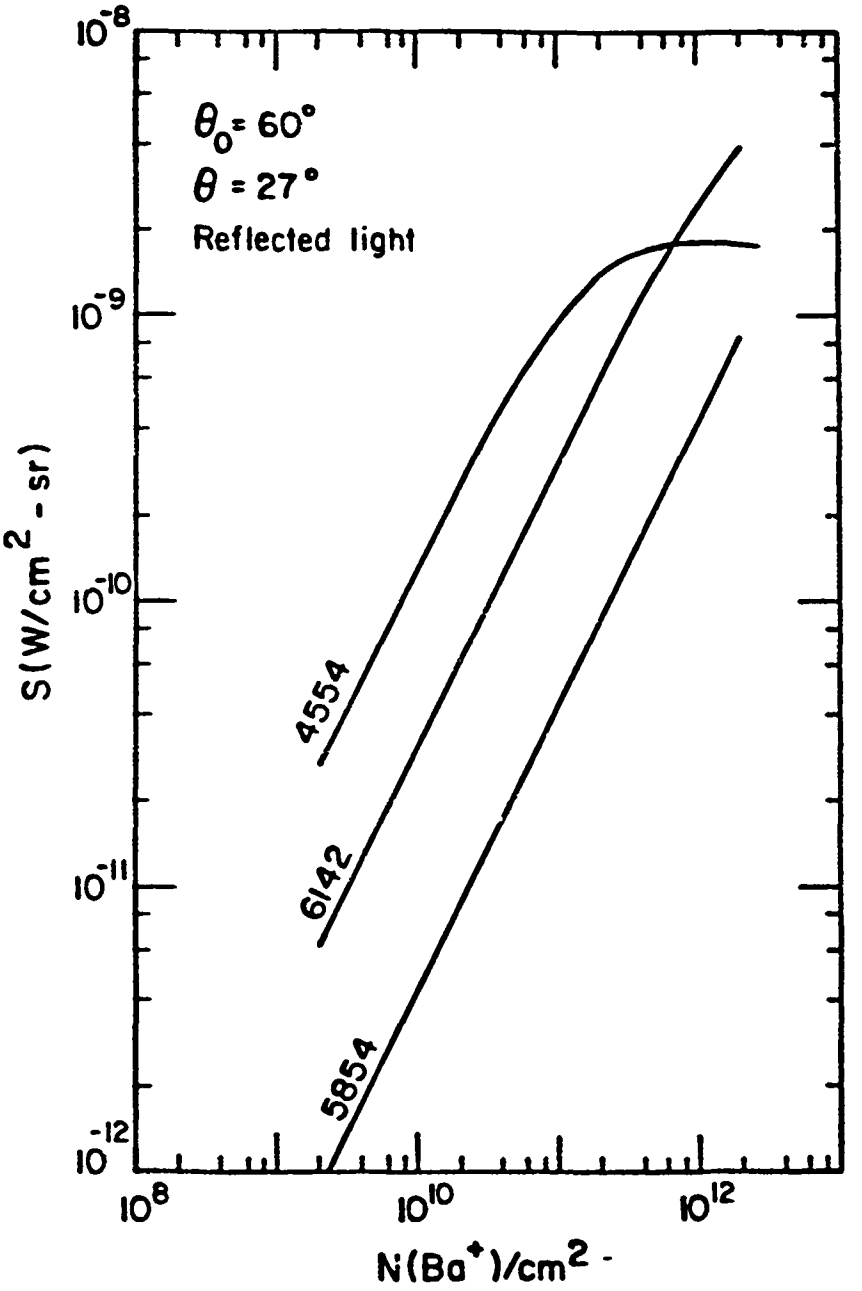

Figure 22 Curve of growth for one resonance transition (4554A) and two fluorescent transitions (5854A and 6142A). Note that the resonance transition saturates at high column densities of Ba^+ ions. Thus observations at 4554A cannot be used to correctly measure Ba^+ column densities above $\sim 2 \times 10^{11}$ cm^{-2}, whereas observations at the other two wavelengths could extend measurements by at least an order of magnitude. After Horak and Whitaker (1980).

saturate. It can be seen in Fig. 22 that even 6142A is beginning to saturate at column densities of 10^{12}Ba+ cm^{-2} for the viewing geometry indicated on the figure. So long as the cloud remains optically thin in the resonance lines, there is no ambiguity, if the spectra are "pure."

However, another problem that has arisen in the past and which further argues for some redundancy in the spectral observations is the leakage of filters to undesired emission. Particularly, the 4607A line of Sr is strong and seems to be an inevitable contaminant of barium. Unlike barium the strontium is essentially unionizable, and the 4607A line may penetrate the 4554A filter.

Because the forthcoming "PLACES" experiments will produce optical thicknesses in the range 40-60, it is important that the curve-of growth effects be anticipated. It should be noted that curve-of-growth effects depend strongly on the hyperfine structure of the scattering atom or ion (J. W. Chamberlain, 1960). In the LASL work of Horak and Whitaker, the complex array of HFS from the variety of isotopes has been accounted for.

ACKNOWLEDGMENTS

During this work a number of JASON members participated in discussions and briefings, but are not authors of this report. We appreciate the efforts of Jonathan Katz, Robert LeLevier, and Allen Peterson in this regard.

The authors also thank the many people who came to La Jolla during the 1980 JASON Summer Study, both to educate us and to participate in discussions, namely W. G. Chesnut and C. L. Rino (SRI International), M. B. Pongratz and D. J. Simons (LASL), R. Kilb (MRC), S. L. Ossakow (NRL) and J. Dawson, H. Goede and D. Humanic (UCLA, TRW and UCLA respectively). Major Leon Wittwer of DNA was a continuing participant both in the educational and discussional aspects of the Summer Study. His careful reading of the draft improved the final version of this report in many ways. For this he has our special thanks. Many others provided useful information by telephone or letter. Among these we are particular y grateful to the following: D. R. McDaniel, D. L. Neilson and G. R. Smith (SRI International); J. A. Stamper and R. W. Clark (NRL); and K. Papadopoulos and C. Parsons (University of Maryland). The Staff of SRI International--in particular, Jan Fanning, Don LeVine, Elaine Matthews and Kathy Zacher--have our gratitude for their help both during the Summer Study and with the preparation of the manuscript.

REFERENCES

1. Baker, K. D., J. C. Ulwick, M. C. Kelley, L. C. Howlett, G. D. Allred, D. Delorey, and N. Grossbard. "Electron Density Structure in Barium Clouds--Measurements and Interpretations," in McDaniel, ed., 1978: 69-104.

2. Baumann, E. J., V. E. Hatfield, and J. Owen. "Documentation of NUCOM II--an Updated HF Nuclear Effects Code" (U). Menlo Park, CA 94025: DNA 3108F, Final Report, Contract DASA-01-71-C-0138, Stanford Research Institute, April 1973. CONFIDENTIAL.

3. Bogusch, R. L., M. J. Barret, D. L. Knepp and B. E. Sawyer. "Signal Propagation Effects of Selected Satellite Systems" (U). Santa Barbara, CA: MRC-R-405, Mission Research Corp., July 1978. SECRET.

4. Boquist, W. P. "High-Resolution Ground Optics Measurements." in McDaniel, ed., 1978: 11-52.

5. Chamberlain, J. W., D. M. Hunten, and J. E. Mack. J. Atmos. Terr. Phys., 12, 1960: 153-165.

6. Chesnut, W. G. Discussions during the 1980 JASON Summer Study, La Jolla, CA 92038, 1980.

7. Clark, R. W. NRL, (1980). Private communication.

8. Costa, E., and M. C. Kelley. J. Geophys. Res., 83, 1978a: 4359.

9. Costa, E., and M. C. Kelley. J. Geophys. Res., 83, 1978b: 4365.

10. Davies, K. Ionospheric Radio Propagation. Washington, D.C.: N.B.S. Monograph 80, U.S. Government Printing Office, 1965.

11. Dean, S. O., E. A. McLean, J. A. Stamper, and H. R. Griem. Demonstration of collisionless interactions between interstreaming ions in a laser-produced-plasma experiment, Phys. Rev. Lett., 27, 1971: 487.

12. Dungey, J. W. Cosmic Electrodynamics. Cambridge University Press, 1958.

13. Dupree, J. H. Phys. Fluids, 21, 1978: 783.

14. Fejer, B. G., and M. C. Kelley. Ionospheric irregularities. Rev. Geophys. and Sp. Phys., 18, 1980: 401-454.

15. Flatté, S. M. (ed.), R. Dashen, W. H. Munk, K. M. Watson, and F. Zachariasen. Sound Transmission Through a Fluctuating Ocean. Cambridge University Press, 1979.

16. Francis, S. H., and F. W. Perkins. J. Geophys. Res., 80, 1975: 3111.

17. Friedman, H. W., and R. M. Patrick. Momentum transfer in plasma flows at high Alfven mach numbers. Phys. Fluids, 14, 1971: 1889.

18. Goede, H. UCLA Doctoral Dissertation, April 1980.

19. Goede, H., J. Dawson, and D. Humanic. Particle simulation of the collisionless interchange. Briefing delivered at the JASON Summer Study, La Jolla, CA, 1980.

20. Hangstad, B. Effects of the inhomogeneous background on radioactive propagating through turbulent planetary atmospheres. Radio Sci., 13, 1978: 435-440.

21. Hasegawa, A., and K. Mima. Phys. Fluids, 21, 1978: 87.

22. Hendrick, R. W. "Propagation of Microwave Satellite Signals through Striated Media." Santa Barbara, CA: DNA 4412T, Mission Research Corp., September 1977. UNCLASSIFIED.

23. Hess, W. N. The Radiation Belt and Magnetosphere. Waltham, MA, Blaisdell, 1968.

24. Holmgren, G., R. Boström, M. C. Kelley, P. M. Kintner, R. Lundin, U. V. Fahleson, R. A. Bering, and W. R. Sheldon. J. Geophys. Res., 85, 1980: 5043.

25. Horak, H. G. and R. W. Whitaker. Resonance-fluorescence lines in barium-ion clouds. Draft, 1980.

26. Huba, J. D., P. K. Charturvedi, S. L. Ossakow, and D. M. Towle. Geophys. Res. Lett., 5, 1978: 695.

27. Huba, J. D., and S. L. Ossakow. Phys. Fluids, 22, 1979: 1349.

28. Ishimaru, A. Wave Propagation and Scattering in Random Media. Single Scattering and Transport Theory, vol. 1. Multiple Scattering, Turbulence, Rough Surfaces and Remote Sensing, vol. 2. N.Y.: Academic Press, 1978.

29. Johnson, S. C., W. G. Chesnut, and C. L. Rino. "Comparison of Performance of DPSK and Incoherent FSK Systems Operating in a Scintillation-Induced, Finite-Fading Bandwidth Environment" (U). Menlo Park, CA: DNA 3957T, Stanford Research Institute, 1976. CONFIDENTIAL.

30. JTAC (Joint Technical Advisory Committee). Radio transmission by ionospheric and tropospheric scatter. Proc. IRE, 48, 1960: 4-44.

31. Keskinen, M. J., S. L. Ossakow, and P. K. Chaturvedi. "Preliminary Report of Numerical Simulations of Intermediate Wavelength $\hat{E} \times \hat{B}$ Gradient Drift Instability in Ionospheric Plasma Clouds." Washington, D.C.: NRL Memo, Rpt. 4133, Naval Research Laboratory, 1979.

32. Keskinen, M. J., B. E. McDonald and S. L. Ossakow. Preliminary numerical study of the outer scale size of ionospheric plasma cloud striations. J. Geophys. Res., 85, 1980: 2349-2352.

33. Kilb, R. Briefing at 1980 JASON Summer Study, La Jolla, CA 92038, 1980.

34. Knepp, D. L. "Multiple Phase Screen Propagation Analysis for Defense Satellite Communication Systems." Santa Barbara, CA: DNA 4424T, Mission Research Corporation, September 1977. UNCLASSIFIED.

35. Koopman, D. W., and R. R. Goforth. Phys. Fluids, 17, 1974: 1560-1565.

36. Lawrence Livermore Laboratories. Laser Program Annual Report, 1978. Livermore, CA: Lawrence Livermore Laboratories, 2, 1979: S-22 through S-45.

37. Linson, L. M., and J. B. Workman. J. Geophys. Res., 75, 1970: 3211.

38. Mandelbrot, B. B. Fractals, Form, Chance and Dimension. San Francisco, CA: W. H. Freeman Co., 1977.

39. Manes, K., R. Kauffman, and V. Rupert. LLL, (1980). Private communication.

40. McDaniel, D. R., ed. Proceedings of the Stress Data Review Meeting, 29-30 November 1977. Menlo Park, CA 94025: Topical Report Project 4960, SRI International, June 1978.

41. McDaniel, D. R., ed. Proceedings of the DNA/LASL High-Altitude Nuclear Weapons Effects Summer Study (U). Working Group Reports, vol 2 (U). Menlo Park, CA: DNA 4736P-3, Stanford Research Institute, November 1978. SECRET.

42. McDonald, B. E., S. L. Ossakow, and S. T. Zalesak. "A Fluid Model for Estimating Minimum Scale Sizes in Ionospheric Plasma Cloud Striations." Washington, D.C.: NRL Memo, Rpt. 3864, Naval Research Laboratory, 1978.

43. McDonald, B. E., S. L. Ossakow, S. T. Zalesak, and N. J. Zabusky. In Proceedings of 1978 Symposium on the Effect of the Ionosphere on Space and Terrestrial System, ed. J. M. Goodman. Washington, D.C.: U.S. Government Printing Office, 1978.

44. McDonald, B. E., M. J. Keskinen, S. L. Ossakow, and S. T. Zalesak. Computer simulation of gradient drift instability processes in Operation Avefria. J. Geophys. Res., 85, A5, 1980: 2143-2154.

45. Nielson, D. L. "The Effects of Nuclear-Burst-Produced Acoustic Gravity Waves on HF Communications Systems." In Effects of Atmospheric Acoustic-Gravity Waves on FM Propagations. AGARD Conference Proceedings CP-115, April 1972.

46. Neilson, D. L., J. B. Lomax, and H. A. Turner. "The Prediction of Nuclear Effects on HF Communications." Menlo Park, CA 94025: DASA 2035, Final Report, Contract DA-49-XZ-436, Stanford Research Institute, November 1967. UNCLASSIFIED.

47. Okuda, H., and J. M. Dawson. Phys. Fluids, 16, 1973: 408.

48. Ossakow, S. L. 1980. Private communication.

49. Ossakow, S. L., S. T. Zalesak, and N. J. Zabusky. "Recent Results on Cleavage, Bifurcation and Cascade Mechanisms in Ionospheric Plasma Clouds." Washington, D.C.: NRL Memo, Rpt. 3579, Naval Research Laboratory, 1977.

50. Ossakow, S. L. "The Relevance of Barium Cloud Experiments." In McDaniel, ed., 1977.

51. Ossakow, S. L., P. K. Chaturvedi, and J. B. Workman. J. Geophys. Res., 83, 1978: 2691.

52. Owen, J., and K. K. Bailey. "Users Manual for NUCOM III: A HF Nuclear Effects Code Incorporating WPH VI-Mod I." Menlo Park, CA 94025: DNA 4824T, Stanford Research Institute, November 1978. UNCLASSIFIED.

53. Papoulis, A. Probability, Random Variables and Stochastic Processes. N.Y.: McGraw-Hill, 1965.

54. Parsons, Charles. University of Maryland, 1980. Private communication.

55. Perkins, F. W., N. J. Zabusky, and J. H. Doles, III. J. Geophys. Res, 78, 1973: 697.

56. Pitteway, M.L.V. The reflection of radio waves from a stratified ionosphere modified by weak irregularities, II. Proc. Roy. Soc. A., 254, 1960a: 86-100.

57. Pitteway, M.L.V. "The Reflection of Radio Waves from an Irregular Ionosphere." Cambridge, MA: Tech. Rpt. 382, Research Laboratory of Electronics, Massachusetts Institute of Technology, November 8, 1960b.

58. Pitteway, M.L.V. Interpretation of ionospheric radio drift measurements, 3. Validation of correlation analysis by computer simulation. J. Atm. Terr. Phys., 33, 1971: 635.

59. Pongratz, M. B., and D. Simons. "Impact of the Drift Cyclotron Loss Cone Instability upon Starfish Phenomenology." Los Alamos, NM 87545: Memo J-10-4349, Los Alamos Scientific Laboratories, 1979.

60. Rino, C. L. A power law phase screen model for ionospheric scintillation, 1. Weak scatter. Radio Sci., 14, 1979a: 1135-45.

61. Rino, C. L. A power law phase screen model for ionospheric scintillation, 2. Strong scatter. Radio Sci., 14, 1979b: 1147-55.

62. Rino, C. L. "A Striation Microstructure Model for Propagation Calculations," (U). Menlo Park, CA: DNA 4626T, SRI International, 1978.

63. Rino, C. L., R. R. Vondrak, and V. E. Hatfield. "An Analysis of Scintillation Effects for Communication and Radio Systems," (U). Menlo Park, CA: DNA 3748F, Stanford Research Institute, August 1975. CONFIDENTIAL.

64. Scannapieco, A. J., S. L. Ossakow, S. R. Goldman, and J. M. Pierre. J. Geophys. Res., 81, 1976: 6037.

65. Scwartz, M., W. R. Bernett, and S. Stein. Communications Systems and Techniques. N.Y.: McGraw-Hill, 1966).

66. Simons, D. J., M. B. Pongratz, G. M. Smith, G. E. Bararch, and T. J. Fitzgerald. "Prompt Striations Observed in a Barium Thermite Release at 335 km." Los Alamos, NM 87545: Report LA-UR 80-1180, Los Alamos Scientific Laboratories, 1980.

67. Simons, D. J., M. B. Pongratz, and S. P. Gary. J. Geophys. Res., 85, 1980: 671.

68. Stamper, J. A., K. Papadopoulos, R. N. Sudan, S. O. Dean, E. A. McLean, and J. M. Dawson. Phys. Rev. Lett., 26, 1971: 1012.

69. Stamper, J. A. NRL, (1980). Private communication.

70. Uscinski, B. J. The Elements of Wave Propagation in Random Media. N.Y.: McGraw-Hill, 1977.

71. Volk, H. J., and G. Haerendel. J. Geophys. Res., 76, 1971: 4541.

72. Wittwer, L. A. "Satellite Communications in a Scintillated Environment." Kirtland Air Force Base, NM 87117: AFWL-TR-75-240, Air Force Weapons Laboratory, January 1976.

73. Wittwer, L. A. et al. "UHF Propagation Effects in Scintillated Environments." AFWL-TR-76-304, Air Force Weapons Laboratory, August 1977. UNCLASSIFIED.

74. Wittwer, L. A. "The Performance of Advanced Frequency Shift Key Modulation Techniques in Scintillated Environments II," (U). AFWL-TR-78-49, Air Force Weapons Laboratory, April 1978. SECRET.

75. Wittwer, L. A. "Radio Wave Propagation in Structured Ionization for Satellite Applications." Washington, D.C.: DNA 5304D, Defense Nuclear Agency, 1980a. UNCLASSIFIED.

76. Wittwer, L. A. "A Trans-Ionospheric Signal Specification for Satellite C^3 Applications." Washington, D.C.: DNA/RAAE Tech. Note, Defense Nuclear Agency, 1980b. UNCLASSIFIED.

77. Wittwer, L. A. 1980c. Private communications.

78. Wright, J. W. Interpretation of ionospheric radio drift measurements, 1. Some results of experimental comparisons with neutral wind profiles. J. Atm. Terr. Phys., 30, 1968: 919.

79. Zabusky, N. J., and J. Block. NRL Memo, Rpt. 3586, 1978.

80. Zinn, J., h. Hoerlin, and A. G. Petscher. "The Motion of Bomb Debris Following the Starfish Test." In Radiation Trapped in the Earth's Magnetic Field, ed. B. M. McCormac. Dordrecht, Holland: D. Reidel Co., 1966, 671-692.

DISTRIBUTION LIST

ORGANIZATION	NO. OF COPIES
Dr. Joseph W. Chamberlain 18622 Carriage Court Houston, TX 77058	1
Dr. John M. Cornwall Department of Physics University of California Los Angeles, CA 90024	10
Defense Documentation Center Cameron Station Alexandria, VA 22314	3
Defense Nuclear Agency Hybla Valley Federal Bldg. 6801 Telegraph Road Alexandria, VA 20305	
ATTN: Maj. Leon Wittwer	1
Dr. E. Conrad	1
Dr. E. Sevin	1
Dr. G. Soper	1
Dr. Adam Drobot Science Applications, Inc. 8400 Westpark Drive McLean, VA 22102	1
Dr. David D. Elliott SRI International 333 Ravenswood Avenue Menlo Park, CA 94025	1
Dr. Stanley M. Flatté University of Cambridge Dept. of Applied Math & Theoretical Physics Silver Street Cambridge, CB3 9EW, ENGLAND	1
Dr. Henry Foley Department of Physics Columbia University New York, NY 10027	1
Director National Security Agency Fort Meade, MD 20755 ATTN: Mr. Richard Foss, A052	2
Dr. Robert Fossum, Director DARPA 1400 Wilson Boulevard Arlington, VA 22209	1
Dr. George Gamota OUSDRE (R&AT) Room 3D1067, The Pentagon Washington, D.C. 20301	2
Dr. David A. Hammer 109 Orchard Place Ithaca, NY 14850	1
Dr. Bjorne Haugstad Norwegian Defense Research Establishment Oslo, Norway	1
Dr. Jonathan I. Katz Department of Astronomy University of California Los Angeles, CA 90024	1
Dr. Michael C. Kelley School of Electrical Engineering Cornell University Ithaca, NY 14850	1
Lawrence Livermore Labs P.O. Box 808 Livermore, CA 94550	
ATTN: K. Manes	1
R. Kauffman	1
V. Rupert	1
Mr. Ray Leadabrand SRI International 333 Ravenswood Avenue Menlo Park, CA 94025	1

ORGANIZATION	NO. OF COPIES
Dr. Robert E. LeLevier R&D Associates P.O. Box 9695 Marina Del Rey, CA 90291	1
Dr. Donald M. LeVine SRI International 1611 N. Kent Street Arlington, VA 22209	3
Dr. L. M. Linson Science Applications, Inc. 1200 Prospect La Jolla, CA 92037	1
Los Alamos Scientific Labs P.O. Box 1663 Los Alamos, NM 87544	
ATTN: Dr. D. J. Simons	1
Dr. M. B. Pongratz	1
Dr. G. M. Smith	1
Dr. G. E. Bararch	1
Dr. T. J. Fitzgerald	1
Dr. H. G. Horak	1
Dr. R. W. Whitaker	1
Dr. S. P. Gary	1
Dr. R. A. Jeffries	1
Report Library	1
Dr. Gordon F. MacDonald 4300 Old Dominion Drive Apartment 1017 Arlington, VA 22207	1
Prof. B. B. Mandelbrot Department of Mathematics University of California Los Angeles, CA 90024	1
Mission Research Corporation P.O. Drawer 719 Santa Barbara, CA 93102	
ATTN: E. J. Baumann	1
R. W. Hendrick	1
D. L. Knepp	1

ORGANIZATION	NO. OF COPIES
Dr. Julian Nall P.O. Box 1925 Washington, D.C. 20013	1
Naval Research Laboratory 4555 Overlook Ave., S.W. Washington, D.C. 20375	
ATTN: Dr. R. W. Clark,code4707	1
Dr. S. O. Dean,code____	1
Dr. E. A. McLean,code4732	1
Dr. J. A. Stamper,code4732	1
Dr. H. R. Griem,code4730	1
Dr. J. D. Huba,code4780	1
Dr. P. K. Charturvedi____	1
Dr. S. L. Ossakow,code4780	2
Dr. D. M. Towle___	1
Dr. M. J. Keskinen,code4780	1
Dr. B. E. McDonald,code4780	1
Dr. S. T. Zalesak,code4780	1
Prof. William A. Nierenberg Scripps Inst. of Oceanography University of California, S.D. La Jolla, CA 92093	1
Dr. Francis W. Perkins, Jr. Plasma Physics Laboratory P.O. Box 451 Princeton, NJ 08540	1
Dr. Allen M. Peterson SRI International, (L-1057) 333 Ravenswood Avenue Menlo Park, CA 94025	1
Dr. K. Papadopoulous Science Applications, Inc. 8400 Westpark Drive McLean, VA 22102	1
Dr. C. L. Reufenach NOAA/WPL R45X5 Sea State Studies Group Boulder, CO 80302	1

ORGANIZATION	NO. OF COPIES
SRI International 333 Ravenswood Ave. Menlo Park, CA 94025	
ATTN: Dr. W. G. Chesnut	1
Dr. C. L. Rino	1
Dr. D. R. McDaniel	2
Dr. R. A. Nelson	1
Dr. R. L. Leonard	1
Dr. D. L. Nielson	1
Dr. G. Smith	1
Ms. J. Owen	1
Ms. V. E. Hatfield	1
Ms. K. K. Bailey	1
SRI/MP Reports Area G037 333 Ravenswood Avenue Menlo Park, CA 94025 ATTN: D. Leitner	2
Dr. Art Shef P.O. Box 1925 Washington, D.C. 20013	1
Dr. Joel A. Snow Senior Technical Advisor Office of Energy Research, U.S. DOE, M.S. E084 Washington, D.C. 20585	1
Stanford University Department of Electrical Engineering Stanford, CA 94305	
ATTN: Prof. O. G. Villard, Durand Bldg	1
Dr. T. Frazier-Smith Durand Bldg	1
Mr. David Hinson SCRA, 233 Durand Bldg	1
Dr. R. N. Sudan, Director Laboratory of Plasma Studies Cornell University Room 309, Upson Hall Ithaca, NY 14853	1

ORGANIZATION	NO. OF COPIES
University of California Department of Physics Los Angeles, CA 90024	
ATTN: Dr. H. Goede	1
Prof. John Dawson	1
Dr. D. Humanic	1
Dr. H. Okuda	1
University of Maryland Department of Physics College Park, MD 20740	
ATTN: Dr. R. R. Goforth	1
Dr. C. Parsons	1
Dr. John F. Vesecky Center for Radar Astronomy Stanford University Stanford, CA 94305	5
Dr. J. B. Workman Berkeley Research Associates 125 University Avenue Berkeley, CA 94701	1
Ms. Alice Wright SRI International 333 Ravenswood Avenue Menlo Park, CA 94025	1
Dr. N. J. Zabusky Bell Laboratories Holmdel, NJ 07733	1